

Dissertation
for the degree of
Doctor of Natural Sciences
submitted to the
Combined Faculties for the Natural Sciences and for Mathematics
of Ruperto-Carola University of Heidelberg, Germany

presented by
Dipl.-Biomath. Hannah Schmidt-Glenewinkel
born in Frankfurt am Main

Oral examination: October 8, 2008

Diese Arbeit ist meiner Großmutter

Dr. rer. nat. Annemarie Schmidt-Glenewinkel, geb. Wallach

gewidmet.

Acknowledgements

I would like to thank a whole group of colleagues who have become friends, without whom the dissertation here would not have been completed.

First, there is Ivayla, who was the first person I ever worked with 'seriously' on a common project - I am afraid that she spoiled the standards for all successors in this role, as it is difficult to live up to the helpfulness and insightfulness that she offered to me. Her quiet way of contributing, helping me to develop my own thoughts, as well as her sharp analytic mind have remained a role model for me.

I would also like to thank Joel, for his sheer endless patience and his generosity to offer his comprehensive knowledge and experience. He sat numerous hours with me at the microscope, looking at images that were barely recognizable, in my earliest efforts to do 'real experiments'. One of our first conversations, after I had decided to enter his lab, started with him asking "So, did you ever hold a pipette in your hand?" - the fact that he didn't throw me out immediately, after my vaguely mumbled response (i did remember that there were two steps in emptying the pipette all the way!), characterizes his optimism which I have witnessed often afterwards seeing him work with other students. I am deeply thankful for the positive response he gave me on my advances from time to time, they are like gasoline which keep you going for another while.

I would also like to thank Sven for being a great colleague. We have shared the office for almost three years, and I estimate that he has saved me about 100 working hours with his knowledge on all kinds of things, from LaTeX to image formats to classes of differential equations. I would like to thank Yvonne and Annika, for their patience in listening to my complaints about 'how hard it is'. I also want to thank the other lab members: Leo, Yara, Dani, Philip, Leo, Hee-Kyong and Marti, whose presence is enjoyable and makes lab life much more cheerful. Special thanks goes to Sabine, who has helped me in the lab numerous times, despite me being very unreliable about my lab tasks. Michaela has helped me with her knowledge on all things that concern cells - I have not been able to come up with a question that she doesn't know the answer to or doesn't have experience with. She is another

example of the fact that in the lab 'experience counts everything'.

Nathan was the one who actually pushed the project into fields where things became meaningful for biology and not just modeling. He has the eye of an experienced experimentalists and while it was sometimes painful for me to depart from my mathematician's view, his requirements for biological research have become standards for me to aspire to.

Eunice has entered my personal scene late, but just at the right time, and I have learned valuable lessons from her in 'letting go' of things, such as, for example, half-finished dissertations. Thanks for this.

Finally, the advisors. Benedikt has helped me only a few time (although I am not in his group), but I can remember all of them and everytime they brought me a big step forward. I remember that my first question to him, after I had been here for a week or so, was "So, Benedikt, what IS a model?". His answer was very helpful.

I would like to give special thanks to my second PhD advisor Ivan Dikic. His energy and love for science, as well as his deep understanding of his subject, have been inspirational and deeply motivating. I'm glad and grateful to have him as an advisor.

Roland Eils, my supervisor, I would like to thank for giving me the freedom to pursue the projects as I wished to, with almost no limitations when it came to lab material and conferences to attend. His generosity has allowed me and other students to develop projects according to our own taste and possibilities. It has been a pleasure to work in his lab.

Als nächstes möchte ich meinem Onkel Thomas danken, der mich im dritten Studiensemester nach New York gelotst hat, mich bei sich hat wohnen lassen und immer wieder versucht hat, mir die 'ernste, deutsche Art' auszutreiben ('Science is fun!'). Außerdem hat er gegen meinen Willen darauf bestanden, dass ich einen Programmierkurs belege, was im weiteren schwerwiegende Folgen hatten.

Als letztes und am meisten von allen möchte ich meinen Eltern dafür danken dass sie mich seit Beginn meines Studiums der Naturwissenschaften bedingslos unterstützt haben, sei es finanziell oder 'gemütlich'. Ohne euch wäre das alles hier viel schwieriger gewesen.

Theoretical and Experimental Examination of EGF Receptor Endocytosis

Referees: Prof. Dr. Roland Eils

Prof. Dr. Ivan Dikic

The work presented in this thesis was carried out in the Division of Professor Dr. Roland Eils, Applied Systems Biology at the German Cancer Research Center (DKFZ) in Heidelberg from January 2005 to March 2008. The thesis was supervised by Professor Dr. Roland Eils and Professor Dr. Ivan Dikic.

The work was financed by the German Cancer Research Center.

List of Publications

- Hannah Schmidt-Glenewinkel, Ivayla Vacheva, Daniela Hoeller, Ivan Dikic and Roland Eils. An ultrasensitive sorting mechanism for EGF Receptor endocytosis. *BMC Systems Biology*, 2008 vol. 2 (1) pp. 32.
- Hannah Schmidt-Glenewinkel, Roland Eils and Nathan Brady. Systems biological analysis of EGF receptor internalization dynamics for altered receptor levels. (accepted in the *Journal of Biological Chemistry*)
- Hannah Schmidt-Glenewinkel, Eileen Reinz, Roland Eils and Angel Alonso. Automated Analysis of Vesicle Features and Colocalization in Microscopy Images. (submitted)
- Hannah Schmidt-Glenewinkel, Nathan Brady, Joel Beaudouin, Michaela Reichenzeller, Roland Eils. Investigations of EGFR endocytic sorting into clathrin- or caveolin-dependent pathways (in preparation)

List of Presentations

- Talk (Invited Speaker) 'Systems Biology of EGFR endocytic sorting' at the IPCMB 2008 at Bose Institute, Kolkatta, India.
- Talk 'Theoretical and Experimental Investigation of EGFR Endocytosis' at the Symposium 'Modelling of Cellular Biosystems' at the Faculty of Mathematics, Informatics and Mechanics, University of Warsaw, Poland, March 2008.
- Talk 'Mathematical Modeling of Cellular Signal Transduction' at the DKFZ Student Retreat in Weil der Stadt, Juni 2006
- Poster 'Multiparametric Flow Cytometry and mathematical modeling to assess EGFR internalization dynamics' at the EMBO meeting on 'Cellular Signaling and Molecular Medicine', Cavtat, Croatia, June 2008.

- Poster 'An ultrasensitive sorting mechanism for EGF Receptor endocytosis', at the Keystone Meeting in Systems Biology, Taos, New Mexico, USA, March 2006.
- Poster 'Automated image analysis of confocal microscopy data ' DKFZ, Heidelberg, October 2006.

Contents

0.1	Zusammenfassung	15
0.2	Summary	17
0.3	List of Abbreviations	19
I	Introduction	20
1	Introduction to EGF receptor signaling and endocytosis	22
1.1	Receptor signaling and downstream events	22
1.2	Receptor endocytosis	25
1.2.1	Endosomal compartments and intracellular routes	27
1.2.2	Clathrin- vs Caveolae-mediated internalization pathways	29
1.2.3	Mathematical modeling of EGFR endocytosis	38
2	General Mathematical Models of Cellular Decision Making	41
2.1	Bistability in signaling : Switches between steady-states as cellular decisions	41
2.1.1	A model of Positive Autoregulation	42
2.1.2	Applications of the model	48
2.1.3	Mutual Repression can lead to Bistability	51
2.1.4	Numerical description of bistability - Models of Apoptosis	63
2.2	The monostable case: Models of Ultrasensitivity	68

2.2.1	Multiple Binding and Cooperativity	69
2.2.2	Signaling Cascades	71
2.2.3	Zero-order Ultrasensitivity	74
II	Objectives	77
III	Results	80
3	Quantification of EGFR endocytosis by multiparametric Flow Cytometry	81
3.1	Background on modeling and experimental quantification of early endocytosis events	81
3.2	Flow Cytometric detection of Rhodamine-EGF to measure Endocytosis of EGFR . . .	83
3.3	A quantitative prediction of EGF uptake dynamics for different receptor expression levels	88
3.2	Internalization dynamics for cells with different receptor expression levelsl	92
3.3	Discussion	95
4	A Model of EGFR Endocytic Sorting	97
4.1	Biological Basis of the Model	99
4.2	Ultrasensitivity in EGFR endocytosis	101
4.3	CIE-internalization depends on number of receptors and strength of EGF-stimulation	102
4.4	Conditions on receptor number for switch-effect of CIE-internalization	103
4.5	Correspondence to distinct classes of steady-state	104
4.6	Conditions on initial values for steady-states	106
4.7	New mechanism of ultrasensitivity - steepness of switch effect	107
4.8	Robustness of solution	110
4.9	Role of Receptor modifications	112
4.10	Ultrasensitivity with inclusion of receptor modification	113
4.11	Discussion	115

5	Experimental investigation of EGF receptor sorting into clathrin- vs. caveolin-dependent endocytosis	118
5.1	<i>ColocalizationFinder</i> : an ImageJ plugin for automated image analysis of vesicle features and colocalization	119
5.2	EGF colocalizes with GFP-Clathrin at early and with GFP-Caveolin at later timepoints upon internalization	120
5.3	Effect of inhibition of clathrin-mediated endocytosis or Caveolin-1 expression on EGF uptake and endocytic trafficking	128
5.3.1	RNAi-kockdown of Caveolin does not reduce EGF uptake but intereferes with intracellular trafficking	128
5.3.2	Inhibition of Clathrin-mediated endocytosis reduces, but does not block EGF internalization	134
5.3.3	Overexpression of AP180-mut leads to accumulation of Caveolin in perinuclear region, suggesting a connection between the clathrin- and caveolae-pathways .	135
5.4	Discussion	137
IV	Material and Methods	139
6	Experimental Procedures	140
6.1	Flow Cytometry	140
6.1.1	Laser and Filter	140
6.1.2	Sample preparation	143
6.2	Cell Culture	143
6.2.1	EGF internalization studies	143
6.2.2	Transfection of cells, cell lines and plasmids	143
6.3	Confocal microscopy	144
6.3.1	Sample Preparation	144

6.4	Image Processing	144
6.4.1	Image Background Reduction and Segmentation	144
7	Differential equations	148
7.1	Modeling internalization with a single pathways (chapter 3, page 81)	148
7.1.1	Deriving $r(t)$ for non-constant $\hat{R}E_s$	148
7.2	Modeling of endocytic sorting into two pathways (section 4, page 97)	150
7.2.1	Numerical Simulations and Steady-State Analysis	150
7.2.2	Approximability by Hill-curve	152

0.1 Zusammenfassung

In der hier präsentierten Arbeit behandeln wir die Zusammenführung von prädiktiven mathematischen Modellen und experimentellen Daten zu EGF Rezeptor Endozytose. Dieser Rezeptor ist vor allem für die Weiterleitung von Wachstumssignalen verantwortlich. In der Arbeit wurde insbesondere die Internalisierung selbst, sowie die Sortierung in Clathrin-abhängige wie -unabhängige Pathways untersucht. Das genaue Verständnis der Mechanismen von EGF Rezeptor Endozytose ist aus mehrfacher Hinsicht erstrebenswert: Endozytose, d.h. die Verlagerung des aktivierten Rezeptors von der Zelloberfläche in intrazelluläre Kompartimente, dient dazu, die Signalweiterleitung (Spezifität, Stärke, Dauer) zu kontrollieren. Entsprechend können abnorme Veränderungen des Endozytoseapparats z.B. durch Mutationen oder virale Infektion schwerwiegende Folgen für den zellulären Haushalt (Krebs) haben.

Im ersten Teil der Arbeit präsentieren wir eine Kombination aus mathematischer Modellierung, konfokaler Mikroskopie und Mehrfarben-Flow Cytometry, um die Internalisierung in einzelnen Zellen quantitativ zu erfassen. Das Modell wird benutzt, um die Wirkung von Rezeptorüberexpression auf den Internalisierungsvorgang zu untersuchen (H.S-G *et al*, zur Publikation akzeptiert in JBC).

Im zweiten Teil der Arbeit legen wir ein mathematisches Modell vor, welches die Sortierung von aktivierten Rezeptoren in unterschiedliche Endozytosewege beschreibt. Dies ist nicht nur aus biologisch-medizinischen Gründen, sondern auch aus Sicht der mathematischen Modellierung und Systembiologie interessant, da sie als Beispiel für einen allgemeinen zellulären Entscheidungsprozess aufgefasst werden kann. Das hier vorgelegte Modell beinhaltet den Mechanismus eines Schalterverhaltens, welches kontinuierliche Signale in ein 'Alles-oder-Nichts' Outputverhalten umwandelt (H.S-G *et al*, BMC Systems Biology, 2008). Die mathematische Struktur und die Relevanz für zellbiologische Prozesse dieser Art von Modellen wird in der Einleitung ausführlich besprochen.

Schließlich, um das erarbeitete Modell experimentell zu testen, wurden quantitative Vorhersagen abgeleitet, die vor allem mit Hilfe von konfokaler Mikroskopie untersucht wurden. Um die Bilddaten auszuwerten, wurde im Rahmen dieser Arbeit eine Bildverarbeitungssoftware entwickelt, mit der sich

Vesikelstrukturen automatisch detektieren und quantifizieren lassen (Manuskript zur Veröffentlichung eingereicht). Diese experimentellen Untersuchungen werden im dritten Ergebnisteil vorgestellt. Hierbei wurde insbesondere selektive Hemmung von Clathrin- oder Caveolin-abhängigen pathways auf das Endozytoseverhalten des EGF Rezeptors untersucht. Das Hauptergebnis dieses Teils der Arbeit ist, dass aktivierte Rezeptoren vorrangig über Clathrin-abhängige Mechanismen internalisieren. Caveolin hingegen ist für den intrazellulären Transport und die Inaktivierung des internalisierten Rezeptors wichtig (Manuskript in Vorbereitung).

Insgesamt stellt die Arbeit einen biomathematischen Ansatz zur Beschreibung von Wachstumsfaktoren auf zelluläre Prozesse dar und liefert damit einen Beitrag zu dem sich im Entstehenden befindenden Gebiet der Systembiologie.

0.2 Summary

In the here presented thesis we attempt the integration of experimental measurements with mathematical models of EGF Receptor endocytosis. Hereby we sought to describe both the internalization itself as well as subsequent endosomal sorting into clathrin-dependent or -independent pathways by quantitative experimental techniques and mathematical modeling. The EGF Receptor is mainly responsible for the transmission of growth factor signals.

EGF Receptor endocytosis is interesting both from a biomedical as well as from a biomathematical viewpoint: The receptor as well as its associated signaling partners are powerful proto-oncogenes, associated with a variety of different cancers. Endocytosis and endocytic mis-sorting has emerged as a source of cellular transformation. One open problem is the uncertainty regarding existence of alternative endocytosis pathways and which adaptor molecules are involved in these. We describe a framework based on flow cytometry, confocal microscopy and mathematical modeling, to assess EGFR internalization in a high-precision, single-cell manner and discuss its application in screening for unknown components in the internalization machinery. In particular, we employed the hereby developed model to assess the effect of EGF receptor overexpression on the internalization process (H.S-G *et al*, accepted in JBC).

Also from a biomathematical, systems-biology point of view the question of how the decision between different pathways is achieved is interesting. In the second part we present a mathematical model based on ordinary differential equations, which describes a 'switching mechanism' through which a continuous input signal is translated into an 'all or nothing' output ((H.S-G *et al*, BMC Systems Biology, 2008). The mathematical structure as well as the relevance for cell-biological processes is discussed in detail in the introduction.

From the model we derive experimentally testable predictions, which we present in the third part of the thesis: Confocal microscopy was chosen as the principal tool to assess EGFR sorting into clathrin- or caveolin-dependent pathways. In order to evaluate the images in an objective manner, an imaging software was developed which allows the automated detection of vesicle features such as size,

intensity and shape as well as the quantification of colocalization with endocytic proteins (manuscript submitted for publication). The main result of these experimental investigations is that the EGF receptor mainly internalizes via clathrin-dependent pathways. Caveolin instead is required for proper endocytic trafficking and inactivation of the receptor. Thus it plays an important role in signal control (manuscript in preparation).

Taken together this work presents a biomathematical approach for the investigation of cell-biological processes, in particular the transduction of growth signals, and with this forms a contribution to the emerging field of systems biology.

0.3 List of Abbreviations

AAK1	Adaptor-associated kinase 1
AP-2	Adaptor Protein 2
CDE	Clathrin-dependent endocytosis
CIE	Clathrin-independent endocytosis
DER	Drosophila EGF Receptor
DUSP	Dual-specificity Phosphatase
EGF	Epidermal Growth Factor
EGFR	Epidermal Growth Factor Receptor
EPS15	EGFR Pathway Substrate 15
HPV	Human Papilloma Virus
MAPK	Mitogen-activated Protein Kinase
MVB	Multi-vesicula body
PTB	Phosphotyrosine-binding
SH-2	Src-homology domain 2
TfR	Transferrin Receptor
TGF	Transforming Growth Factor
UIB	Ubiquitin-interaction domain
Ub	Ubiquitin

Part I

Introduction

The topic of this thesis is the synchronization of quantitative experimental techniques with mathematical modeling of Epidermal Growth Factor (EGF) receptor (EGFR) endocytosis, in particular the question of sorting into alternative endocytic pathways.

The thesis is organized as follows: In the first Introduction part we describe the relevance of EGFR signaling and the role of endocytosis (chapter 1). The main focus lies on the mechanisms of clathrin- or caveolin mediated endocytosis and their role in EGFR signaling.

The second part of the introduction is devoted to mathematical modeling of cell biological processes by ordinary differential equations (chapter 2). In particular, models are considered which have the property of translating a continuous input signal into an all-or-nothing output ('switches' or ultrasensitivity), as the model we present in chapter 4 falls into this class.

In the first Results chapter (chapter 3) we describe detection of EGFR internalization by Flow Cytometry. The experimental measurements are accompanied by a mathematical model which relates internalization kinetics to receptor expression level.

In the second Results chapter (chapter 4) we address the problem of ligand-induced sorting of EGF receptors into clathrin-dependent vs clathrin-independent/caveolae pathways. We present a model based on ordinary differential equations which proposes how sorting could be achieved as a function of EGF-stimulation.

In the last Results chapter (chapter 5) we investigate by confocal microscopy combined with automated image analysis as well as flow cytometry the distribution of internalized receptors into clathrin- vs caveolae pathways.

Chapters 4 and 3 are published or submitted for publication, respectively. Chapter 5 is currently in preparation for publication.

Chapter 1

Introduction to EGF receptor signaling and endocytosis

1.1 Receptor signaling and downstream events

Cells respond to their environment through cytoplasmic transmembrane receptors which bind ligands such as hormones and growth factors. Binding of a specific ligand can induce a series of intracellular events which dictates cell behaviour. The epidermal growth factor receptor (EGFR) is a cell-surface receptor which is found in epithelial cells and tumors arising from epithelial tissue [83].

The EGFR, a 170-kDa glycoprotein, belongs to the ErbB family of receptors, a subfamily of four closely related receptor tyrosine kinases: EGFR (ErbB-1), HER2 (ErbB-2), Her 3 (ErbB-3) and Her 4 (ErbB-4).

ErbB receptors are made up of an extracellular region which contains approximately 620 amino acids, a single transmembrane spanning region and a cytoplasmic tyrosine kinase domain.

EGFR binds to ligands EGF, Transforming Growth Factor (TGF)- α , amphiregulin and betacellulin [83]. Upon activation by its growth factor ligands, EGFR undergoes a transition from an inactive monomeric form to an active homodimer. In addition to forming homodimers after ligand binding,

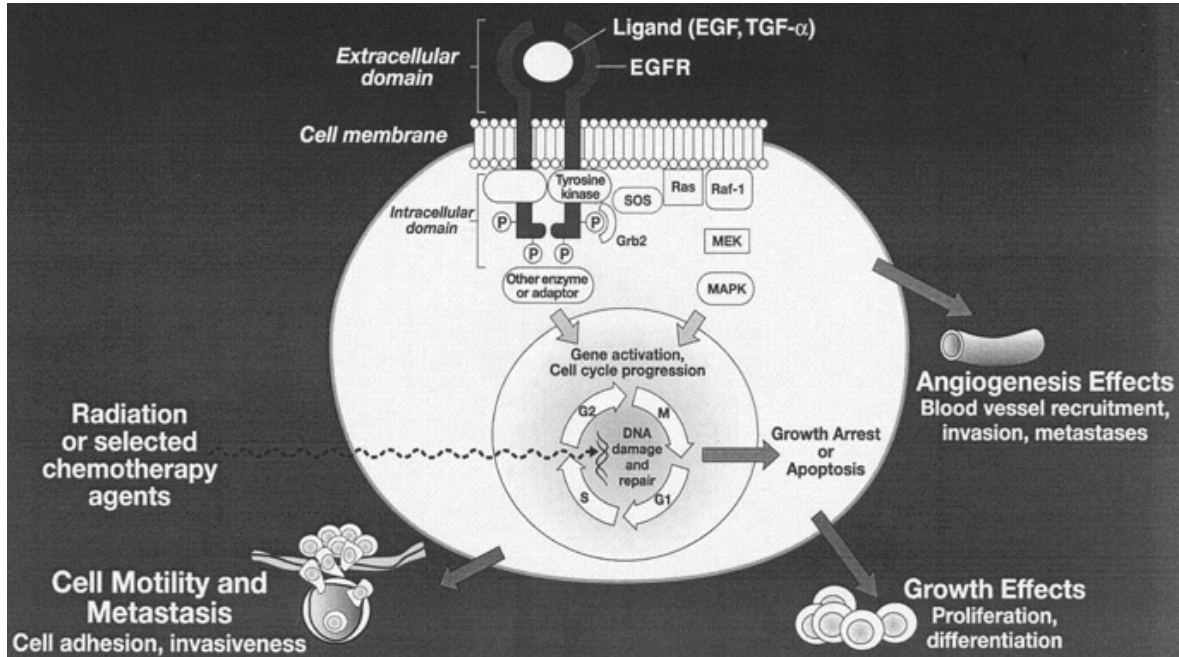


Figure 1.1: **EGFR Endocytosis** Cartoon of Epidermal Growth Factor Receptor (EGFR) signal transduction. Ligand-binding induces dimerization and transphosphorylation of receptor monomers. Phosphorylated tyrosine residues serve as binding sites for cytosolic adaptor proteins which initiates a signaling cascade via several pathways, eventually targeting nuclear proteins. EGFR signaling is involved in many cellular programs such as cell motility, growth and angiogenesis. See main text. Figure from [83]

EGFR may pair with another member of the ErbB receptor family, such as ErbB2/Her2, to create an activated heterodimer (see section 1.2).

Ligand binding induces dimerization and trans-phosphorylation of the monomers at specific tyrosine residues [168]. This phosphorylation creates binding sites for cytosolic adaptor proteins containing Src-Homology (SH) 2 or Phosphotyrosine-binding (PTB) domains [93, 143, 168]. Through the combinatorial binding to these transitional interaction interfaces, a signaling network is created which allows the translation of external stimuli into actions carried out inside the cell by initiation of several signal transduction cascades, principally the MAPK, Akt and JNK pathways. EGFR mediated signaling leads to altered gene expression patterns, as measured by, e.g., microarrays [6] and, depending on the gene module activated, to different phenotypes such as cell proliferation, migration, adhesion, and proliferation [6, 83] (Figure 1.1).

Knockout studies of the *ErbB1* gene in mice showed that *ERBB1* (as the *EGFR* is referred to in mice) has an important role during epithelial-cell development in several organs. Along with brain defects, most of the observed abnormalities involve aberrant proliferation, migration or differentiation of specific epithelial cells (for example, skin, lung, intestine and placenta). Mutant mice that survive after birth develop a strain-independent progressive neurodegeneration [29].

Nematodes and insects express a single *ERBB* orthologue. A single epidermal-growth factor (*EGF*)-like ligand is found in worms, whereas four stimulatory ligands and one inhibitory ligand, *Argos*, bind to the fly orthologue of *EGF* receptor (*DER*). In worms, *EGFR* controls vulva development, hermaphrodite sterility, differentiation of the male tail and posterior-ectoderm development [29].

Attenuation of ligand-induced signaling occurs on several levels. First, as a result of ligand-binding, receptors are routed for lysosomal degradation [200], which is mediated through poly-ubiquitination of the receptor ([43], see below). The removal of receptors results in a refractory period during which cells are insensitive to recurring stimulation. Secondly, inhibitory processes act upon the molecules that are activated in the early phase of signaling, such as the Mitogen-activated protein kinase (*MAPK*) pathways and immediate-early-genes expressed in the first wave of signal response [6]. Signal attenuation involves activation of Dual-Specificity Phosphatases (*DUSPs*), a family of phosphatases where the individual members show different specificity for different *MAPK* modules [6] as well as production of transcriptional repressors [203, 6].

Besides phosphorylation, receptor ubiquitination is an important modification induced by receptor activation [84, 85, 124]. The protein *Cbl* is a ubiquitin E3-ligase which transfers ubiquitin (*Ub*) moieties onto the *EGFR* upon *EGF* stimulation [43]. The *EGFR* is mono-ubiquitinated at multiple sites (multi-mono-ubiquitination) as well as poly-ubiquitinated (chains of ubiquitin) upon *EGF* stimulation [75]. The importance of ubiquitination is two-fold: first, poly-ubiquitination serves to route activated receptors for lysosomal degradation [43, 72]. Secondly, mono-*Ub* serves as a recognition site for proteins carrying a ubiquitin-interaction modules (*UIM*), a collection of modular protein domains

that non-covalently bind to ubiquitin [85]. Proteins that participate in EGFR endocytosis carrying a UIM include EGFR-Pathway Substrate 15 (Eps15), epsins and Hrs [152, 172, 38].

As expected from their role in cell proliferation, abnormalities in the ErbB receptor family are associated with cancer. Overexpression of HER2, which occurs in 25% to 30% of breast cancers, is associated with a poor prognosis and shorter survival [174, 201]. In normal cells, the expression of EGFR ranges from 40,000 to 100,000 receptors per cell [83]. In contrast, EGFR is overexpressed in the majority of solid tumors, including breast cancer, head-and-neck cancer, nonsmall-cell lung cancer (NSCLC), renal cancer, ovarian cancer, and colon cancer [124, 77]. For example, some breast cancers may express up to $2 \cdot 10^6$ EGFR molecules per cell [54]. Such overexpression produces intense signal generation and activation of downstream signaling pathways, resulting in cells that have more aggressive growth and invasiveness characteristics [83].

A process which has emerged as an important regulator of EGF receptor signaling is receptor endocytosis which is reviewed in the following.

1.2 Receptor endocytosis

Endocytosis of the Epidermal Growth Factor Receptor (EGFR) describes the process of translocation of the transmembrane receptor to the cell interior. The importance of this process lies in the diverse nature of its function: continuous internalization and recycling back to the membrane vs targeting for lysosomal degradation serves to keep receptor numbers at an appropriate level, thereby defining the cell's sensitivity to a presented stimulus. Stimulation with EGF induces lysosomal degradation of the majority of receptors within two hours, resulting in a refractory period during which cells are non-responsive to EGF stimulation. Misbalance of degradation and synthesis of the EGFR results in cellular defects as indicated by EGFR gene amplification and overexpression in various human cancers (previous section, [124]) or the transforming character of non-internalizing EGFR mutants [195].

The notion of endocytosis as a modulator of signal transduction appeared in [188] where it was found that preventing internalization not only inhibited signal attenuation, i.e. receptor degradation,

but also prevented activation of certain downstream targets. This discovery gave rise to the more recently developed notion of internalized receptors as active signaling compartments ('signalosome') [88, 130, 27], which, along the endocytic routes, associate with and selectively activate downstream signaling targets.

Internalization of the receptor begins immediately after ligand binding ([198, 189] and chapter 3). Dimerization, which induces trans-phosphorylation of the monomers, seems to be the crucial internalization signal, as pharmacologic inhibition of EGF-induced receptor phosphorylation or the use of a kinase-dead receptor mutant (K721A) had no effect on the rate of internalization [189]. Prevention of dimerization by deleting the dimerization loop of EGFR [64], however, abolished internalization, whereas the construction of an artificial EGFR-dimer using cross-linking reagents drove endocytosis in the absence of ligand [189].

Another important signal in receptor internalization is ubiquitin, whose role, however, is somewhat controversially discussed. As shown through the use of a chimaera EGFR where the cytosolic part was replaced by a single ubiquitin moiety [75], ubiquitin is sufficient to drive internalization. The rate of internalization, however, was reduced, which might mean that there exist internalization pathways which do not accept ubiquitinated cargo, as was discussed in another study ([172], see sections 4 and 1.2.2).

Regarding the necessity of EGFR ubiquitination for internalization, there exist conflicting reports, but it seems that ubiquitination is not strictly required for this initial step of endocytosis [91], again pointing at the possibility of internalization pathways for non-ubiquitinated cargo. Experimentally, it is not trivial to prevent ubiquitination of the receptors altogether. Some studies made use of the Y1045F mutant, which lacks the tyrosine residue at position 1045 whose phosphorylation is necessary for interaction with the E3-ligase Cbl [43] and thus decreases, but does not fully prevent receptor ubiquitination [193, 60]. Studies employing the Y1045F mutant report a slowed down kinetics of internalization [193], while other studies employing site-directed mutagenesis of lysine residues, thus preventing ubiquitination, report that this had no effect on internalization rate as long as kinase

activity was unaffected [91]. The role of ubiquitin is most clearly associated with intracellular sorting or internalized receptors to degradative compartments (see below).

1.2.1 Endosomal compartments and intracellular routes

Receptor internalization and endosomal trafficking constitute an important mechanism of signal regulation through compartmentalization. Temporal and Spatial control of active receptors determine signal specificity, as has arisen in many different contexts by now, reviewed in [88].

It has been appreciated for some time that upon internalization, different fates await the receptors, most easily observed in different fractions that are routed either for recycling and re-integration in the membrane or lysosomal degradation [200]. For EGFR, the relative fractions of receptors destined for different fates depend on the degree of homo- vs heterodimerization of EGFR with itself or ErbB2 [114] as well as the type of ligand: EGF binding directs the majority of EGF receptors to degradation within 2 hours, whereas stimulation with TGF- α results mostly in receptor recycling. A higher fraction of recycling receptors is accompanied by a stronger proliferative signaling effect [27, 191].

The question of how this sorting into distinct endocytosis pathways is regulated is now a major focus of research on receptor signaling.

Three major endosomal compartments are generally distinguished: early and late endosomes, as well as multivesicular bodies (MVBs) which are thought of as a sorting organelle, an intermediate compartment between early endosomes, from which on cargo can be sent to recycling, and late endosomes which mature into or fuse with lysosomes [192, 72], see Figure 1.2.

An important question both from a theoretical point of view as well as its biomedical relevance is how sorting of internalized cargo into distinct fates is regulated.

The sorting into degradative vs recycling pathways seems to be partly directed by the endosomal pH and its effect on dissociation of the ligand-receptor complex. Internalized vesicles acidify along the endocytic route through an ATP-dependent proton-pump [27]. This consecutive decrease of endosomal pH functions as an intrinsic clock which indicates the endosomal stage and forces ligand-

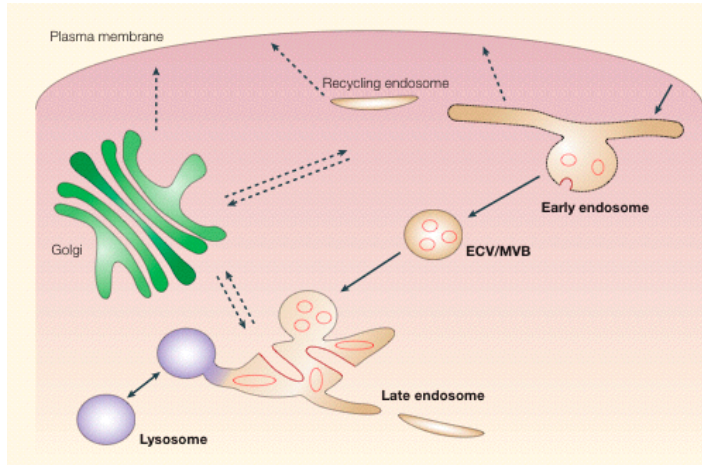


Figure 1.2: **Endosomal compartments reached upon internalization** Upon internalization, receptors are found in early endosomes, from which they can be routed for recycling and re-integration into the membrane. Other receptors are routed to multi-vesicular bodies where they are found in the internal vesicles as a function of ubiquitin-modification [97]. From MVBs cargo is transported to late endosomes which lead to lysosomal degradation. Figure from [72]

receptor dissociation at a certain point. The distinct pH dependence of binding seems to explain the different trafficking properties of different ligand-receptor pairs: A receptor mutation of the Low density lipoprotein receptor stabilizing receptor-ligand binding at low pH results in accelerated receptor degradation, indicating that the receptor binding state is an important regulator of endosomal sorting [36]. Indeed, TGF- α dissociates from EGFR at higher pH-values than EGF [191], and treatment of cells with the ionophor monensin, which increases endosomal pH forces an elevated fraction of receptors to degradation upon TGF- α stimulation, supporting the idea that ligand-receptor binding is an important signal for endocytic routing (see Figure 1.3) [191, 27].

Viral proteins have evolved to modify the endosomal acidification apparatus in order to prevent receptor degradation and enhance signaling. This way, mis-sorting of internalized receptors qualifies as a mechanism of cell transformation, which is an important, new concept in cancer research. The E5 protein of Human Papilloma Virus (HPV) results in cell transformation by inhibiting ligand-induced receptor degradation, despite a normal initial internalization of ligand-receptor complexes [182, 181]. However, the E5 proteins associates with the endosomal proton pump and prevents endosomal acidification, which re-directs endosomes into the recycling pathway. The result is enhanced

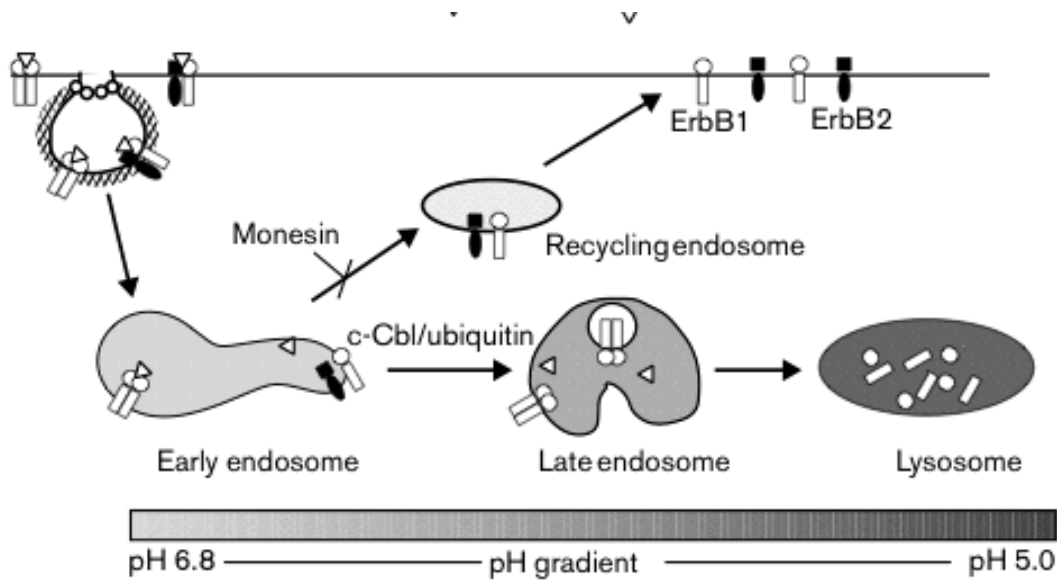


Figure 1.3: **pH dependence of endosome sorting** Figure from [27]

EGFR signaling and an enhanced mitogenic effect.

The discovery of the existence of not only different intracellular endosomal routes but different internalization mechanisms -clathrin-dependent vs -independent pathways - led to the quest to identify which internalization pathway is associated with which endosomal route. Along with this question comes the question whether these different pathways interact, and how sorting into the different routes is regulated. In the following, we review the processes of clathrin-mediated endocytosis and clathrin-independent, caveolae-mediated endocytosis.

1.2.2 Clathrin- vs Caveolae-mediated internalization pathways

Clathrin-dependent endocytosis (CDE) of EGFR was the first to be discovered [104] and is considered the dominant pathway, responsible for most of internalized EGFR. Clathrin is a triskeletoin protein which spontaneously forms cage-like structures in solution [144]. The different steps of CDE, with formation of clathrin-coated membrane regions which eventually pinch off are well described and considered the best understood pathway of internalization of transmembrane receptors [26, 192]. Vesicles

emanating from coated-pits regions give rise to early endosomes from which on cargo can either be routed to recycling or subcellular distribution such as location to MVBs and late endosomes.

Adaptor proteins involved in clathrin-mediated endocytosis

A series of adaptor proteins are involved in CDE, though not all are essential and it could be that different subsets of these adaptors define different 'sub-pathways' of CDE. AP-2 is a hetero-tetrameric protein, whose β -subunit interacts with clathrin and whose $\mu 2$ -subunit is capable of binding specific tyrosine-based motifs in membrane proteins [137] thereby mediating the recruitment of cargo to the vesicles [192, 104, 26, 176]. Despite its important role during cargo recognition, several studies confirm that CDE can still occur in the absence of functional AP-2, as seen from normal internalization of the Transferrin Receptor (TfR) [32, 132, 135]. Transferrin Receptor is a recycling receptor which strictly depends on CME and is often used as a marker for it. RNAi-mediated depletion of AP-2 [132] or specific disruption of its $\mu 2$ subunit, which mediates cargo recognition, abolished TfR internalization, while still allowing efficient clathrin vesicle formation and EGF internalization [132, 135]. The same result was obtained from overexpression studies of Adaptor-associated kinase (AAK1), an AP-2 binding partner, which modulates AP-2 function by phosphorylating its $\mu 2$ subunit. AAK1 overexpression decreased the phosphorylation of the adaptin subunits of AP-2 and disrupted AP-2 distribution, selectively blocking transferrin receptor endocytosis but leaving EGF uptake unaffected [32]. These results suggest that AP-2 is more involved in the cargo-selecting step than actually required for clathrin vesicle formation. The question remains, however, whether these AP-2 dependent or -independent CDE-pathways have different functional roles.

The pinching off of clathrin vesicles is dependent on the small GTP-ase dynamin [34, 27]. Dynamin is also required for caveolae-mediated endocytosis (see next section) and consequently dominant negative dynamin mutants are able to inhibit EGFR uptake, where the stage of inhibition depends on the type of mutation [34, 92].

For clathrin vesicle formation and receptor internalization to occur signaling downstream of EGFR

is necessary. EGF-induced EGFR activation results in phosphorylation of clathrin at tyrosine 1477, which lies in a domain controlling clathrin assembly [196]. Clathrin redistribution to the cell periphery upon EGF stimulation requires EGFR-mediated activation of SRC kinase as treatment with a specific SRC family kinase inhibitor, reduces EGF-induced clathrin phosphorylation and redistribution [196].

Caveolin and cellular signaling

Besides clathrin-mediated pathways receptor endocytosis can occur through clathrin-independent pathways [159]. One important non-clathrin endocytic route involves the raft-resident protein Caveolin, which induces the formation of caveolae at the cell surface membrane. Caveolae are special membrane regions that are enriched in sphingolipids and cholesterol and are defined by their sensitivity to cholesterol-depletion such as by nystatin-treatment [153, 172, 98]. They can take on different forms and are described as 50-100nm size membrane invaginations or tunnels which are involved in membrane transport processes such as transcytosis and receptor endocytosis. Caveolin-1, now the defining member of caveolae regions, was first discovered as a protein which was tyrosine phosphorylated upon infection of cells by the Rous Sarcoma Virus [158]. Immunogold electron microscopy revealed a striking colocalization of caveolae regions with this new protein which was consequently named caveolin [158]. Overexpression of caveolin leads to the formation of new caveolae, whereas downregulation of caveolin results in loss of these membrane regions [153], highlighting its principle role in caveolae's biogenesis. The Caveolin gene family consists of three members, Caveolin-1 (the original), -2 and -3, which have different behaviour and function with respect to their effect on cellular signaling [33]. We here focus on the biology of caveolin-1, to which we will simply refer as caveolin.

Caveolin plays a directive role in the inhibition of growth signals. Caveolin is able to bind through a 20 amino acid long domain, termed the caveolin scaffolding domain, to a number signaling proteins including EGFR [33] on which it has a negative effect. For example, it was found that caveolin binding to EGFR inhibits EGFR's autophosphorylation activity *in vitro* [33]. One model of caveolae functioning in EGFR signaling is that caveolae hold receptors in an inactive state in the membrane

and that receptors migrate from caveolae to clathrin-coated regions upon stimulation [131, 192].

This notion of caveolin-containing signaling platforms termed caveosomes, which keep signaling molecules in an inactive state [33, 53] also extends to G-protein Ras or the kinase c-Src whose enzymatic activities are inhibited by binding to caveolin [165].

Cellular regulation of caveolin expression levels strongly correlates with growth inhibition [105, 62]. Cells grown to confluency as well cells deprived of growth factors upregulate caveolin expression, with lowest caveolin levels found during exponential growth phase [62]. In fact, it could also be shown that RNAi mediated inhibition of caveolin expression is sufficient to transform NIH 3T3 cells, as indicated by the loss of contact inhibition, as well as to form tumors upon injection in immunodeficient mice [62]. Further, transformation of NIH 3T3 cells by overexpression of a constitutively active mutant H-Ras(G12V) results in downregulation of Caveolin-1 transcription and protein expression [53, 105]. This downregulation is directly regulated by the Ras-p42/44 kinase cascade and can be restored by inhibition of this kinase [53]. A further link to the role of caveolin in cellular oncogenesis is the observation that MTLn3 cells, a metastatic rat mammary adenocarcinoma cell line fails to express caveolin. In these cells, EGF stimulation induces lamellipod extension and cell migration while restoring caveolin expression inhibits these processes [206].

Together, this data led to the model of EGFR endocytosis shown in Figure 1.4, according to which caveolae regions in the membrane function to retain receptors in an inactive state from which they migrate to the clathrin-regions upon stimulation.

Caveolae-mediated endocytosis

Caveolae-mediated endocytosis is defined as a clathrin-independent, but dynamin-dependent internalization pathway of membrane cargo and marked by the presence of a member of the caveolin protein family [125, 73, 148, 153] (see Figure 1.5).

The characteristics of caveolae endocytosis have been well described during cell-invasion by viruses, which hijack the pathway to enter cells. Simian Virus 40 enters cells by first associating with caveo-

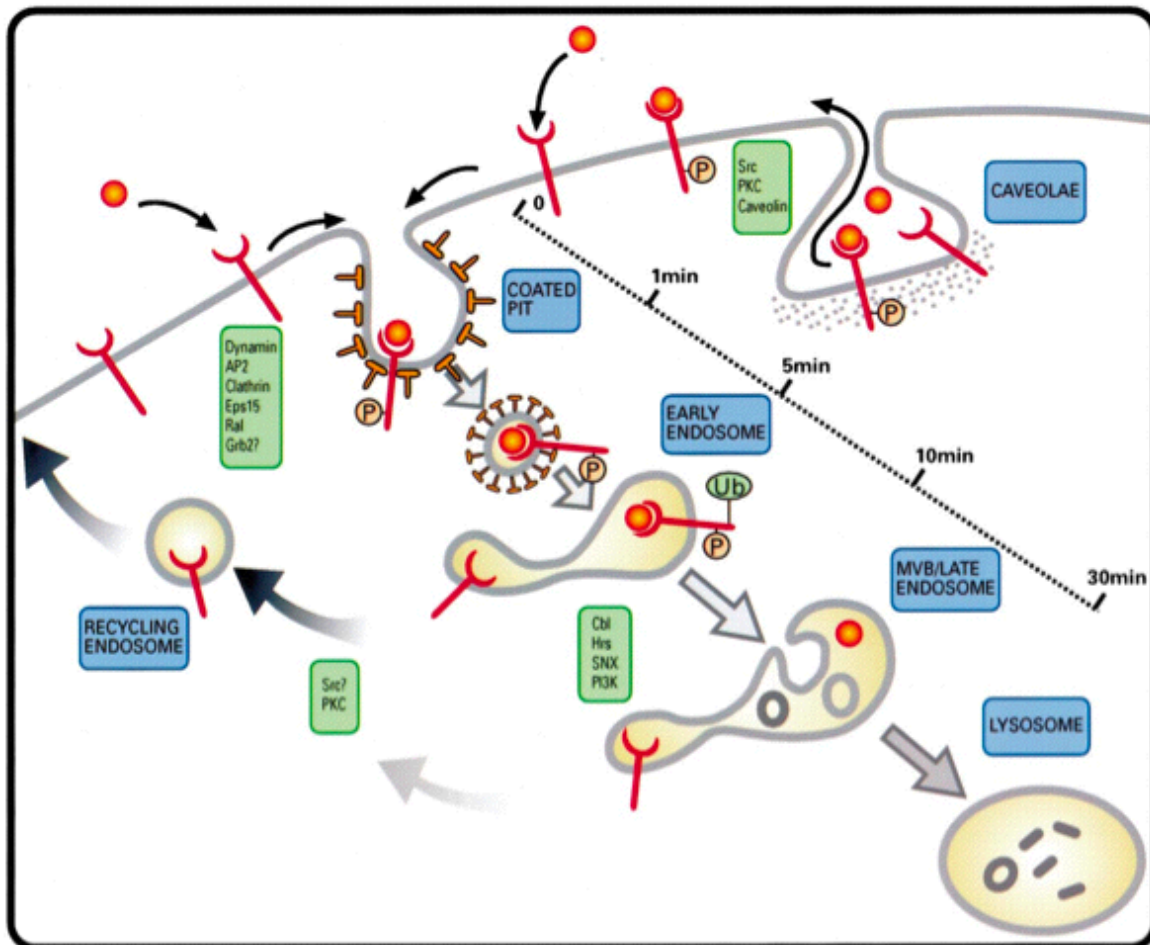


Figure 1.4: **One model of Caveolae-association and Clathrin-mediated EGFR internalization** According to one model of EGFR internalization, non-stimulated receptors locate to caveolae regions from which they translocate to clathrin-coated regions upon activation. Indicated are the timeline and major players of clathrin-mediated endocytosis and sorting into distinct endosomal populations. According to this model, caveolae do not pose an independent internalization mechanisms but function to retain receptors in an inactive state. Figure from [192]

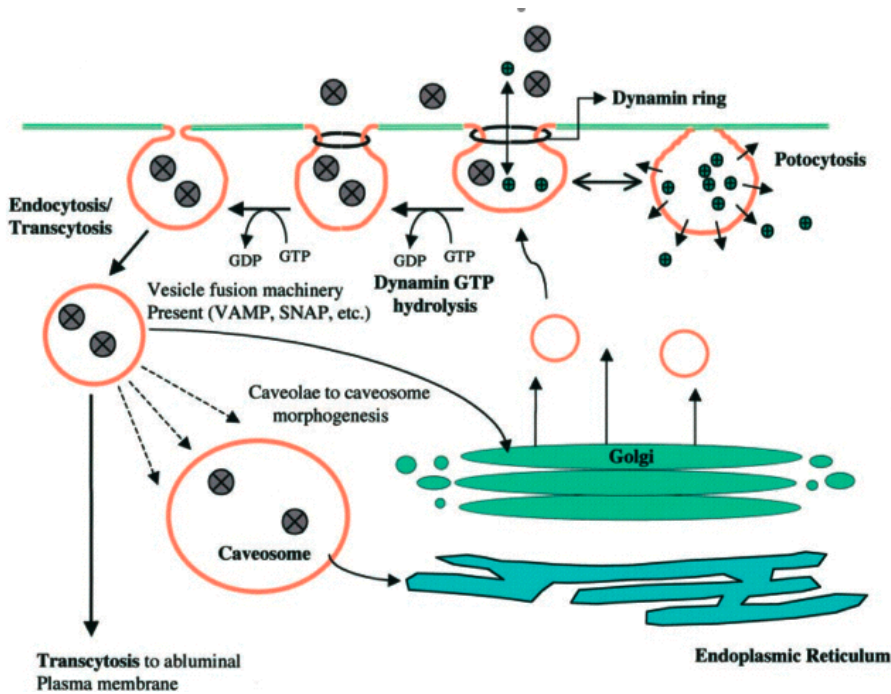


Figure 1.5: **Caveolae endocytosis** Caveolae-mediated endocytosis is a clathrin-independent, but dynamin-dependent internalization pathway of membrane cargo. Upon internalization Figure from [153]

lae at the plasma membrane and inducing the detachment of caveolin-containing vesicles which fuse with caveosomes [7, 179, 145]. This detachment and initial vesicle formation depends on a transient association of dynamin and actin rearrangement around the forming vesicle. From the caveosome, virus-containing vesicles then pinch off and are targeted to the endoplasmic reticulum (ER), whereas caveolin itself does not fuse with the ER, but travels back to the plasma membrane [145]. Pelkmans and coworkers who investigated caveolae endocytosis in a series of studies [145, 146, 149] point out that this SV40 trafficking route defines the principal characteristics of caveolae endocytosis: First, it is not constitutive as the clathrin-pathway, but is strictly ligand-triggered [185, 148]. During caveolae trafficking, the endosomal pH remains neutral [145], which is different from clathrin-mediated trafficking. Further, clathrin-mediated endocytosis does not strictly depend on a functional cytoskeleton [61, 27], whereas the temporary depolymerization of actin and assembly of actin monomers around caveolae-vesicles is important for this initial vesicle formation.

The role of caveolae-mediated endocytosis in EGFR signaling is controversially discussed. Some reports claim it to be an independent internalization mechanism which may occur in addition to clathrin-dependent endocytosis upon EGF stimulation [172] or oxidative stress [99]. This conclusion was drawn from microscopy studies where co-localization of EGFR with Caveolin was observed. In addition, some reports claim that downregulation of clathrin itself does not fully abrogate EGF internalization [87], suggesting the existence of clathrin-independent EGFR internalization, which has, however, been challenged by other reports [132, 92]. Similarly, while some groups report that nystatin treatment, which disrupts caveolae, decreases EGF uptake [172], other groups challenge this observation [98], arguing against its role as an independent internalization mechanism.

In [73] it was investigated whether clathrin- vs caveolae pathways (indicated by the markers EEA1 or caveolin, respectively) could be distinguished in their functional role for signaling, and specifically their role in signaling vs receptor degradation.

Based on a series of mutant/disruption experiments, using nystatin treatment to inhibit caveolae formation and overexpression of a dominant negative EPS15 mutant to inhibit clathrin-dependent internalization, the authors concluded that clathrin-dependent pathways are mainly responsible for proper signal distribution whereas caveolae-mediated receptor trafficking is necessary for receptor degradation (Figure ??).

In a different study the effect of different types of stimuli on EGF receptor distribution into clathrin vs caveolae-mediated pathways was investigated [99]. The authors found that caveolin-1 phosphorylation, which is required for its activation, is observed only under stimulation by reactive oxygen species and not by EGF. The study concluded that receptor internalization and signaling induced by reactive oxygen species leads primarily to a caveolin-dependent trafficking, whereas EGF stimulation directs the receptor to clathrin-pathways leading to the model shown in Figure 1.7.

Finally, another hypothesis regarding the sorting of EGFR into clathrin-dependent or -independent endocytosis was proposed in [172] where it was observed that (i) at low EGF concentrations (1.5 ng/ml) receptors primarily internalized via a clathrin-dependent pathways, whereas at high EGF

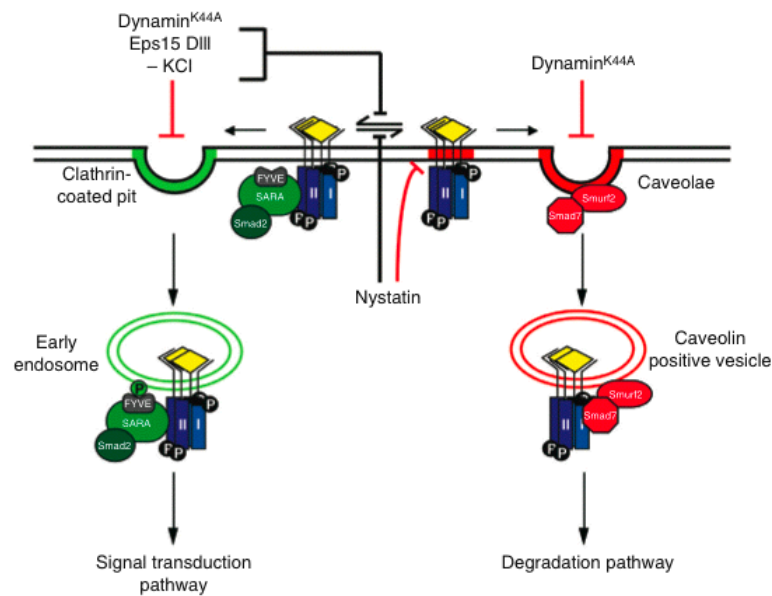


Figure 1.6: **Model of TGF- β -Receptor distribution into clathrin- vs caveolae endocytosis and effect on receptor signaling proposed in [73]** DiGuglielmo et al propose a model according to which clathrin-mediated endocytosis of the TGF- β -Receptor leads to formation of early endosomes and induction of signaling pathways. Caveolae-mediated endocytosis leads to receptor degradation. Expression of a dominant negative mutant Dynamin^{K44A} disrupts both pathways. Eps15dIII expression or nystatin treatment selectively disrupts clathrin- or caveolae-endocytosis, respectively. See text for details. Figure from [73].

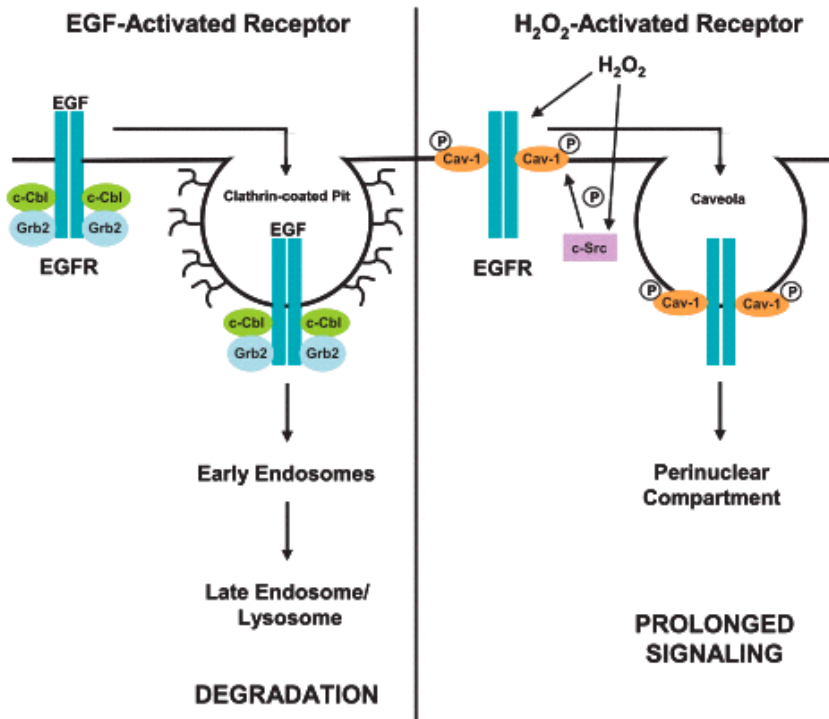


Figure 1.7: Model of EGFR distribution into clathrin- vs caveolae endocytosis depending on type of stimuli and their effect on receptor signaling Figure from [99]

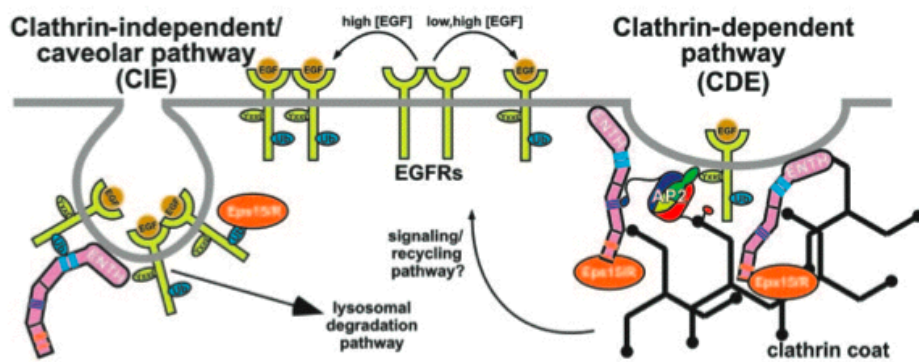


Figure 1.8: Model of EGFR distribution into clathrin- vs caveolae endocytosis depending on strength of EGF stimulation Figure from [2]

concentrations (20 ng/ml), a clathrin-independent pathway was employed and (ii) that at high EGF stimulations receptors were ubiquitinated. These results led the authors to propose that in an EGF-concentration dependent manner, the activated receptors are sorted between the pathways, with mono-Ub as a sorting signal for clathrin-independent endocytosis ([172, 2], see Figure 1.8).

The main interest of this work lies in the question of how sorting into distinct endocytosis pathways of the EGFR is regulated. We present a model addressing the question of how this sorting is achieved in Results section 4 on page 97 [166]. Considering the very different models proposed in Figures 1.6, 1.7 and 1.8, however, it is obvious, that the role of caveolae in EGFR signaling and in particular during endocytosis is still controversial. In chapter 5 we present our experimental investigations of clathrin- or caveolae-mediated EGFR endocytosis.

While the EGFR system has been subject to modeling for a long time, to our knowledge the model we presented was the first attempt to address the question of endocytic sorting theoretically. It falls into the broader class of model that describe the translation of continuous input signals into binary output. For this class of model we give a detailed introduction in the next chapter 2, page 41.

In the following, we give a brief review of models of EGFR signaling which address the internalization process itself as well as downstream signaling (reviewed in [200, 29, 101, 110]).

1.2.3 Mathematical modeling of EGFR endocytosis

In the earliest studies, models of EGFR were mainly used to describe the temporal evolution of receptor internalization [198, 140, 141, 197], which was feasible because it was experimentally possible to determine the internalized receptor fraction. Using these models, important concepts such as the saturability of the EGFR internalization pathway (in contrast to, for example, internalization of the transferrin receptor) were developed [198, 197]. Comparison of model predictions to experiments of binding affinities using Scatchard-analysis also revealed the existence of different internalization pathways which are entered with distinct affinities [197, 180, 120]. This discovery has laid a fruitful foundation for the current ongoing investigations on the mechanisms and role of endocytic sorting (see

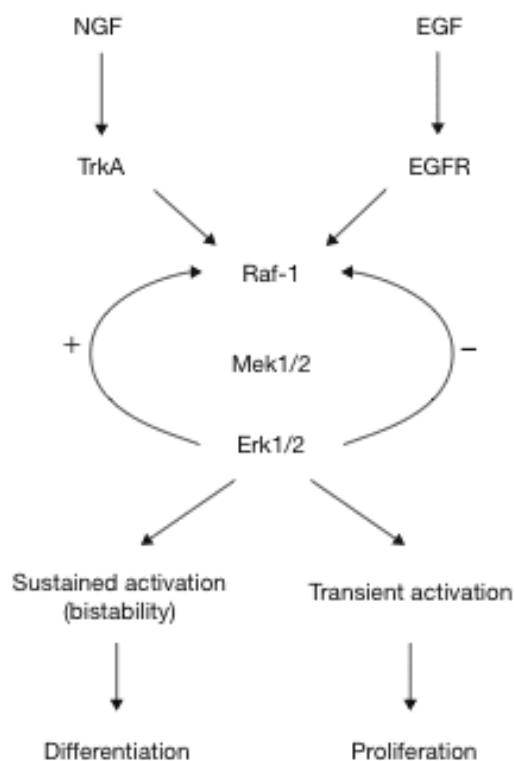


Figure 1.9: **Transient vs sustained activation of Erk and associated cellular response** EGF treatment results in transient Erk activation and proliferation, NGF treatment in sustained Erk activation and differentiation. Figure from [101]

previous section).

From these early studies on using models to describe EGFR endocytosis, interest shifted to the question how information is transmitted to cellular signaling proteins, most prominently the MAPK pathway, and in particular how signaling specificity is achieved. Since the modeling of downstream events is not the focus of this thesis, we here only briefly mention the key ideas and refer to other work for extensive reviews [101, 200].

In [163] Santos et al investigate by which means two different receptors (EGFR vs TrKA), respectively stimulated by their two cognate ligands EGF vs neuronal growth factor (NGF), can lead to different types of MAPK activation: If PC-12 cells, a model for neuronal differentiation, are treated with EGF, MAPK is phosphorylated only transiently, with a peak at ca 5 minutes, followed by a rapid

decline to basal levels. To this stimulation, cells react with proliferation, cell division. If, however, cells are treated with NGF, Erk activation shows a sustained pattern and the stimulus induces cell differentiation (see Figure 1.9). The NGF-induced sustained Erk activation had previously been proposed to result from a Protein Kinase C (PKC) mediated positive feedback from Erk (the MAPK) to Raf (the MAPKKK) [20] (Figure 1.9). Indeed, it turned out that a pharmacologic inhibitor of PKC changed the Erk-activation pattern as induced by NGF from a sustained to a transient one. Even more astounding, the phenotypic response of cell was altered as well, in that through the disruption of the feedback, cells responded to NGF treatment with proliferation instead of differentiation. This study thus showed that network topology determines cellular response.

Other models addressed the question of how EGFR dimerization partner affects signal outcome [80, 81, 82]. HER2 is a member of the EGFR family whose overexpression is frequently observed in cancer. HER2 overexpression decreases its own as well as EGFR's degradation rate [201] and heterodimerization of EGFR with HER2 enhances signaling potency [114]. Hendriks et al used ordinary differential models to compare different mechanisms of how HER2 competes with EGFR.

When work on this thesis began, evidence had appeared that the sorting of EGFR into clathrin-dependent vs -independent endocytosis was a function of strength of EGF stimulation presented to cells. This observation led us to propose a model of ultrasensitivity for the sorting process. In the following chapters we give a broad review to mathematical models of this type. Particular attention is paid to discussing the mathematical structure of the models, rather than just describing simulations.

Chapter 2

General Mathematical Models of Cellular Decision Making

2.1 Bistability in signaling : Switches between steady-states as cellular decisions

In this chapter, we introduce what is termed a 'switching mechanism': mathematical models where initial situations are sorted into two distinct outcomes. These bistable models have a particular underlying structure and serve as descriptions for cellular decision processes, in which gradually varying inputs are translated into qualitatively distinct responses. These types of models contain positive feedback circuits [40]. We begin with a simple model of positive feedback with which we illustrate the principle of switching between steady-states (section 2.1.1). We then discuss a more detailed model of a positive feedback (mutual inhibition, section 2.1.3), which can exhibit four qualitatively different types of behaviour depending on the parameter-regimes. The chapter is concluded with *in vivo* applications of the presented mechanisms.

2.1.1 A model of Positive Autoregulation

In this section we derive a basic mechanism of how a continuous input signal can be translated into two distinct outcomes. The underlying mathematical model describes a dynamical system which possesses one or two stable steady-states, depending on the strength of the input signal. The arising or disruption of a steady-state upon some parameter variation is called bifurcation [76].

This example model originally arose in the context of morphogens directed embryonic patterning [115]. I introduce the model in its original context and then proceed to point out applications in the current literature of cellular signaling.

Morphogens are diffusible proteins that are secreted from a restricted source and provide spatial information via a concentration gradient along a matrix of cells [94, 44, 127]. The interpretation of a continuous morphogen gradient to lead to qualitatively different behaviour is a classic example of mathematical modeling of cellular all-or-nothing decisions [46, 127].

Consider a matrix of cells. Originally, the cells are identical. During the process of differentiation two different 'types' of cells are being established, for example pigmented vs unpigmented cells (see Figure ??). We will consider a simple mathematical model of this process.

It is thinkable that the nature of the differentiation into different cell types is manifested in distinct abundance levels of some protein G that is produced upon the cell's encounter with a signal S, which in our case plays the role of the morphogen. We assume that S stimulates the production of G (either by acting on the DNA or by enhancing protein production).

Further, we will use the model to analyze the consequences of G stimulating its own production (positive feedback). Finally, we will take into account the degradation of G. The level of G could then be described by the equation:

$$\frac{dg}{dt} = f(g) = k_1 s - k_2 g + \frac{K g^2}{k_n + g^2} \quad (2.1.1)$$

The last term reflects the positive feedback G is assumed to exert on itself: it is sigmoid in shape,

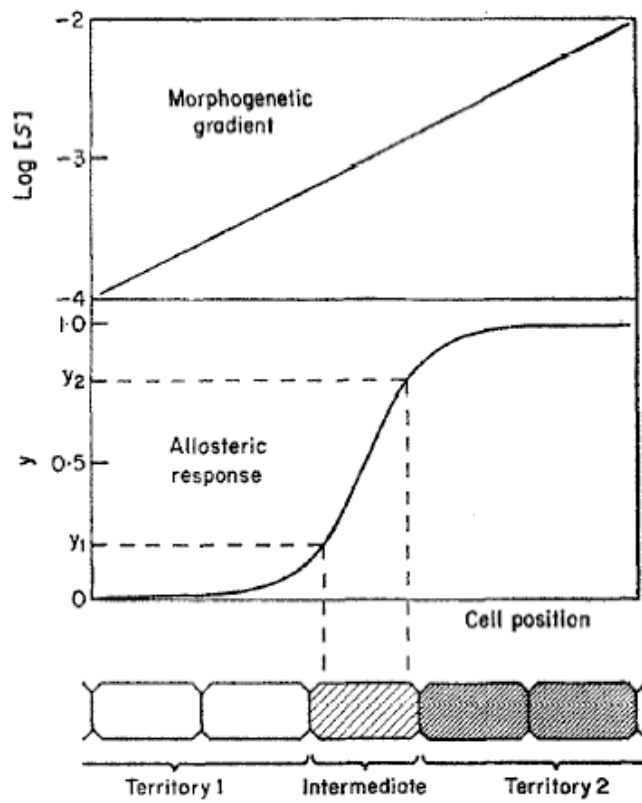


Figure 2.1:

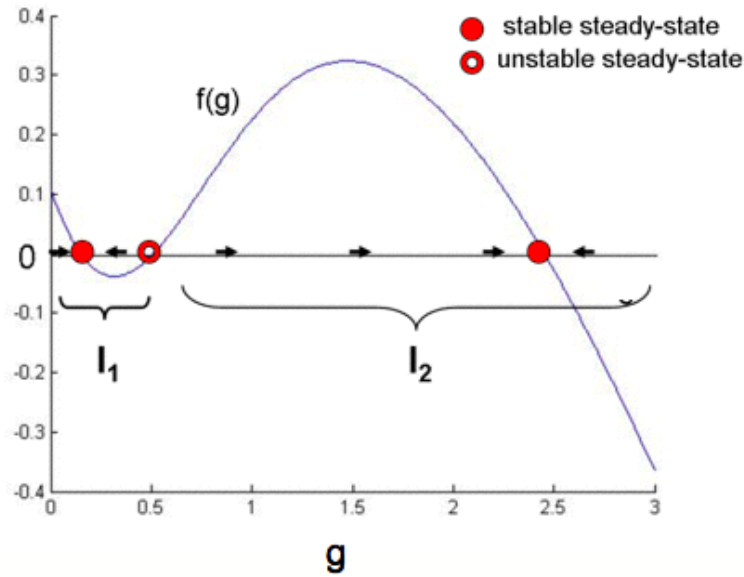


Figure 2.2:

its effect on the rate of change being very small for small levels of G and reaching the threshold of K for high levels of G . In section 2.2.1 we derive how this term arises from the assumption of multiple binding events. Note that although this model is motivated from an example of transcriptional control, the form of the equation very generally describes the effect of a protein on itself.

To understand the implications of 2.1.1, we study the graph of $f(g) = dg/dt$ vs g , i.e. the rate of change as a function of the level of G . First, observe that whenever the graph intersects the g -axis, i.e. $f(g) = 0$ the rate of change is zero, that is, the system has reached a steady-state.

For our purpose, it is sufficient to distinguish two types of steady-states: if the graph $f(g)$ intersects the g -axis at a point \bar{g} while it is decreasing ($f'(\bar{g}) < 0$), the steady-state is **stable**, meaning that the system will come back to this steady-state for small perturbations. If $f(g)$ is increasing at the intersection \bar{g} ($f'(\bar{g}) > 0$) the steady-state is **unstable**. This follows from the fact that g is increasing with positive $f(g)$ and decreasing if $f(g)$ is negative (for proofs on the stability of steady-states see [46, 76]). Figure 2.2 illustrates this, with black arrows indicating whether g in- or decreases. It can be seen that the first and third steady-states are stable steady-states (solid circle), the second one (open

circle) is unstable.

We will study the form of the graph $f(g)$ vs g for different signal strengths s and derive how small differences in s cause the system to tend towards the first vs the third stable steady-state.

First note that independently of the values for the parameters k_1 , k_2 , K and k_n , $f(g = 0) = k_1s$, since all other terms are zero. This means that cells which possess no G at all, will initially respond with a production rate of k_1s .

Secondly, for very high levels of g , the degradative term in 2.1.1 ($-k_2g$) predominates and the rate of change is negative: $\lim_{t \rightarrow \infty} f(g) = -\infty$. Thus, the graph of dg/dt vs g will always have a *qualitative* behaviour as shown in figure 2.2. The *number and positions of intersections with the g -axis*, the steady-states, however, do depend on the precise parameter values of k_1 , k_2 , K and k_n , as well as on the strength of signal S .

Figure 2.3 illustrates how this bears an explanation for how small differences in level of S may account for drastic differences in level of G .

In Figure 2.3A we see different graphs of $f(g)$ vs g for gradually increasing signal strength S (from left to right in both rows, with lowest s in the upper left and highest s in the lower right panel). As noted before, $f(0) = k_1s$ and thus the strength of S determines where the graph starts (indicated by a black bar in the upper left panel in Figure 2.3A). For S lower than a critical threshold (whose exact value depends on the other parameters in equation (2.1.1)), the graph intersects the g -axis three times, resembling the graph in Figure 2.2. This is the case in the upper row of Figure 2.3A.

What does this mean for the steady-state value of G ?

If we consider a cellular situation in which, prior to encounter with the stimulus S , cells possess no or very little of the protein G ($g(\text{time}=0) \approx 0$), as production of G starts and g increases, it will hit the first stable steady-state (cf Figure 2.2). This means that for signal strength s lower than the critical value S^* , the production of G will reach a steady-state precisely at that low value of g corresponding to the first intersection of the g -axis.

If on the other hand, the signal strength s is higher than S^* (lower row in Figure 2.3A), the graph

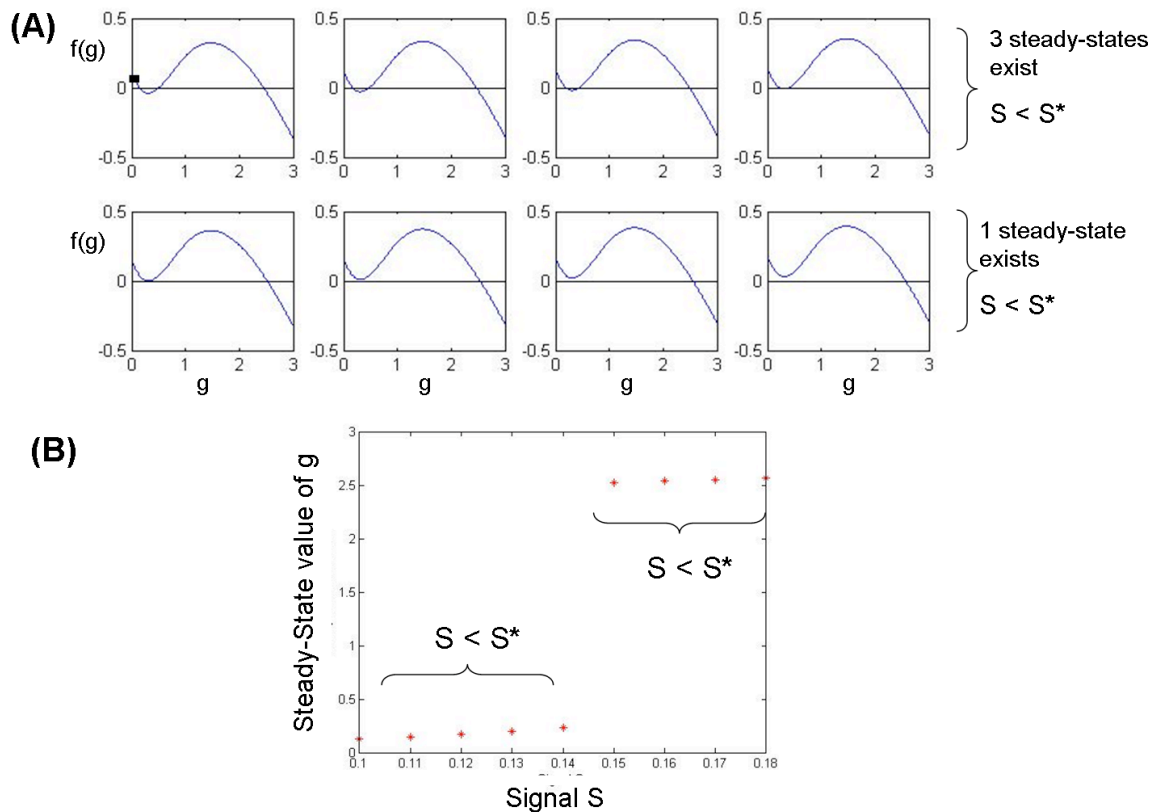


Figure 2.3:

$f(g)$ will intersect the g -axis only once, the system exhibits only one steady-state. This means that production of g will not come to a rest before it reaches this second, 'higher' steady-state.

In Figure 2.3B the steady-state value of G is plotted against signal S , for the same parameters as in A. We see that when S passes a threshold the steady-state level of G 'switches' from low to high.

A different interpretation of the model

We saw how varying a parameter of equation (2.1.1), in our case the signal s , can lead to the arisal of a new steady-state: a bifurcation occurred. For signal strengths for which $f(g)$ intersects the g -axis three times, G remains at a low level, assuming that initially, as the cells start to encounter signal S , protein G is absent in the cells, i.e. $g(0) = 0$.

The same model, however, can be interpreted as a switching mechanism without a bifurcation but

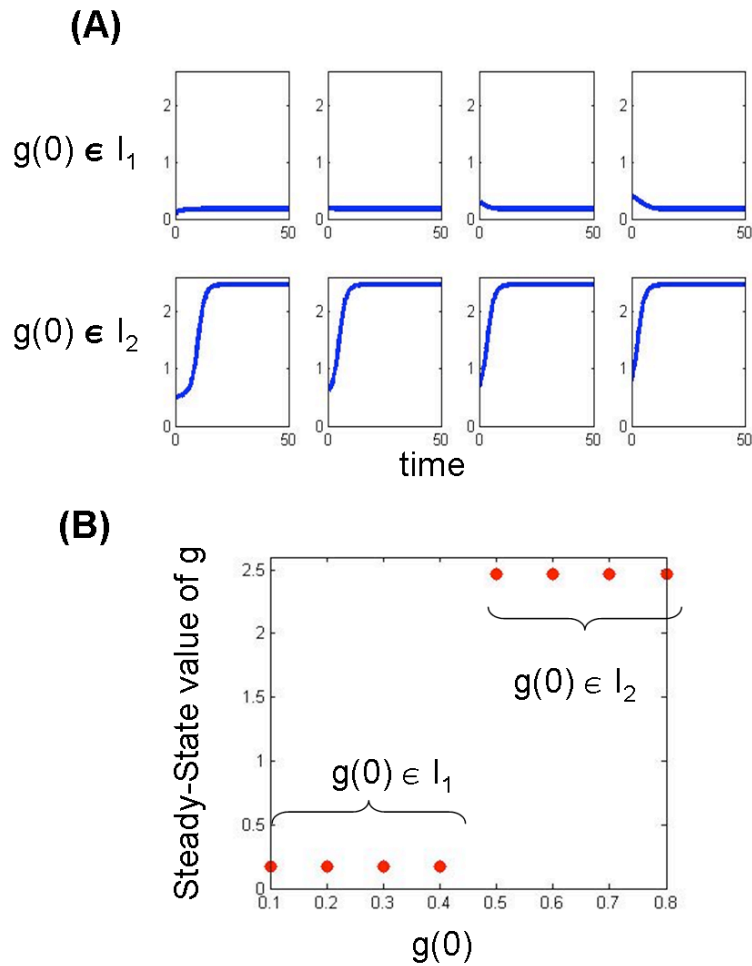


Figure 2.4: Different steady-states are reached depending on initial value of G , $g(0)$. (A): temporal evolution of g for $g(0) \in I_1$ (upper row) or $g(0) \in I_2$ (lower row). (B) Steady-state values of g plotted against $g(0)$ for same values as in (A).

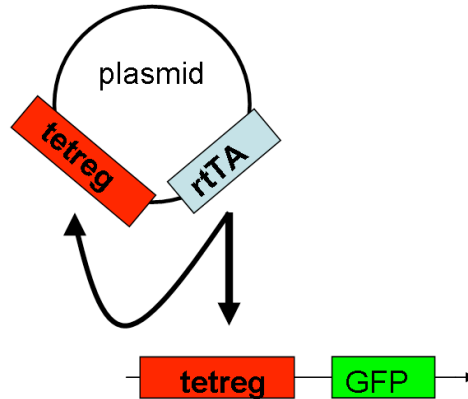


Figure 2.5: Architecture of an autocatalytic positive feedback of the rtTA system. rtTA binds and activates its own promoter as well as that of a reporter GFP gene (tetreg).

by means of *different initial values* of g .

If we assume that the signal strength is such that the graph $f(g)$ intersects the g -axis three times, then which one of the two stable steady-states will be reached depends on the initial value of g . With each steady-state a so called basin of attraction is associated [1] which denotes the subspace for which the motion of the system tends towards this steady-state. In our case, these are the intervals I_1 and I_2 , as shown in Figure 2.2.

As explained before and indicated by the black arrows, g increases if $f(g)$ is positive and decreases if $f(g)$ is negative. It follows that if $g(0)$ lies in the interval I_1 g will approach the lower steady-state, whereas if $g(0)$ lies in I_2 it will approach the higher steady-state. This is shown in Figure 2.4.

We have thus derived two different mechanisms by which the model (2.1.1) could explain a switch-like behaviour: the first is by variation of the signal strength and the occurrence of a bifurcation (Figure 2.3). The second mechanism gives rise to a switch for constant signal strength, but for cells possessing different initial values of the protein under consideration (Figure 2.4).

2.1.2 Applications of the model

Becksei and Serrano [13] implemented a transcriptional positive feedback mechanism in *Saccharomyces cerevisiae* using a plasmid-encoded tetracycline-responsive transactivator (rtTA). In the presence of

inducer doxycycline rtTA is activated and binds DNA containing appropriate binding sites. Figure 2.5 illustrates the architecture of an autocatalytic positive feedback of the rtTA system used in [13]. GFP expression was used to assess activity. Indeed, upon induction, the population of cells split into two distinct subpopulations with cells either fully expressing GFP or not at all (cf. Figures 3,4A in [13]) indicating the existence of two distinct steady-states as predicted by equation (2.1.1)

An important property of bistable systems is a memory-effect: By reaching a new stable state upon encounter of a signal, this state is retained even if the stimulus is taken away.

In an interesting study by Santos *et al* [164] positive feedback was shown to result in sustained activation of Erk upon Neuronal Growth Factor (NGF)-stimulation in PC-12 cells. Very interestingly, the existence of a positive feedback (implemented in the MAPK cascade) and bistability is dependent on the type of growth factor used to stimulate the cells: Epidermal Growth Factor (EGF) stimulation does not invoke a positive feedback. This difference between the two ligands is manifested in the different nature of Erk-activation: NGF-stimulation leads to sustained Erk-activation even after addition of NGF-neutralizing antibodies (cf. Figure 3 [164]) and a switch-like response of Erk on the population level (cf. Figure 2 in [164]). This observation are in accord with two steady-states caused by the existence of the positive feedback. In contrast, EGF stimulation activates Erk in a graded manner and loses its effect upon the addition of EGF-neutralizing antibodies. The existence of a positive feedback upon NGF- but no feedback upon EGF-stimulation was also postulated by a reverse-engineering approach called Modular Response Analysis [102, 164].

In [202] a study was presented in which the role of positive feedback in cellular differentiation of *Xenopus* oocytes was investigated. Immature oocytes remain in a 'G2-like phase' of the cell cycle. Upon stimulation with steroids, they undergo germinal vesicles breakdown (GVDB), complete meiosis I and then again are arrested in meiosis II [202, 58]. Mediators of this process are the kinases Mos, Mek, p42 MAPK and the cell-division cycle kinase Cdc2 (see Figure 2.6).

The objective of the study was to find out whether the positive feedback operating between the kinases MAPK and Mos was the critical element in allowing the cells to irreversibly commit to differ-

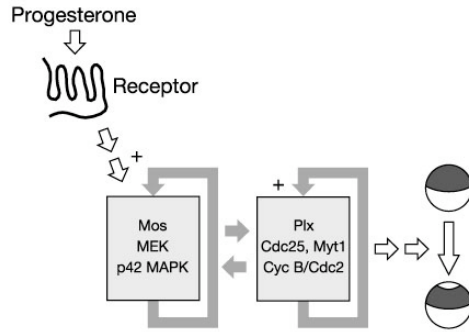


Figure 2.6: Upon stimulation with steroids such as Progesterone, oocytes undergo maturation. This is mediated by the kinases Mos, Mek and p42MAPK. A positive feedback from MAPK results in activation and accumulation of Mos [69]. Figure from [202]

entiation once a threshold of stimulation is exceeded: even if the stimulus (Progesterone) is removed from the cells, the key kinases p42MAPK and Cdc2 remain phosphorylated and differentiation is completed (cf. Figure 2 in [202]).

To find out, whether the positive feedback from MAPK to Mos was responsible for this memory-effect, the authors blocked protein synthesis using cycloheximide. It is claimed that protein synthesis is not essential for differentiation [204], but that it is necessary for the positive feedback from MAPK to Mos [69, 160].

Both cycloheximide, as well as the introduction of a Mos antisense oligonucleotide (inhibiting the synthesis of Mos) abrogated the ability of the system to remain in the activated state: after the stimulus progesterone was removed by washing, both p42MAPK- and Cdc2-activation were abolished (cf. Figure 2 in [202]).

The authors proposed equation (2.1.1) as a model for their observation (cf. Box 1 in [202]). Indeed, similar to how the variation of signal strength s in Figure 2.3 leads to disruption of a steady-state, so does variation of K , the strength of the feedback, allowing for the conclusion that a sufficiently positive feedback is necessary to obtain bistability.

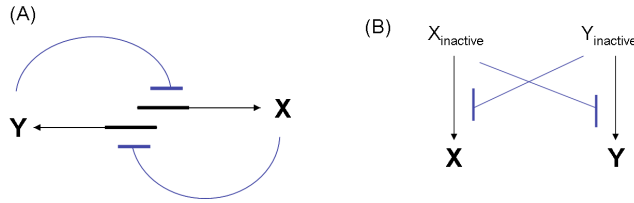


Figure 2.7: Mutual inhibition of two molecules on the gene (A) or protein level (B)

2.1.3 Mutual Repression can lead to Bistability

In the previous section we saw that positive feedback can lead to bistability. We saw that for different values of parameters such as signal strength, or the magnitude of the effect of the feedback, equation (2.1.1) exhibited one or three steady-states. In this section we'll see how negative interaction of two molecules can give rise to a bistable system. This motif of *mutual inhibition* is in fact a positive feedback circuit too and can be viewed as a more detailed description of the processes giving rise to the dynamics of the earlier example. We start out by explaining the mathematical basis of this phenomenon and will then discuss examples in different signaling contexts, where mutual repression has been identified as a plausible mechanism to underlie the cellular decision process.

Consider two molecules X and Y which directly or indirectly repress each other. 'Repress' is a rather vague expression and indeed could include different scenarios. For example, X and Y could be transcription factors which bind and block each other's promoters, thus preventing transcription (Figure 2.7A). This negative effect does not need to be direct: protein X for example could be involved in the activation of a repressor Z of Y's promoter, and vice versa. We will introduce an example of a switch on the gene level in section 2.1.3.

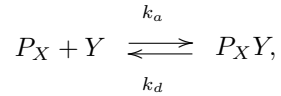
On the protein level, the inhibition could be envisioned as, for example, part of a signaling cascade where X and Y stand for the *activated form* of two proteins and where the repression takes place at the level of the conversion from precursor to active state (Figure 2.7B). An example of this is discussed in section 2.1.3.

Generally, the interaction between X and Y is described by the system of equations

$$\begin{aligned}\frac{dx}{dt} &= f(y) - \mu_1 x \\ \frac{dy}{dt} &= g(x) - \mu_2 y\end{aligned}\tag{2.1.2}$$

where the first term in each equation describes the effect of the opposing molecule and the last part describes degradation; μ_1 and μ_2 are positive constants. Since we consider mutual inhibition, f and g are decreasing functions.

What could their specific form be? As described, we want to explore the case that Y represses the formation of (the active form of) X . To avoid confusion, we will derive $f(y)$; $g(x)$ has the analogous form. Assume that Y directly binds to the promoter region of gene X (or the inactive precursor of protein X). The binding kinetics could then be described as



where P_X is the fraction of unblocked precursor/promoter of X , which we expect our production function $f(y)$ to be proportional to. We thus need to derive its specific form.

In steady-state we have

$$\frac{k_d}{k_a} \equiv K_d = \frac{Y \cdot P_X}{P_X Y}$$

and hence

$$P_X = \frac{K_d \cdot P_X Y}{Y}\tag{2.1.3}$$

The conservation equation of P_X , $P_{X_{tot}} = P_X + P_X Y$, which we may set equal to 1, tells us that $P_X Y = 1 - P_X$. Equation 2.1.4 becomes

$$\begin{aligned}
P_X &= \frac{K_d \cdot (1 - P_X)}{Y} \\
P_X \cdot Y &= K_d \cdot (1 - P_X) \\
P_X(Y + K_d) &= K_d \\
P_X &= \frac{K_d}{Y + K_d}
\end{aligned} \tag{2.1.4}$$

which, measuring the amount of y in units of K_d and setting $y = \frac{Y}{K_d}$ we may write as

$$P_X = \frac{1}{1 + y}.$$

The production of X is proportional to this fraction of unblocked P_X and we thus derived

$$f(y) = k_1 \frac{1}{1 + y}$$

for some positive k_1 .

Performing the same for $g(x)$, equations (2.1.2) become

$$\begin{aligned}
\frac{dx}{dt} &= \frac{k_1}{1 + y} - \mu_1 x \\
\frac{dy}{dt} &= \frac{k_2}{1 + x} - \mu_2 y
\end{aligned} \tag{2.1.5}$$

This system describes two interacting genes mutually repressing each other by binding each other's promoter/precursor on a single binding site.

Mutual inhibition is a positive feedback loop: X (Y) represses its own repressor. Intuitively, we can see that the system can potentially have two different steady states: Either X is synthesized and

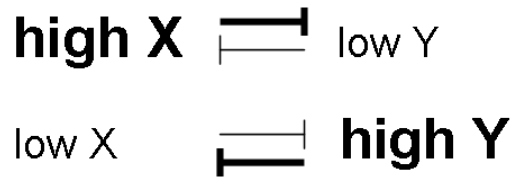


Figure 2.8:

represses the formation of Y, or vice versa (Figure 2.8).

Nevertheless, we will derive that with the dynamics of equations (2.1.5) it is impossible to obtain these two steady-states. We can show that

- (i) independently of the parameters repression strengths (k_i) or degradation rate (μ_i), the system of equations (2.1.5) is monostable.
- (ii) in order to obtain bistability, cooperative reaction kinetics of the binding of repressor to its target are needed.
- (iii) by extending equations (2.1.5) for cooperativity, we obtain a system which can have four distinct types of steady-state behaviour. Varying the strength of the repressor-target interactions or degradation rates, allows for transition between these four types.

To show that simple binding kinetics as in (2.1.5) describe a monostable system, we follow the method by Cherry and Adler [28].

Steady-states are the points (x,y) where both equations are equal to zero, i.e. $\frac{dx}{dt} = \frac{dy}{dt} = 0$. Each of these equations describes a curve in the (x,y) -plane, which are called the *nullclines* of the system. Steady-states are intersections of these two curves, since in these both nullcline equations are fulfilled.

The nullclines are given by

$$\begin{aligned}
 x &= \bar{f}(y) = \frac{k_1}{\mu_1} \left(\frac{1}{1+y} \right) \\
 y &= \bar{g}(x) = \frac{k_2}{\mu_2} \left(\frac{1}{1+x} \right)
 \end{aligned}$$

We can identify intersections of these curves by composing the two functions

$$\begin{aligned}
 x &= \bar{f}(\bar{g}(x)) \\
 &= \frac{k_1}{\mu_1} \left(\frac{1}{1 + \bar{g}(x)} \right) \\
 &= \frac{k_1}{\mu_1} \left(\frac{1}{1 + (k_2/\mu_2)(1/1 + x)} \right) \\
 &= \frac{k_1}{\mu_1} \left(\frac{1 + x}{1 + (k_2/\mu_2) + x} \right) := h(x)
 \end{aligned} \tag{2.1.6}$$

The question of multiple intersections of the nullclines can now be restated to whether there exists more than one value for x for which $h(x) = x$. A simple argument tells us that this is not possible. Consider the left- and right-hand-sides of the last equation as two curves in the plane. The left-hand-side, x , is simply the first diagonal. We ask whether the right-hand-side, $h(x)$, can cross this diagonal more than once. We find the first derivative to be

$$h'(x) = \frac{k_1}{\mu_1} \left(\frac{k_2/\mu_2}{(1 + k_2/\mu_2 + x)^2} \right) \neq 0 \quad \forall x \tag{2.1.7}$$

Hence, $h(x)$ has no maxima or minima and cannot cross the diagonal more than once. Thus, a model of a single binding site, following simple mass-action kinetics can not account for a switching mechanism.

What do we obtain if we extend equations (2.1.5) for cooperativity in repressor-binding? In section 2.2.1 on page 69 we demonstrate that in cooperative reactions equations take on the form

$$\begin{aligned}
 \frac{dx}{dt} &= \frac{k_1}{1 + y^n} - \mu_1 x \\
 \frac{dy}{dt} &= \frac{k_2}{1 + x^n} - \mu_2 y,
 \end{aligned} \tag{2.1.8}$$

with $n > 1$.

In [28] it is proved that the nullclines of this system can cross three times for certain regions of the parameters k_i and μ_i , i.e. three steady-states can arise for values of $n > 1$.

The dynamical behaviour of a system described by equations (2.1.8) is exemplified in Figure 2.9. Depending on the relative strengths of the two components degradation and mutual inhibition, four different scenarios can occur [28, 46].

- Case 1: X dominates over Y, independently of the initial values.
- Case 2: Y dominates over X, independently of the initial values.
- Case 3: X dominates over Y **or** Y over X, depending on the initial values.
- Case 4: X and Y are both being expressed and remain at a fixed ratio.

Figure 2.9 illustrates these scenarios. Depicted is the direction field of mutual inhibition (equations 2.1.8) for different parameter combinations. The direction field shows for which starting points which steady-states will be reached, i.e. whether X or Y will dominate. Black circles indicate initial values (X_0, Y_0) and red circles are stable (solid) or unstable (open) steady-states. In all subgraphs, the initial points are equal, yet the outcome is different: Depending on the parameters k_i and μ_i the system shows one or three steady-states.

(A) and (B): Parameters are chosen such that the nullclines of equations (2.1.8) cross only once and hence only one steady-state exists ($k_1 = 0.5$ (A) or 3 (B), $k_2 = 3$ (A) or 0.5 (B), $\mu_1 = 1, \mu_2 = 1$). Independently of the initial values this steady-state will be reached and the system can not show switch-like behaviour. (A) corresponds to Case 1, (B) to Case 2. In (C) Parameters are chosen such that nullclines cross three times ($k_1 = 1, k_2 = 1, \mu_1 = 0.1, \mu_2 = 0.1$), two stable steady-states exist. One lies on the y-axis, representing high Y-activity and low X, the other the opposite situation. Which one of these two stable states is reached depends on the initial values: if $X_0 > Y_0$ X will predominate, and vice versa (cf. Figure 2.10). In (D) coexistence of X and Y is reached: only one steady-state exists and X and Y remain at a fixed ratio.

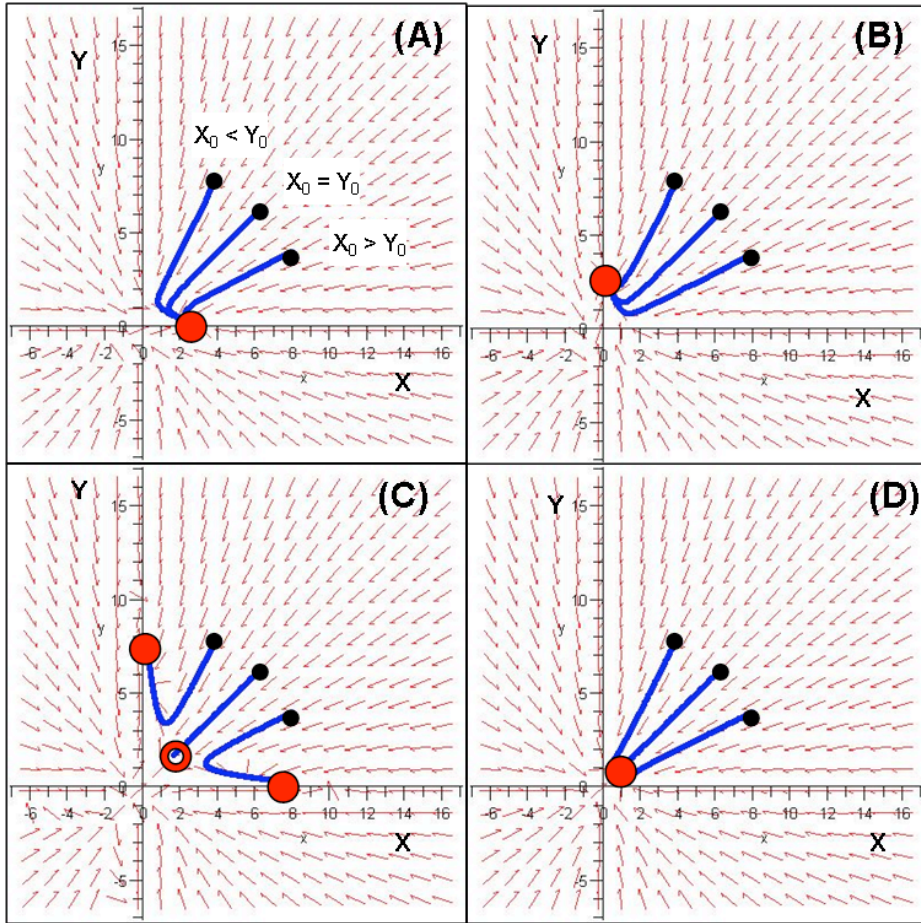


Figure 2.9: Illustration of the four cases that can arise from equations (2.1.8). See text for explanation and parameter values used.

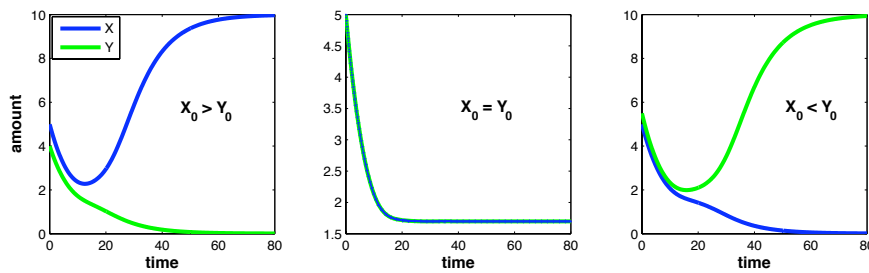


Figure 2.10: Simulation of the mutual inhibition mechanism (equation 2.1.8). Small differences in the initial values (X_0, Y_0) are sorted by the system into two distinct steady-states, with high or low value of one of the variables. (Parameters used are $k_i = 1, \mu_i = 0.1, n = 3, i = 1, 2$)

Similar to the one-dimensional example in the previous section, we also see how bistability can explain the translation from a graded signal into an all-or-nothing response, see Figure 2.10, where the temporal evolution of X and Y is shown for three different initial situations. The parameter setting is such that the behaviour of the system corresponds to Figure 2.9C and two stable steady-states exist. In all three panels in Figure 2.10 X_0 is the same, but Y_0 is varied from a value smaller than (left), equal to (middle) or larger than X_0 (right panel). We see that this slight change in initial values is sorted into different steady-states.

Mutual Inhibition in cellular signaling

In this section, we will discuss two examples of where the model of mutual inhibition has been identified as a plausible mechanism to guide a cellular decision process. The first example is from the field of synthetic biology: a toggle switch was designed using the very architecture of repressor-repressor system just discussed [63].

The next example stems from MAPK signaling. Here the switch is used by the cell to reach signaling specificity [126].

Implementation of a Genetic Switch in E.Coli

One of the first studies to show that the mechanism proposed by the abstract set of equations just discussed can actually work *in vivo* was presented in [63]. Gardner *et al* constructed a switching mechanism of two genes that implements the architecture shown in Figure 2.8B. As mentioned, the parameters in equations 2.1.8 are important for the existence of bistability. To account for this, Gardner *et al* used different plasmids, with different strengths of promoter repression as well as ribosome binding sites, to identify combinations for which bistability could be observed. The plasmids used in the study contained multiple binding sites for their respective repressors. The repressors were proteins that formed dimers or tetramers, giving rise to cooperative effects (personal communication with T.Gardner).

The basic form of mutual inhibition are two promoters, each controlling the expression of a re-

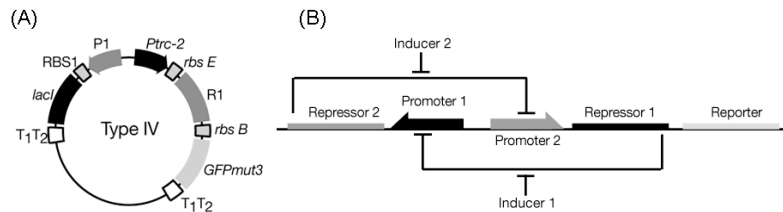


Figure 2.11: Design of Toggle Plasmid. Promoter 2 (*Ptrc-2*) controls Repressor 1 (+ GFP); Promoter 1 controls *lacI* (Repressor 2); IPTG (Inducer 2) blocks *lacI*-repression of Promoter 2; Temperature shift (Inducer 2) blocks repression of Promoter 1. Modified from [63]

pressor of the opposing promoter. In addition, two inducers are needed which specifically block the interaction of one repressor:promoter pair - inducers can then be added to the reaction to shift the system between the two steady-states. Finally, in order to report which of the two promoters is currently active, one needs a reporter gene, i.e. GFP, under the control of one of the promoters (see Figure 2.11).

In the current study, the authors used two types of plasmids: pTAK and pIKE plasmids, which differ in the identity of one of the two promoters used, but not in the dynamic principles of the experiment. For the sake of shortness, I will only describe pTAK plasmids.

The design of the switching plasmid is shown in Figure 2.11. IPTG (Inducer 1) can be used to block repression of the *Ptrc-2* Promoter (Promoter 2 in Figure 2.8B) by *lacI* (Repressor 2). A pulse of IPTG thus can be used to induce transcription of the Promoter 2, which also controls the expression of GFP to report promoter activity. The second part of the inhibition loop (Promoter 1, Repressor 1 in Figure 2.8B) is formed by the P_{Ls1con} -promoter (Promoter 1) in conjunction with a temperature-sensitive λ repressor (Repressor 1): shift to $42^\circ C$ inactivates Repressor 1, allowing transcription of *lacI* and hence repression of GFP expression.

Thus, IPTG switches the system into GFP-expression, whereas a temperature-shift induces transcription of *lacI*, resulting in a repression of GFP-expression.

With this design, knowing of the cooperative nature of the promoter binding events, we thus recognize the architecture described in equations 2.1.8.

How does it work in practice?

As mentioned before, one property of bistability is that once a steady-state is reached, the inducer does not need to remain present to maintain that state. Consequently, to test whether the synthetic construction of mutual inhibition did indeed lead to bistability, the authors showed that transient induction with IPTG (temperature shift) turned on (off) GFP-expression, which remained high (low) even in absence of inducer (cf. Figure [63]).

Decision Making in Signaling

The problem of cellular decision making arises in the context of overlapping signaling pathways: if pathways which transmit signals of different nature, each with their own specific response, share common components, we need to ask how signaling specificity is maintained [107, 11]. This problem has been intensively studied in the yeast *Saccharomyces Cerevisiae*, which has three MAPK pathways, the pathways for invasive growth, pheromone/mating signaling and osmotic shock response. What has caused many speculations is the fact that these pathways function via common components: For example, between the pathways for pheromone signaling and osmotic shock, the MAPKKK Ste11 is shared [169, 23], see Figure 2.12A.

This brings up the interesting question, how stimulation by pheromones exclusively result in activation of the mating pathway, whereas stimulation with sorbitol activates osmotic shock response [169, 126]. Further, when presented to both stimuli simultaneously, individual (wildtype) cells exclusively show one of the two responses, never a mix (cf. Figure 3 in [126]). Figure 2.12B illustrates how the mutual exclusiveness of the two pathways is demonstrated experimentally: yeast cells expressing GFP under a Fus3- and RFP under a Hog1-controlled promoter, express only one of these reporter genes upon costimulation with both Sorbitol and pheromone. The fraction of cells of the population choosing one or the other response, however, varies with the strengths of the respective signals. This means that each cell undergoes a decision process for one of the pathways.

Indeed, the authors showed that the decision process is history dependent (hysteresis), for which

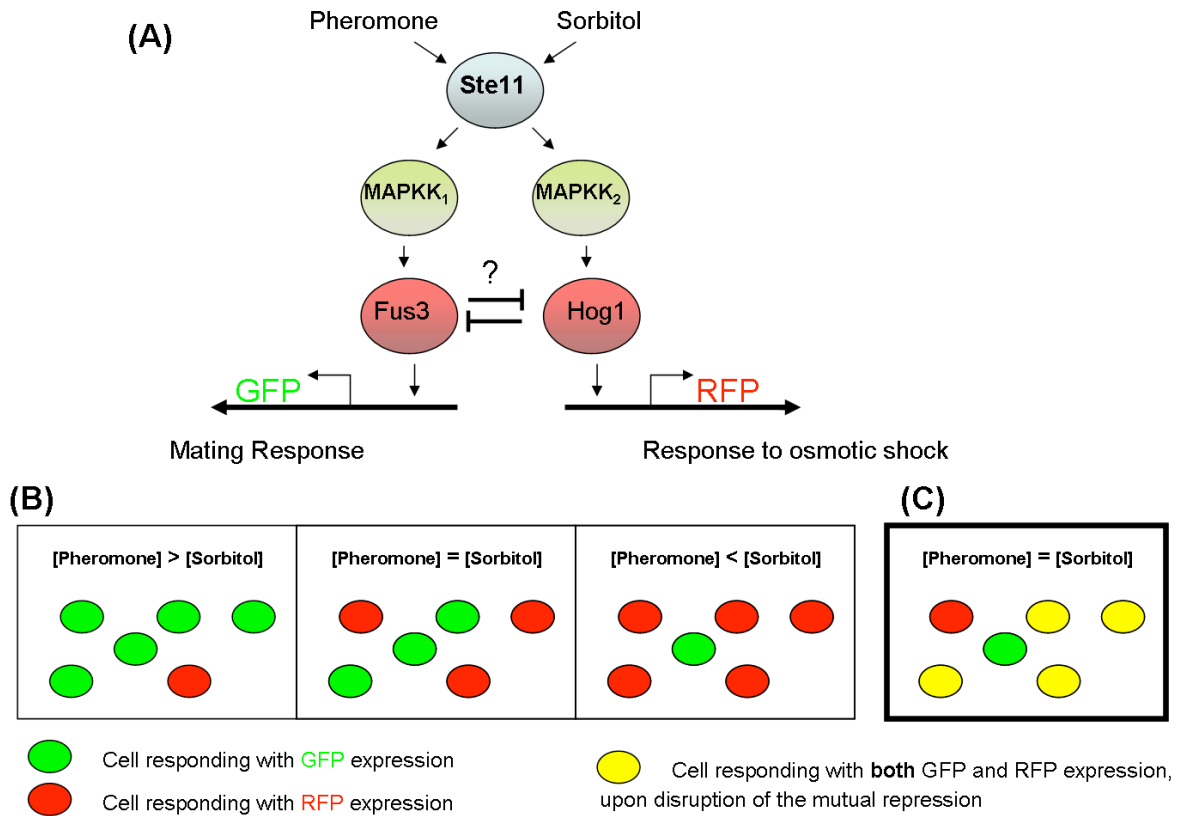


Figure 2.12: (A) In yeast, the two MAPK modules responsible for pheromone signaling or osmotic shock share the first element of the cascade, Ste11. One possibility to ensure signaling specificity is mutual inhibition of the target MAPKs Fus3 and Hog1. (B) and (C) schematic depiction of cellular response upon costimulation in wildtype (B) or mutant (C) cells, see main text.

bistability is a prerequisite (cf. Figure 4 in [126]). They further provided strong evidence that mutual inhibition of Fus3 and Hog1 is the mechanism behind this observed bistability, by employing mutant yeast cells in which the postulated mutual inhibition of the respective MAPK-elements of the two pathways (cf. Figure 2.12) was disrupted. More specifically, they showed that

- Δ hog1 cells, i.e. cells with the hog1 gene deleted, respond with mating pathway activation upon sorbitol signaling (cf. [126] Fig.5a). This indicates that the inhibition by Hog1 is needed to repress mating pathway response upon Sorbitol stimulation.
- Δ fus3 cells, i.e. cells with the fus3 gene deleted, respond with osmotic shock pathway activation upon pheromone stimulation (cf. [126] Fig.5b). This indicates that the inhibition by Fus3 is needed to repress osmotic shock response upon pheromone stimulation.
- cells expressing a Hog1-repression-resistant mutant of Fus3 (Fus3^{D63S}) respond with a mixed activation of both the pheromone as well as the osmotic shock response upon co-stimulation with Sorbitol and Pheromone (cf. [126] Fig.5, Figure 2.12C)

Thus, the model of mutual inhibition of the two opposing MAPKs and the bistability of the system is a very plausible model to explain the exclusiveness of the two responses in yeast cells.

2.1.4 Numerical description of bistability - Models of Apoptosis

The study of Apoptosis, the phenomenon of how apoptotic stimuli are incorporated into a signaling network and are translated into a cellular program to kill the cell in a 'programmed fashion', has inspired the development biologically plausible models of cellular decision making, a selected few of which we want to discuss here [112, 10, 48, 194]. These models are also representative examples of how a biological mechanism can be inferred from equations which, unlike the examples presented above, are not amenable to an analytic treatment but instead are analyzed by computational means. In sight of the limitedness of most mathematical techniques to small systems, classifying models based on parameter scans is an important way to identify possible model behaviour [47].

The process of apoptosis seems to be suited for modeling by a bistable system because it seems that at some level, cells 'decide' whether or not to succumb to apoptosis: either the full cellular program is activated or not at all. Obviously, cell death itself is -by definition- an 'all-or-nothing' phenomenon: in the end the cell will be either dead or not. What we are interested in, however, is the fact that already the cellular signaling network that communicates apoptosis stimuli acts in that 'all-or-nothing' manner: A recent study [134] showed that if a population of isogenetic cells is treated with an apoptotic stimulus such as hydrogenperoxide, individual cells invoke either one of two opposing cellular programs, favoring either cell death or cell survival by activation of cytoprotective proteins such as Erk [89, 74]. This observation suggests that the signaling network responsible for detecting the apoptotic stimulus, before passing on the signal, in some way 'evaluates and decides' whether or not the program of apoptosis is to be invoked or not. Further observations that support the idea of a signal evaluation step prior to activation of an all-or-nothing response, are, for example, that the apoptosis-protein p53, which is activated upon DNA-damage and takes important part in invoking apoptosis, is activated in a switch-like manner [95]. Although transcription of p53 is increased in a graded manner, *activation* of p53 in the form of phosphorylation is activated in a discrete fashion, as shown by FACS-analysis [95]. Other studies have shown that the activation of caspases (cleavage proteins that are generally considered the 'executioners' of apoptosis) is a rapid process and their

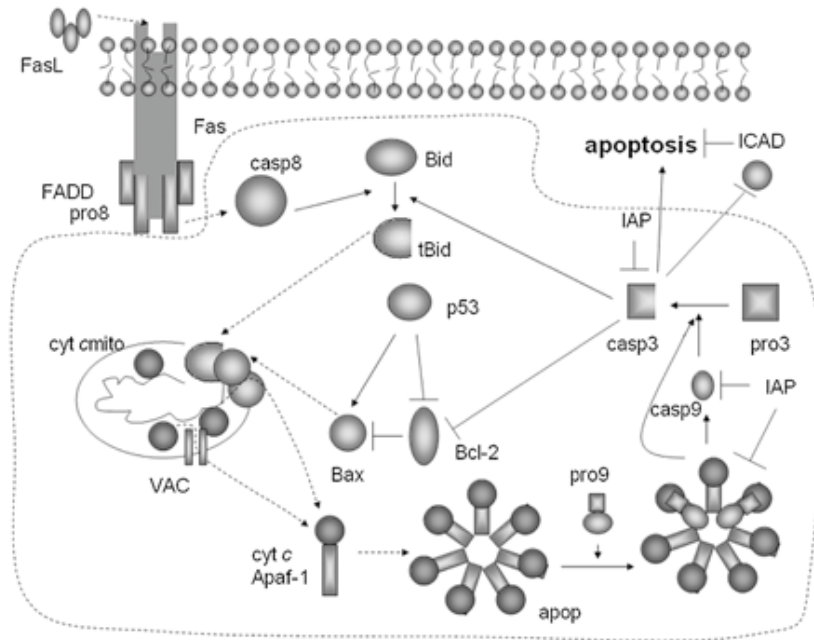


Figure 2.13: The full model of apoptosis considered in [10], from which this figure is taken . See text for explanation.

degree of activation does not decrease with a decrease of apoptotic stimuli. Rather, with reducing the stimuli, caspase-activation stays at the same level (apoptotic state) until at some minimal threshold of stimuli, caspase-activation stays out altogether [156]. In this study caspase activity was detected by measuring the loss of FRET signal of a protein chimera carrying caspase cleavage sites. The same observation was made in [17], where it was demonstrated that below a certain threshold of apoptotic stimulus (CD95L) invocation of cell death stays out, even though death receptors were still being activated.

These observations have inspired the development of mathematical models that exhibit two main features. First, the model should be consistent with the existence of two different states of the system, one representing the non-apoptotic state in which the level of executioner caspases is low, and a second, apoptotic state, which the system can reach upon encounter with an apoptotic stimulus. Secondly, the model should hold an explanation for the 'signal evaluation step': if the stimulus stays below a threshold, the system should remain in the non-apoptotic state.

Most theoretical studies of apoptosis concentrate on the establishment of bistability [10, 48, 194, 112], where the existence of several feedback loops from the endpoint of apoptosis-invocation, i.e. executioner Caspase-3, to upstream events stand at the core of the analysis, but there are also monostable models which concentrate on the description of the critical threshold of apoptosis invocation [17].

After a brief summary of the main events leading to Caspase-3 activation, we will discuss the results of the different modeling approaches.

Figure 2.13 shows the mitochondria-dependent (intrinsic) apoptotic pathway considered in the study by Bagci *et al* [10] (for a review on apoptotic pathways see, e.g. [155, 133]).

Briefly, binding of a ligand induces oligomerization (trimerization) of the receptor Fas, plus subsequent recruitment of FADD adaptor molecules [133]. The resulting Death Inducing Signaling Complex (DISC) recruits multiple procaspase-8 molecules, which leads to their cleavage and activation (induced proximity model). In type I cells the amount of active caspase 8 generated at the DISC is sufficient and can directly lead to apoptosis. In Type II cells, the number of caspase-8 is amplified via the mitochondria pathway (see Figure 2.13): caspase-8 molecules cleave Bid to generate truncated Bid (tBid), which then translocates to the mitochondria to induce release of cytochrome c into the cytoplasm [205, 151]. This process depends on the opening of the mitochondrial permeability transition pores (MPTPs).

An important component of the apoptotic pathway is p53, which represses Bcl-2 (an antiapoptotic protein that inhibits the release of cytochrome c [9]) and activates Bax (a pro-apoptotic protein which promotes mitochondrial permeability). Cytochrome C release supports the formation of an apoptosome complex which leads (via Caspase-9) to the activation of Caspase-3, the endpoint of the apoptosis invocation promoting DNA fragmentation [116, 52].

There exist at least four positive feedback circuits from Caspase-3 to upstream events involved in its activation (see Figure 2.14):

1. Cleavage of Bid by Caspase-3, producing tBid and leading to increased permeability of mitochondria pores [121, 175]

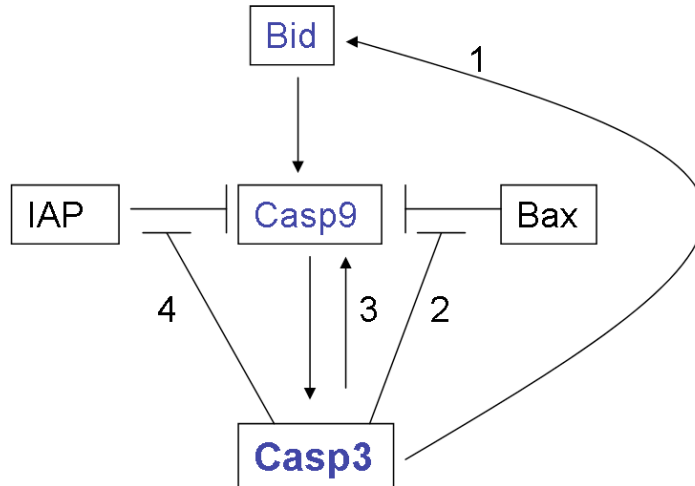


Figure 2.14:

2. Cleavage (inhibition) of Bcl-2 by Caspase-3, suppressing its negative effect on the pro-apoptotic protein Bax [103]
3. Cleavage (activation) of Caspase 9 by Caspase-3, presenting a direct positive feedback [208, 178]
4. Sequestration of IAPs away from Caspase 9 by activated Caspase-3 [112, 42, 41]

In theory, each of these mechanisms can cause bistability [112, 10, 48], but different studies focus on different subsets of the feedback circuits. The general procedure is to computationally define parameter ranges for the specific models which lead to bistability. The principle of robustness of biological pathways [4, 12] is then applied to reason that those mechanisms with the largest 'bistability range' of parameters are the most plausible ones.

Several interesting conclusions arise from these investigations:

Bagci find that cooperativity in apoptosome formation is required for robust bistability. Again, as we have seen earlier, cooperativity was modeled by applying a Hill-term with an exponent n greater than one (cf. equation 2.1.2 on page 52, equation XX in [10]). They show that (at least in the admittedly arbitrary parameter range of their search), one of the two positive feedbacks from Caspase-3 via cleavage of Bid or Bcl-2 alone show bistability only in a small parameter range (cf. Figure 3 in [10]). In their model, the action of IAPs does not lead to stability, which is in contrast to

the results of Legewie *et al* [112].

Another study [194] focuses on the activation of p53 vs activation of cytoprotective response such as Erk or Akt [35, 136], thereby following up on observations of the single cell bifurcation of these two mutually exclusive responses upon presentation to apoptotic stimuli [134, 109]. Their focus is a positive feedback between p53 and Akt, involving MDM2 and PTEN.

The biological interpretation of these largely numerical studies proves difficult, since the true range of cellular parameter combinations is hard to assess.

One interesting result, however, is the interpretation of pathologic cell behaviour in the light of disruption of the bistability property. As explained earlier (section 2.1.3; Figure 2.9 on page 57), bistability is not statically encoded into a reaction system, but depends on the proper balance of parameters such as synthesis, repression and degradation rates [46, 76]. A change of these, caused for example by disrupted binding surfaces through oxidative damage (for example in aging [150, 170]), can shift the balance of the system towards one state. In this view, pathological resistance to apoptosis can be interpreted as a shift from the healthy bistable behaviour where different initial situation lead to different outcomes (cf Figure 2.9C) to a state that independently of the input leads to the cell survival state (cf Figure 2.9A or B).

A theoretical identification of those parameter changes that are able to cause this shift may give hints to the cellular events that cause the resistance to apoptosis. In [10] the authors point out that, e.g., increasing the rate of degradation for Bax (a pro-apoptotic protein) results in loss of bistability, such that even for very high stimuli, Caspase-3 levels evolve towards zero.

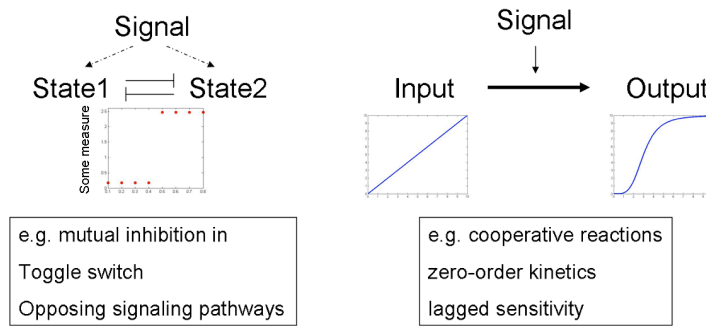


Figure 2.15:

2.2 The monostable case: Models of Ultrasensitivity

In the first chapter we looked at competition between opposing cellular events: cell death vs cell survival (section 2.1.4), mutually exclusive expression of a two-inhibitor system (section 2.1.3) or the invocation of either one of two overlapping pathways: yeast mating signaling is stopped if the osmotic shock response is on. We saw how positive feedback, for example by means of mutual inhibition can generate a bistable system, in which one event will dominate over the other.

But there are other situations where we think of all-or-nothing behaviour, where the phrasing into a competitive framework might not be appropriate. For example, this would be the case for events of multiple subsequent reactions, where one state depends on its predecessor; another example are enzymatic reactions, where the steady-state level of the product shows a sigmoidal dependence curve on substrate level (Figure 2.15).

In this chapter, I introduce three mechanisms that are known to give rise to ultrasensitive responses (cooperative binding (section 2.2.1), cascade arrangements (section 2.2.2) and zero-order ultrasensitivity (section 2.2.3). In the next chapter I then discuss in detail a model of endocytic sorting of EGFR, thereby explaining a different mechanism giving rise to ultrasensitivity.

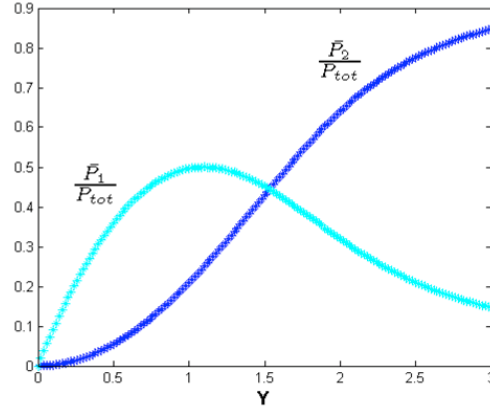


Figure 2.17: Steady-state value of fractions of double-bound ($\frac{\bar{P}_2}{P_{tot}}$, dark blue) or single-bound ($\frac{\bar{P}_1}{P_{tot}}$, light blue) form as a function of modification substrate.

$$\bar{P}_1 = 2\frac{k_+}{k_-}\bar{P}_0Y \equiv 2\bar{P}_0\frac{Y}{K} \quad (2.2.2)$$

$$\bar{P}_2 = \frac{k_+}{2k_-}\bar{P}_1Y \equiv \bar{P}_0\left(\frac{Y}{K}\right)^2 \quad (2.2.3)$$

, with $\frac{k_-}{k_+} \equiv K$.

Further, setting $\hat{Y} = \frac{Y}{K}$, we obtain the fraction of double-bound \bar{P}_2 of total $P = P_{tot}$ as

$$\frac{\bar{P}_2}{P_{tot}} = \frac{\bar{P}_2}{P_0 + P_1 + P_2} = \frac{P_0\hat{Y}^2}{P_0 + 2P_0\hat{Y} + P_0\hat{Y}^2} = \frac{\hat{Y}^2}{(1 + \hat{Y})^2} \quad (2.2.4)$$

The last expression is a sigmoidal curve as a function of \hat{Y} .

Figure 2.17 shows the fraction of \bar{P}_2 (equation 2.2.4, blue) and \bar{P}_1 (cyan) as a function of input Y . It can be seen that \bar{P}_2 , but not \bar{P}_1 , exhibits an ultrasensitive response. This behaviour of \bar{P}_2 reflects its quadratic dependence on input \hat{Y} .

In section 2.1.3 we had described a system of two mutually inhibiting proteins X and Y . The negative effect on each other's synthesis (or activation), we had taken as

$$f(y) = \frac{1}{1 + y^n}$$

, cf. equation 2.1.8 on page 55.

Appearing in the production term of the opposing molecule X ($dx/dt = f(y) - \mu x$) $f(y)$ denoted the fraction of unbound (i.e. unblocked) promoter/precursor of X, P_X , to which the production of X is proportional (cf. page 55). In the scenario of the double bound protein P described here, this 'unblocked' form is represented by P_0 , whose fraction is given by

$$\frac{\bar{P}_0}{P_{tot}} = \frac{\bar{P}_0}{P_0 + P_1 + P_2} = \frac{P_0}{P_0 + 2P_0Y + P_0Y^2} = \frac{1}{(1 + Y)^2}.$$

It can be shown that for the reaction scheme in Figure 2.16, $\frac{\bar{P}_0}{P_{tot}}$ can be approximated by $\frac{1}{1+Y^2}$, if *the second binding reaction occurs with a higher rate than the first one*, that is, $k_+P_1Y \gg k_+P_0Y$ [46]. Hence, if the affinity for further binding is increased with each bound monomer, the fraction of unbound molecule P_0 is given by

$$\frac{\bar{P}_0}{P_{tot}} \cong \frac{1}{1 + Y^2}.$$

This effect is called positive cooperativity. If this dynamic effect can be assumed, the approximation of multiple binding events by equations of the form 2.2.1 is valid.

2.2.2 Signaling Cascades

The sigmoidity of double-modified molecules can be enhanced by consecutive occurrence of this motif in the form of signaling cascades. Instead of having just one layer of double-modification, in these cascades the output of one layer is the input for the next one so that beginning from the second layer, already the *input* function is sigmoid. This effect gets then enhanced in the subsequent double-modification level [122, 56, 57, 21, 90].

Figure 2.18 illustrates the architecture (left) and the output behaviour (right) of such a cas-

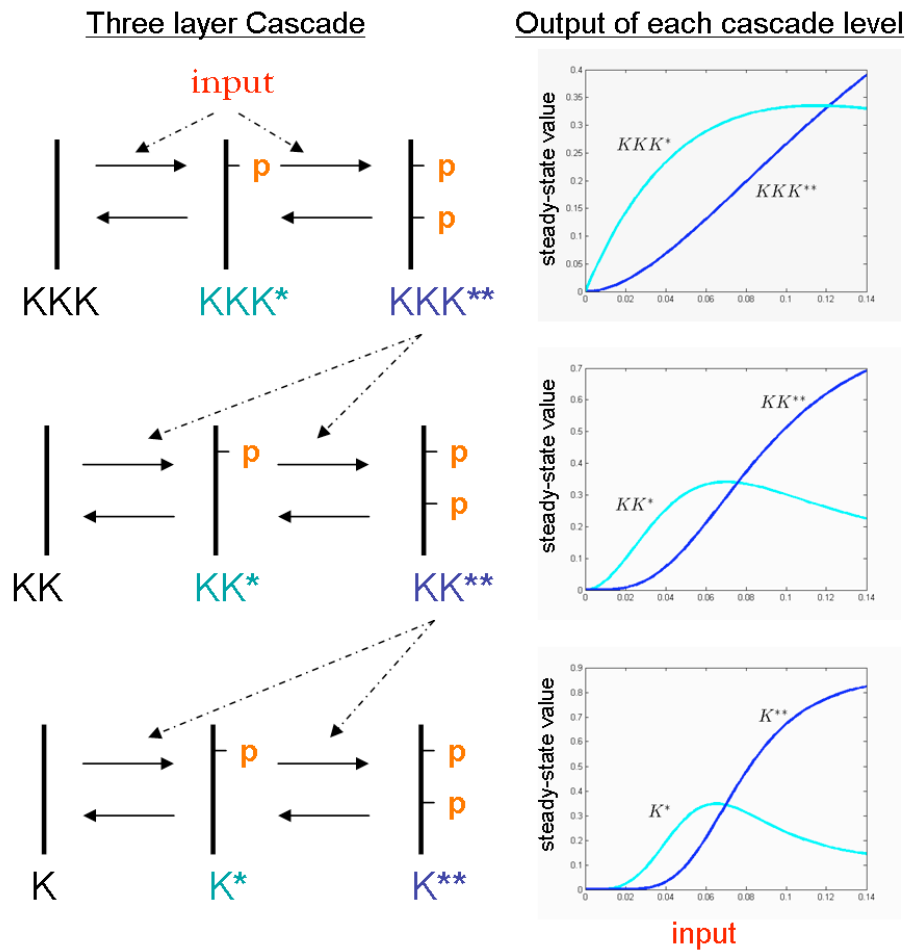


Figure 2.18: The sigmoidity of double-modified molecules can be enhanced by consecutive occurrence of this motif in the form of signaling cascades. See text.

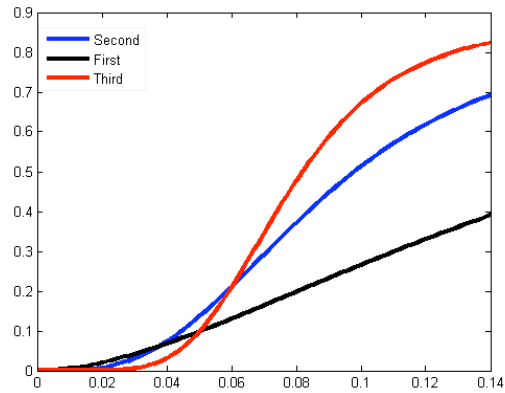


Figure 2.19: Comparison of the steepness of the response of the double-phosphorylated form on each cascade level.

cade arrangement. In this example, each horizontal level of the cascade consists of a kinase in its un-phosphorylated, single- or double-phosphorylated form, where '*' denotes phosphorylation. The double-phosphorylated form on one level activates the kinase on the subsequent level.

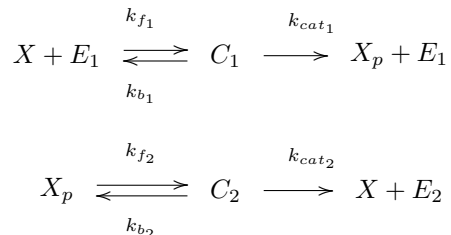
We thus recognize the architecture of double-modification which we just derived has having a sigmoid input-output behaviour (equation 2.2.4). We see this again in the graph showing output behaviour of the first level of the cascade (Figure 2.18, top right). The effect of the cascade arrangement now is simply that this sigmoidal effect gets amplified in each level: clearly, if the input itself is already sigmoid, the double-modification step enhances this effect.

Figure 2.19 indeed shows that with each level, the ultrasensitivity effect is increased. Note that not only does a response get suppressed more strongly for low input levels, but the maximal response is also reached faster.

2.2.3 Zero-order Ultrasensitivity

Another mechanism to achieve highly sigmoidal response curves is the so called zero-order ultrasensitivity [66, 65, 108, 186, 21].

Again, we consider the modification of some protein X by an enzyme E₁, along with the demodification reaction by a second enzyme E₂.



Goldbeter and Koshland [65] derived, how a switching mechanism can arise if the two modifying enzymes work in the 0-order regime, that is the substrates are much more abundant than the enzyme's Michaelis-Menten constant : $X + X_p = X_{tot} \gg K_M$, where

$$K_M = \frac{k_b + k_{cat}}{k_f}.$$

To explain the mechanisms, we follow the description in [18].

Let f denote the level of modified protein X_p and $(1-f)$ the level of unmodified protein X. Then $X_{tot} = 1$. The rate of conversion from X to X_p is given by $\frac{k_1(1-f)}{K_M+(1-f)}$, the rate of demodification is $\frac{k_2 f}{K_M+f}$. Denoting the ratio of the maximal rates of the converter enzymes, $\frac{k_1}{k_2}$ by α we get in steady-state [18]¹:

$$\begin{aligned}
 \frac{k_1(1-\bar{f})}{K_M+(1-\bar{f})} &= \frac{k_2\bar{f}}{K_M+\bar{f}} \\
 \frac{\alpha(1-\bar{f})}{K_M+(1-\bar{f})} &= \frac{\bar{f}}{K_M+\bar{f}}
 \end{aligned}$$

With this, the steady-state level \bar{f} of modified protein X_p is implicitly given as a function of α ,

¹The derivation of this equation is following simple Michaelin-Menten kinetics, similar to equation 2.1.5 on page 53

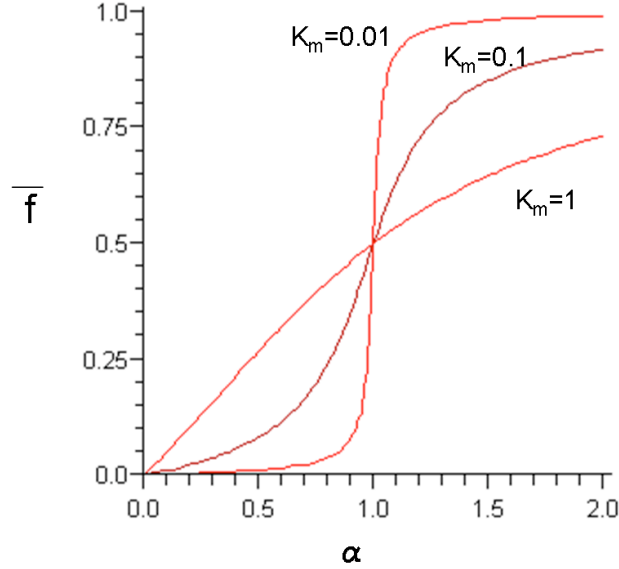


Figure 2.20: Zero-order ultrasensitivity for different parameter values $K_M = \frac{k_b+k_{cat}}{k_f}$

where α denotes the relative strengths of the two opposing reactions.

It is interesting to study, how \bar{f} changes if α is varied from small values to values larger than 1, that is we vary $k_1 < k_2$ to $k_1 > k_2$.

Figure 2.20 shows how the steady-state value of the modified form \bar{f} depends on α for different values of K_M . We see that the smaller K_M , that is, the farther in the zero-order regime the enzymes are working, the steeper is the switch-like response of \bar{f} .

One interesting consequence of zero-order ultrasensitivity and the fact that the enzymes are working at saturation is that upon overexpression of substrate X the time to reach steady-state is extended. This is not trivial and is not true for cooperativity or positive feedback mechanisms. Melen, Levy *et al* used this characteristic to validate zero-order ultrasensitivity experimentally in the context of *Drosophila* embryogenesis. During embryonic development, morphogens direct the formation of body patterns in an initially homogenous cell. In *Drosophila* embryos degradation of the transcription factor Yan is regulated by phosphorylation by MAPK, which in turn is activated upon EGFR stimulation

by its ligand Spitz [138]. Yan degradation, but not MAPK activation, occurs in tight boundaries, opening up the question how the graded input is translated into all-or-nothing degradation of Yan. As we have seen, several mechanisms exist that could lead to this behaviour.

The following was observed upon Yan-overexpression [127]:

- (i) the time to reach steady-state of Yan-degradation extended (cf Figure 6C in [127])
- (ii) the border of Yan-degradation did not change (cf Figure 6E in [127])

These results agree with the prediction of zero-order ultrasensitivity (cf Figures 4 and 5 in [127]) and exclude other possibilities of ultrasensitivity in this context.

Part II

Objectives

The overall aim of this thesis was the synchronization of experimental measurements with mathematical models of EGFR endocytosis, whereby both the internalization step itself (Project 1) as well as subsequent endosomal sorting (Projects 2 and 3) should be described by quantitative experimental techniques and mathematical modeling.

1. In the first Results section I describe a flow cytometry approach to measure internalization of EGFR, which is accompanied by a mathematical model which relates internalization dynamics to EGFR expression levels. The objectives were to, first, improve existing methods of measuring internalization. In this sense, the mathematical model was used to derive quantitative predictions that could be tested experimentally and thus probe the quantitative preciseness of the flow cytometry measurements. Secondly, by extending and refining a previous mathematical description, the model constitutes a theoretical disquisition of the effect of receptor overexpression relative to internalization capacity. This is of interest, considering that (i) internalization is necessary for signal attenuation and (ii) EGFR overexpression is frequently observed in cancer.
2. In the second Results section I describe a mathematical model based on ordinary differential equations, in which we discuss a mechanism of how sorting of EGFR into clathrin- or caveolae-mediated endocytosis might be regulated. The model was developed based on published data, where it was reported, that the sorting of EGFR into these different pathways is a function of the strength of EGF stimulation used, which suggested an ultrasensitive sorting mechanism. The objective of this part of my work was to (i) define a mathematical structure with which the question of pathway sorting could be addressed and in which previous knowledge about EGFR endocytosis could be integrated (ii) test the plausibility of a given model with methods from the theory of modeling (robustness analysis) (iii) derive theoretical predictions which could be tested experimentally and which would allow interpretation of the obtained data in light of possible alternative mechanisms of pathway sorting.
3. In the third Results section, I present a methodology and application of a combination of con-

focal microscopy and flow cytometry to address the problem of endocytic sorting of EGFR into clathrin- or caveolin-dependent pathways. The objective of this project was (i) to develop a framework which would allow the quantitative description of employment of each of the endocytosis pathways. For this I developed an imaging software (ColocalizationFinder.java) to allow the automatic evaluation of colocalization of EGFR vesicles with endocytic proteins; (ii) to conduct experiments which allowed the selective inhibition of one of the pathways which could then be used to derive the relationship of the different pathways and in particular test the model predictions derived in the second part.

Part III

Results

Chapter 3

Quantification of EGFR endocytosis by multiparametric Flow Cytometry

3.1 Background on modeling and experimental quantification of early endocytosis events

The first step of endocytosis is the disappearance of receptors from the membrane. As explained in the introduction (22 ff.), internalization and subsequent intracellular routing are important events in EGFR signal control. For the internalization step itself, there is still a controversy about the existence of alternative pathways (cf. section 1.2 on page 25). To clarify this issue (that is, decide, which proteins are involved in and necessary for internalization), but also to learn about the dynamics of this process in order to compare to mathematical models, high precision methods are needed to measure receptor internalization.

In this chapter we present detection of receptor internalization in a high-throughput manner using

flow cytometry. Flow Cytometry to measure EGFR endocytosis has previously been used by utilizing GFP-tagged EGF [189, 45, 24, 25]. GFP with a molecular weight of 30kDa is expected to exhibit a more serious alteration on the true dynamics of EGF (6kDa)-binding and internalization than Rhodamine (0.5kDa). The results presented here is the first study to use EGF fused to the low molecular weight marker Rhodamine, which is widely applied in confocal microscopy, to measure internalization. The utilization of Rhodamine-EGF has been made possible by the use of a 561nm laser. DPSS lasers emitting at 561 nm have recently emerged as excitation sources in flow cytometry [183, 96], holding the promise of making a whole range of fluorophores emitting in the yellow-red range, such as the many variants of DsRed, which range from mOrange (λ_{ex}) = 548) to mCherry (λ_{ex}) = 587) (fruit basket [171]), as well as Rhodamine and its derivatives such as tetramethylrhodamine (λ_{ex}) = 555), Cy3 (λ_{ex}) = 552) or Alexa Fluor 546 (λ_{ex}) = 561) and 555 (λ_{ex}) = 555), accessible for Flow Cytometry [171, 183].

The detection of EGFR internalization by flow cytometry holds important advantages compared to the traditional biochemical methods such as radioactively [198, 201, 209, 38, 16, 196] or biotin labeling assays [114, 188, 14]. The most important disadvantage of these, besides being very laborious and offering low reproducibility, is that they are not single-cell techniques and instead yield an integrated signal over a whole population of cells.

As an application of the measurements, we develop a mathematical model which relates EGF uptake dynamics to EGFR expression levels. We investigate the temporal evolution of the ratio of internalized vs surface located ligand-receptor complexes $r(t)$, a standard parameter used to estimate the rate of internalization [198] and in particular to assess the effect of certain perturbations on internalization [98, 172, 177, 114]. In [198, 140, 141] it was shown mathematically that, under certain assumptions this ratio describes a straight line with the slope corresponding to the rate of the internalization step. These assumptions were (i) that the number of surface bound ligand-receptor complexes RE_s remains approximately constant during the measurements and (ii) that the internalization step is a first-order process, i.e. that it is proportional to RE_s and independent of a potentially limiting

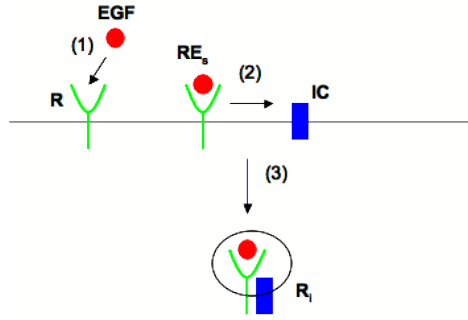


Figure 3.1: EGF binds membrane-located EGFR (1) to give rise to surface-bound EGF-EGFR complex. Via lateral diffusion events, the activated receptor binds internalization adaptors (2), which eventually leads to vesicle formation and internalization (3).

availability of internalization adaptors. A possible restriction of internalization by a limited capacity of internalization adaptors, however, has been suggested for cells expressing abnormally high numbers of EGF receptors [197]. In light of the signal-attenuating character of endocytosis and the oncogenicity of EGFR overexpression, it is important to investigate what the effects of high receptor expression levels relative to internalization pathway capacity on internalization dynamics are [200]. We here provide a mathematically more precise derivation of the internalization process and in particular the temporal evolution of $r(t)$ than previously given [198, 140, 141, 197, 180, 120] by dropping assumptions (i) and (ii) in the mathematical analysis and find that $r(t)$ is not a straight line as previously derived, but a convex or concave curve depending on whether receptors or internalization components are limiting the reaction, respectively. This way, the shape of this curve can be used to determine which of these cases is true for a given cell-type.

3.2 Flow Cytometric detection of Rhodamine-EGF to measure Endocytosis of EGFR

Experiments were performed in the cervical cancer Hela cell line, a cell culture model expressing abundant EGFR and which is well established for studying the various modes of endocytosis and their role in EGFR signaling [5, 130]. Initial experiments were aimed at quantifying the dynamics EGF

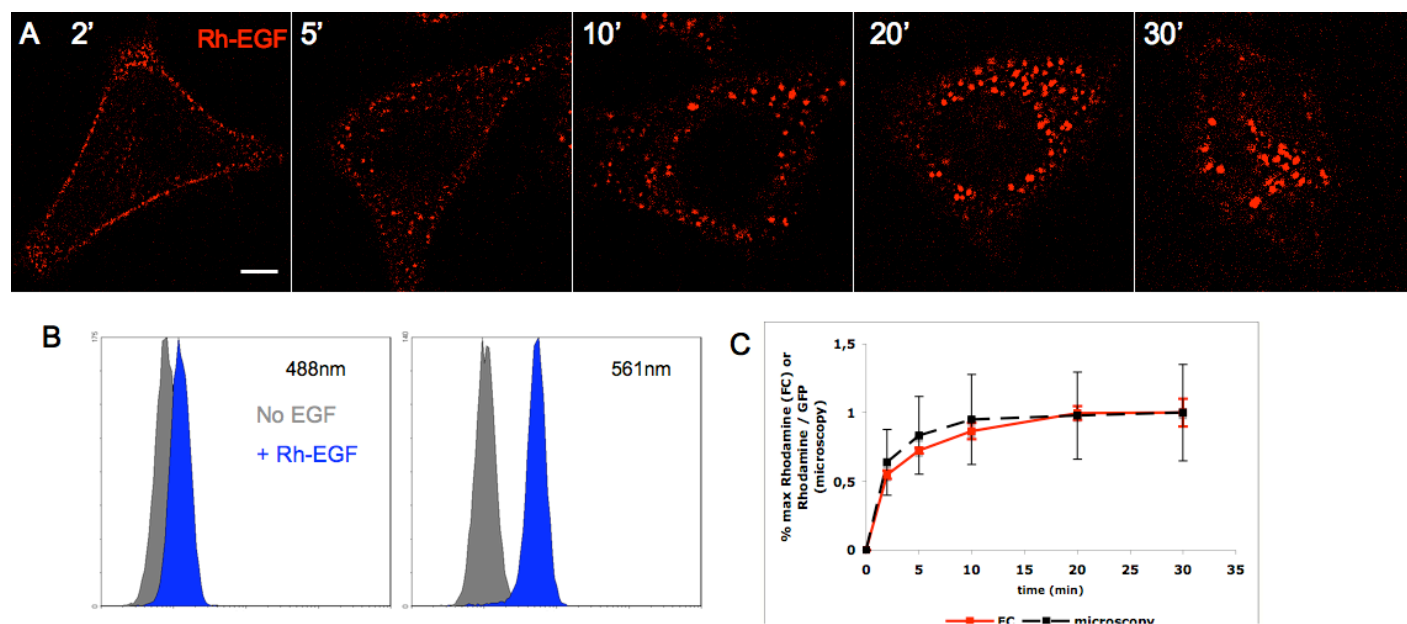


Figure 3.2:

interaction with EGFR using both high content (high-resolution laser scanning confocal microscopy) and high sample size (flow cytometry) approaches.

We first observed Rhodamine-EGF internalization by confocal microscopy (Figure 3.2A). HeLa cells were stimulated with 100ng/ml Rhodamine-EGF at 37 °C for various time periods and subjected to live microscopy. Figure 3.2A shows Rhodamine-EGF as binding and internalization occurs. At 2 minutes, the majority of Rhodamine-EGF is still located at the cell surface, with few small vesicles already internalized. As stimulation time increases, the level of surface-located Rhodamine-EGF declines and instead more and larger vesicles can be seen which locate more towards the cell interior. This increase in size is due to vesicle fusion processes along the endocytic route [130]. Cellular Rhodamine-EGF was quantified from images (figure 3.2D, see below).

While microscopy is an excellent method to observe in detail the process of endocytosis, we sought to test the suitability of flow cytometry as a high-throughput single-cell method to detect Rhodamine-EGF - EGFR interaction. Flow Cytometry has been used previously to study EGFR endocytosis using GFP-fused EGF [189], labeled Quantum dots [117] or polyplexes [37] with a standard 488nm laser

as excitation source. Rhodamine-EGF is widely used in confocal microscopy [161, 172, 184, 119] but has not been applied in Flow Cytometry due to the unavailability of appropriate laser lines. To test the ability of the 561nm laser to serve as an excitation for Rhodamine-EGF, we stimulated HeLa cells with 100ng/ml Rhodamine-EGF and compared the fluorescence intensity obtained from exciting the probes with a 488nm or 561nm laser. Cells were stimulated for 20 minutes at 37 °C, washed in PBS, trypsinated and then returned in medium for measurements. Figure 3.2A shows that, as predicted by the excitation spectra of Rhodamine, the signal-to-noise ratio improved with excitation at 561nm, demonstrating its suitability for detecting EGF-EGFR complexes by flow cytometry.

Subsequently we stimulated HeLa cells with 100ng/ml Rhodamine-EGF for different time periods as described above and measured the Rhodamine-EGF signal.

To determine the accuracy of using Rhodamine-EGF to quantify EGF binding to EGFR by flow cytometry we compared the flow cytometric measurements to detection of Rhodamine-EGF internalization by confocal microscopy. To obtain quantitative information from microscopy images, we fixed the cells at the indicated time points of EGF stimulation prior to imaging and for each time point monitored 30 cells. The sum of pixel values of the Rhodamine-EGF channel was taken as the fluorescence signal, which was normalized to its maximal value at 30 minutes. Plotting the normalized Rhodamine-EGF signal revealed an excellent agreement between these two different single cell techniques (Fig. 3.2D).

For Flow Cytometry, 10,000 cells were measured, whereas for microscopy, for each time point 30 cells were evaluated. Importantly, while the overall shape of the two curves match, the errorbars are significantly reduced for flow cytometry, demonstrating the value of sampling higher numbers of cells. These results demonstrate that 561-nm excitation of Rhodamine-EGF provides a sensitive tool for detecting EGF-EGFR complexes by flow cytometry.

The process of receptor endocytosis begins with a ligand binding event, and followed, on a slower timescale, by binding of the ligand-receptor complex to internalization adaptors, vesicle formation and the actual internalization of the vesicles (cf. Figure 3.1, [32, 192]).

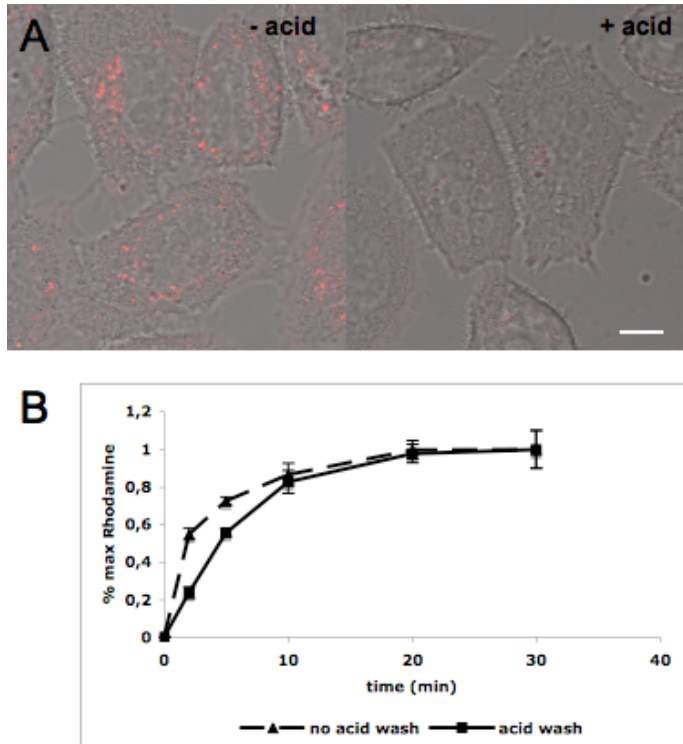


Figure 3.3: (A) HeLa cells were treated with 100ng/ml Rhodamine-EGF at 37C, then washed with PBS (left) or low pH buffer (right) and returned into fresh medium at 37C for 15 minutes before microscopy. Shown are overlays of transmission image and fluorescence image of Rhodamine-EGF. (B) HeLa cells were stimulated with 100 ng/ml Rhodamine-EGF for indicated time points and washed with PBS (solid line) or a low pH buffer (dashed line) before trypsination and flow cytometry. Plotted are mean values of three measurements (10,000 cells each), error bars denote standard deviation.

We sought to determine the suitability of flow cytometric detection of Rhodamine-EGF to discriminate between surface located vs internalized complexes. To distinguish between plasma membrane versus internalized ligand-receptor complexes, cells can be treated with a low pH buffer to remove surface-bound but not internalized labeled-EGF [200, 98, 172, 177].

The efficiency of the acid-induced dissociation of EGF was verified using microscopy (Figure 3.3A). Here, cells were treated with 100ng/ml Rhodamine-EGF for two minutes at 37 °C to allow for formation of EGF-EGFR complexes on the cell surface [172, 192]. Following, cells were washed with PBS (Figure 3.3A, left) or acid buffer (Figure 3.3A, right) and then returned to 37 °C for 15 minutes to allow for internalization prior to imaging. Figure 3.3A demonstrates that the acid wash effectively removed all surface bound Rhodamine-EGF, as in the acid-treated cells no EGF vesicles could be detected.

To determine the time-cours of internalization via flow cytometry HeLa cells were treated with 100ng/ml Rhodamine-EGF for different time periods, then washed with an acid buffer (solid line) or PBS (dashed line), prior to trypsination and subjected to flow cytometry (Figure 3.3B). We observed a significant difference between the Rhodamine-EGF signal for the acid- vs PBS-treated cells for short stimulation times. This difference in fluorescence intensity is highest at early timepoints (< 10 minutes) and corresponds to the fraction of receptors still localized on the membrane. For longer incubation times (> 10 minutes), the two curves coincided, as the majority of receptors were internalized [197, 98, 172, 177]

We conclude that in HeLa cells, up to 10 minutes of EGF incubation, there are still EGF receptors located at the cell surface, which are bound to EGF, but not fully enclosed in membrane pits and hence sensitive to the acid treatment.

This results demonstrates the sensitivity of our measurements and the ability to distinguish the temporal evolution of surface-bound vs internalized EGF by flow cytometric detection of Rhodamine-EGF.

3.3 A quantitative prediction of EGF uptake dynamics for different receptor expression levels

Mathematical modeling combined with high-throughput, quantitative data collection can yield non-intuitive understanding of the complexity of signaling pathways in the living cell. For the EGFR numerous models have been recently developed which focus on signal transduction (reviewed in [200, 29, 101]), yet little focus has been given to understanding new concepts in EGFR endocytosis. While the nonlinearity of the uptake reaction, due to the existence of alternative pathways which are entered with different affinities [120, 200], as well as the saturability of EGFR endocytosis [198, 197] were recognized early, detailed mathematical investigations of how this effects internalization dynamics are still missing. Related to this is the question of how EGFR overexpression relative to internalization capacity influences the uptake process. We here propose a combination of mathematical modeling and single-cell analysis to approach this problem.

In order to quantitatively evaluate the internalization reaction, and in particular to assess the effect of certain perturbations on internalization, typically, the temporal evolution of the ratio of internalized vs surface-associated ligand is monitored [98, 172, 177, 114, 190]. The ratio $r(t)$ is found experimentally by determining the fractions of internalized (labeled) ligand as well as the fraction still associated with the membrane using the acid stripping technique described earlier at different timepoints of stimulation and then calculating the ratio [98, 172, 177, 114, 190].

We asked 'What would a mathematical model predict for the temporal evolution of $r(t)$ and what can be concluded from its form?' Typically, the experimental data of $r(t)$ is approximated by a straight line [198, 98, 172, 177, 114, 190] with the slope corresponding to the rate of internalization k_e . Indeed, in [198] it was mathematically determined, that $r(t)$ describes a straight line with slope k_e , where two main assumptions were posed in the mathematical analysis, namely that (i) the number of surface-bound ligand receptor complexes RE_s remains approximately constant during measurement and (ii) the internalization acts like a first order process, i.e. that it is a function only of the number

of membrane bound ligand-receptor complexes and independent of the presence of any internalization components such as adaptor proteins of the endocytosis pathways [198]. Effectively, the following reaction scheme was considered:



$RE_s \equiv \bar{R}E_s = \text{constant}$, whereby RE_s and R_i denote fractions of surface-bound or internalized ligand-receptor complexes, respectively.

This reaction scheme is described by

$$\frac{dR_i}{dt} = k_e \cdot \bar{R}E_s$$

which immediately yields $R_i(t) = k_e \cdot \bar{R}E_s \cdot t$ and hence $r(t) = \frac{R_i}{RE_s} = k_e \cdot t$ describes a straight line in dependence of time with slope k_e [198, 140, 141].

Note that for the analytical treatment, it is assumed that the ligand binding reaction occurs instantaneously. This simplification is justified since the ligand binding reaction happens on a much faster timescale than the internalization reaction [198, 180, 80, 81, 82]. We adapt this procedure in the following and show later in simulations that the qualitative results are not affected by this simplification.

We extended the above described theoretical derivation of $r(t)$ to include the effect of a potentially limiting availability of internalization adaptors relative to different expression levels of EGFR and considered reaction scheme



We hereby relax assumption (i), i.e. we consider non-constant RE_s as well as assumption (ii), i.e. we include the binding to endocytosis adaptors IC prior to internalization. Note that again the ligand-binding reaction is assumed to occur instantaneously, so that the initial value of surface-bound ligand

RE_{s0} immediately assumes the minimum value of initially available receptors and number of EGF molecules, $RE_{s0} = \min\{R_0, EGF_0\}$ (Generally, X_0 denotes the initial value of the variable X). Since we are interested in deriving a prediction for different receptor numbers relative to internalization capacity we consider experimental situations where EGF-stimulation is not limiting, so that the initial number of surface-bound ligand-receptor complexes RE_{s0} is given by the number of available receptors at the beginning of the reaction R_0 .

The dynamics of reaction scheme (R2) are given by a single equation:

$$d(RE_s)/dt = d(IC)/dt = -d(R_i)/dt = -k_e \cdot RE_s \cdot IC \quad (3.1.1)$$

We consider the temporal evolution of the ratio of internalized vs surface-bound ligand $r(t) = \frac{R_i}{RE_s}$. Whereas using reaction scheme (R1), assuming constant RE_s as well as independence of internalization adaptors, it was derived that $r(t)$ describes a straight line, we can now see what a model without these two assumptions predicts for $r(t)$ for different relative initial values of receptors or internalization adaptors. To decide whether $r(t)$ is a convex or concave function, depending on whether receptors or internalization adaptors are limiting, we consider its second derivative which is given by (see Material and Methods):

$$r(t)'' = k_e \cdot RE_{s0} \cdot \frac{RE_s'}{RE_s^2} \cdot (RE_{s0} - IC_0)$$

where $RE_s' = d(RE_s)/dt = -k_i \cdot RE_s \cdot IC$.

Observe that $k_e \cdot RE_{s0} > 0$ and $\frac{RE_s'}{RE_s^2} < 0$, since RE_s' is always negative. The sign of $r(t)''$ thus depends on $(RE_{s0} - IC_0)$, and $r(t)$ will be a convex function if $RE_{s0} < IC_0$ (receptors are limiting) or concave if $RE_{s0} > IC_0$ (internalization adaptors are limiting).

Our analysis still holds if the ligand-binding reaction is included, so that

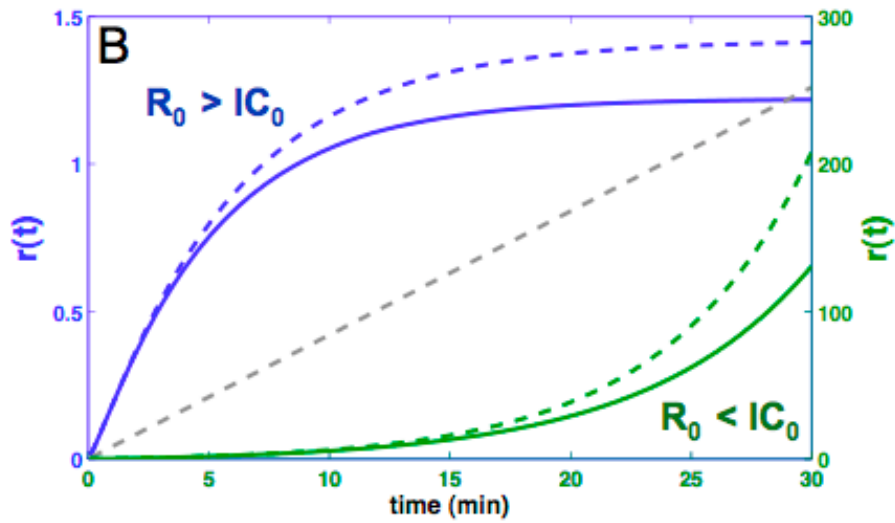
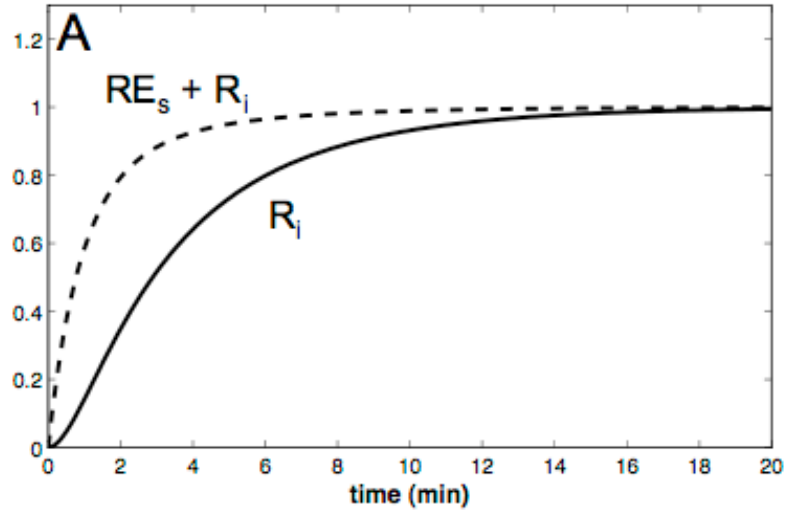
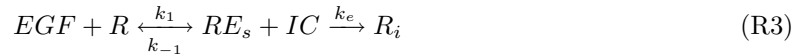


Figure 3.4: (A) Simulations of the full model (reaction scheme (R2)) for internalized ligand-receptor complexes R_i (solid) or the sum of R_i and surface-located ligand receptor complex RE_s (dashed). (B) Simulations of the full model (reaction scheme (R2)) for the ratio of internalized vs surface-bound ligand receptor complexes $r(t) = \frac{RE_i}{RE_s}$ for the two different cases $R_0 < IC_0$ (green) or $R_0 > IC_0$ (blue). Plotted are the time trajectories for $r(t)$ for these two cases, each for two different initial receptor values with R_{01} (dashed) $<$ R_{02} (solid)



(see Material and Methods for equations). Figure 3.4A shows the model simulation for R_i (= internalized EGF-EGFR complex, solid line) as well as for the sum of R_i and surface-located ligand receptor complex RE_s (dashed line). It can be seen that qualitatively, the simulations agree with our measurements of HeLa cells treated with PBS only (cf. Figure 3.2B, dashed or solid line, respectively), demonstrating that the model is in principle able to capture the kinetics of the internalization process. The exact shape of the model simulations depends on parameter values chosen, see Figure caption for parameters used in Figure 3.4.

Figure 3.4B shows simulations for the two different cases $R_0 < IC_0$ (green) or $R_0 > IC_0$ (blue). Plotted are the time trajectories for $r(t)$ for these two cases, each for two different initial receptor values with R_{01} (dashed) $<$ R_{02} (solid). See Figure caption for initial values and parameters used. As derived analytically assuming instantaneous ligand-binding, we see that $r(t)$ is convex if $R_0 < IC_0$ and concave otherwise.

3.2 Internalization dynamics for cells with different receptor expression levels

To apply the derived predictions, we generated HaCat cells stably expressing GFP-EGFR to study EGF internalization dynamics in subpopulations expressing different relative numbers of receptors. These cells showed a heterogeneous expression level of GFP-EGFR (Figure ??A), with an otherwise identical genetic background. In particular, cells from different subpopulations of receptor expression are expected to exhibit highly similar abundance levels of internalization adaptors, making them an excellent model to study EGF uptake as a function of receptor expression level using a single cell technique.

To first test whether the flow cytometric detection is sensitive enough to detect differences in

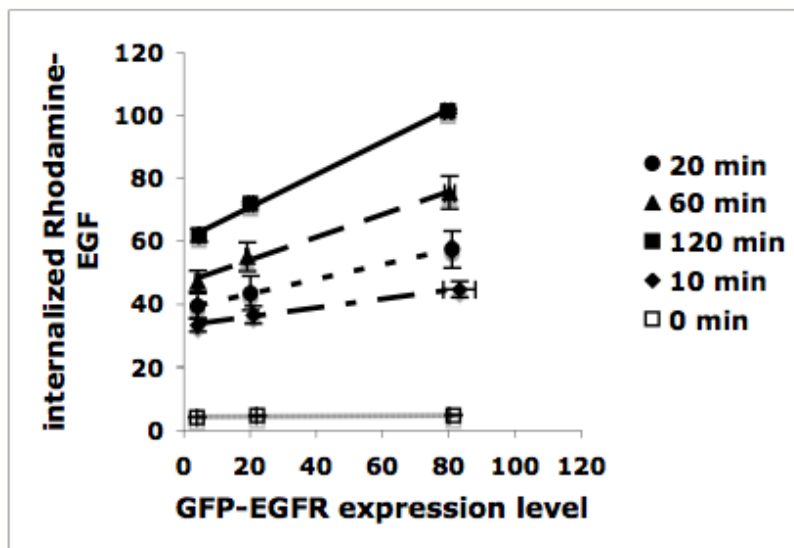


Figure 3.5: HaCat cells stably expressing GFP-EGFR were stimulated with 100 ng/ml Rhodamine-EGF for indicated time points. Rhodamine-EGF uptake is plotted as a function of GFP-EGFR expression level for three subpopulations of cells expressing different levels of GFP-EGFR

Rhodamine-EGF binding between cells expressing different levels of EGFR, we investigated whether cells with higher GFP signal would show an increased level of surface-binding of EGF when compared to cells with a lower GFP signal. For this, we stimulated cells with 100 ng/ml Rhodamine on ice for 1 hour. This allows surface binding but not internalization [172]. Prior to stimulation, cells were starved in serum free medium for 14 hours to force integration of all receptors into the membrane. As expected, we saw an increased Rhodamine-EGF signal for cells with higher GFP-EGFR expression level and surface-binding of Rhodamine-EGF, demonstrating the sensitivity of the measurements (not shown).

We next tested whether cells with higher GFP-EGFR level would also internalize more EGF. This is not obvious because whereas surface binding solely depends on the number of available binding sites, i.e. surface receptors, the internalization reaction also depends on the capacity of the endocytosis machinery.

In the previous section we derived that the ratio of internalized vs surface located ligand-receptor complexes $r(t) = \frac{RE_i}{RE_s}$ is a convex or concave curve depending on whether receptors or internalization

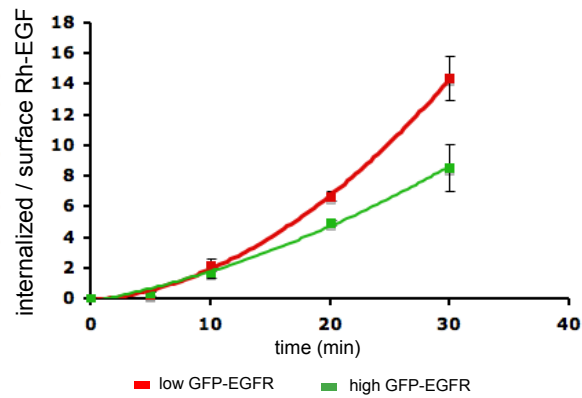


Figure 3.6: GFP-EGFR HaCat cells were stimulated with 100 ng/ml Rhodamine-EGF for the indicated time points. Surface-associated fraction of EGF (RE_s in the model) was determined by subtracting the mean fluorescence value of acid-treated samples from that of PBS-treated (see Material and Methods). Plotted is the ratio of internalized vs surface-bound ligand receptor complexes $r(t) = \frac{RE_i}{RE_s}$ for two subpopulations of GFP-EGFR expression.

adaptors are limiting the EGF internalization.

To judge, which of these two situations on the initial conditions is true in the HaCat cell line and to derive a prediction for the shape of $r(t)$, we compared Rhodamine-EGF internalization in cells with different receptor expression levels.

We found that uptake of Rhodamine-EGF increased linearly with GFP-EGFR expression level at all timepoints measured (Figure 3.5). We conclude that in this cell line receptor number and not internalization components are limiting the uptake.

According to the analysis in the previous section the prediction for the ratio of internalized vs surface located ligand-receptor complexes $r(t) = \frac{R_i}{R E_s}$ is that it is a convex curve with the one for cells with higher GFP-EGFR values lying below the one with lower GFP-EGFR. We determined the ratio of internalized vs surface bound ligand-receptor complex for 2, 5, 10 and 20 minutes of Rhodamine-EGF stimulation using the acid-wash protocol (cf. Figure 3.3). Figure 3.6 shows the results of the measurements. As predicted, $r(t)$ describes a convex curve. Further, we see that for cells with higher expression levels, $r(t)$ lies below, which also agree with the model prediction (cf. Figure 3.4B)

3.3 Discussion

In this study we have shown the applicability of Flow Cytometry to study dynamics of EGF receptor endocytosis using Rhodamine-EGF on a Beckman-Coulter Flow 500/MPL equipped with a Compass 561 nm/40mW laser. An improved fluorochrome to autofluorescence ratio over standard 488-nm excitation was shown as well as agreement to data obtained by confocal microscopy (cf. Figure 3.2).

We have refined a previously developed model by dropping two assumption previously made in the theoretical treatment, which allowed the analysis of receptor overexpression on internalization dynamics. We have validated quantitative predictions obtained from the model by measuring Rhodamine-EGF uptake as a function of receptor expression level using a cell line expressing GFP-EGFR (cf. Figures 3.4 and 3.6).

The biggest advantage we see in using Flow Cytometry to study EGFR endocytosis dynamics is

that is yields single-cell data, as opposed to traditional methods such as using radioactively [198, 177, 201, 209, 38, 16, 196] or biotin-labeled EGF [114, 188, 15].

The two principal tools for single cell measurements in cell biology are high-resolution fluorescence microscopy and flow cytometry. Fluorescence microscopy, using either fluorochrome- or GFP-tagged EGF, EGFR or quantum dots, has been applied at many different levels to study the dynamics of EGFR endocytosis. Dye (e.g. rhodamine)-labeled EGF can be combined with GFP-tagged EGFR to observe spatial and temporal dynamics of endocytosis and endosomal trafficking. However, most applications have been qualitative; reporting highly qualitative/subjective co-localization, or internalization results [172, 75, 99]. Several studies have applied quantitative image analysis demonstrating the ability to obtain statistically significant quantitative data [147, 157]. However, these findings are statistically limited in that even with automated imaging only small populations of cells are analyzed. Furthermore, quantification of imaging data involves pre-processing of the images such as background reduction and segmentation, processes during which quantitative information of the original image is lost.

While Flow Cytometry has been previously applied to studying EGFR endocytosis, these studies were either restricted to single color studies [117, 37, 189].

The EGFR internalization machinery is not fully understood, with the precise role of many components or receptor modifications such as ubiquitin, still uncertain (cf. Introduction, page 25). In this light, the here presented method would be an excellent system to assess the role of certain proteins using single-cell techniques such as RNAi. For EGFR endocytosis, the existence of several independent internalization pathways has been postulated, but their interdependence is not fully understood. The earlier discussed time/EGF concentration dependence for clathrin- vs caveolin/lipid raft-mediated internalization ([172, 166] could be tested for using the here presented high-throughput approach, in combination with mathematical modeling.

In the next chapter we introduce a model of sorting between clathrin- vs caveolae-mediated endocytosis pathways.

Chapter 4

A Model of EGFR Endocytic Sorting

Cellular components interact in time and space. Using mathematical models based on ordinary differential equations one may simulate the dynamic behaviour of signaling pathways and investigate the functional consequences of assumptions about the quantity of involved components as well as the rates of reactions (see Part I of this thesis).

To analyze endocytosis behaviour of EGFR, we constructed a mathematical model of the sorting process of EGF receptors into distinct endocytosis pathways. The biology of EGFR endocytosis was introduced in section 1. After ligand binding, the receptor may internalize via different pathways, thereby altering the cellular response.

It is currently not known whether there exist receptor modifications that specifically target the receptor into one or the other endocytosis pathway. In this section, we describe a system of ordinary differential equations, representing ligand binding plus subsequent binding to endocytosis adaptors, which reproduces previously published data on receptor internalization. With the model we specifically addressed the question, whether a 'sorting effect' between different pathways is conceivable, without

the assumption of receptor modifications to discriminate between these.

To describe 'sorting' of the activated receptor, we searched for a model that reproduced an experimental observation that was published in [172]: the suppression of Clathrin-independent endocytosis for low EGF levels, and an abrupt start of this for high EGF levels. This behaviour implies that for a given strength of stimulations, cells react in distinct and well-defined manners. We found that already very weak assumptions lead to ultrasensitive behaviour and give a mathematical analysis of a mechanism by which ultrasensitive, i.e. all-or-nothing responses based on a graded input signal, can be generated. In particular, the model suggests that one and the same form of the receptor may be internalized by distinct endocytosis pathways while still achieving a clear-cut sorting.

This chapter is organized as follows: After a brief reminder of the relevant biological background of the model (section 4.1), we describe the sorting mechanism as proposed by the model (section 4.2). Specifically, sections 4.3 and 4.4 explain how the occurrence of clathrin-independent endocytosis depends on the strength of EGF stimulation as well as the initial number of available receptors, respectively.

A mathematical analysis of the observed dynamic effects, in particular the correspondence to distinct classes of steady states, as well as the biological interpretation of these is given in section 4.5.

As we have learned in Part I, mathematical models of real life phenomena can be used to gain a different perspective of the phenomena of interest, such as the analysis of certain assumptions, for example assumptions of reaction rates or the number of a certain class of molecules, such as endocytosis adaptors. In order to test the effect of changes of the assumptions, for example certain values for reaction rates, one has to define a measure how to quantify the effects. Section 4.7 shows how we use the approximability of our model by a sigmoidal function (the so called Hill-function) as a measure to assess the change of behaviour of our model upon changes of underlying assumptions. In section 4.8 it is demonstrated that our main result, the ultrasensitive effect, is preserved for large

parameter variations, i.e. that our model is *robust*. This is an important property of a model: a fruitful branch of systems biology is devoted to the question whether robustness of intracellular signaling systems is a feature selected for during evolution. The idea is especially exciting, since it would put in our hands a quantitative measure for the evolution of biological networks. In this case, the robustness of a model speaks for its plausibility and may be used as a selection feature when comparing different possible candidate mechanisms for a certain phenomenon. For groundbreaking work on the application of robustness theory to Chemotaxis in *E. Coli*, see [12, 3, 106]; to Drosophila Development, see [49, 50, 51, 4]; to the evolution of the Circadian Clock see e.g. [30].

The chapter concludes with a discussion of the biological significance and implications of the proposed model.

4.1 Biological Basis of the Model

Ultrasensitivity is a property of signal transduction systems that allows the generation of all-or-nothing responses based on graded inputs [67, 123, 90]. This feature proves especially important in the context of growth factors or apoptosis signals, whose output is 'binary by nature' [21, 68], as well as morphogen directed pattern formation [44, 128, 68].

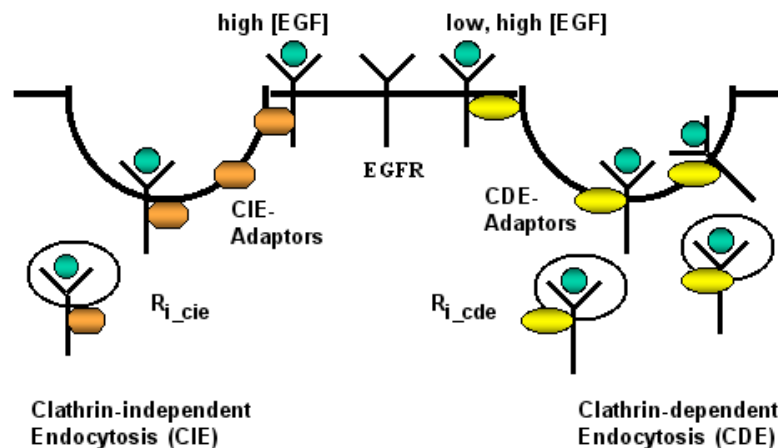


Figure 4.1: CDE and CIE pathways of EGFR. High EGF concentrations induce CIE, whereas CDE is observed at low and high EGF concentrations. The adaptors for the respective endocytosis pathways are referred to as CDE- or CIE-adaptors, respectively.

In a recent study it was observed that the Epidermal Growth Factor (EGF) receptor follows clathrin-independent endocytosis (CIE) in an ultrasensitive, EGF concentration dependent manner [172]: In the presence of low concentrations of EGF, the receptor was exclusively internalized via clathrin-dependent endocytosis (CDE), whereas at high concentrations CIE was abruptly turned on (Fig. 4.1).

Endocytosis is the process by which activated transmembrane receptors are directed into the endosomal system from the plasma membrane [130, 200]. CDE is the major internalization route and was the first to be discovered (reviewed in [104, 111]). In the past years, receptor internalization mechanisms that do not employ the structural protein clathrin, but arise from lipid rafts and caveolin-rich membrane regions have been identified [154, 173, 111]. Still, the important question which molecular events govern the sorting of the EGF receptor into the two different endocytosis pathways remains unanswered [55, 2, 88, 111, 173].

Ligand induced receptor phosphorylation creates docking sites for adaptors, such as EPS15, epsin and AP-2 [104, 176]. Via direct or indirect binding, adaptors recruit the receptor to special membrane regions which are characterized by a particular composition of cage-proteins and/or -lipids [173, 111]. The forming vesicles pinch off the membrane and carry their cargo to distinct intracellular locations, which might account for the specificity of the invoked signal [88]. Endocytosis may direct the receptors for lysosomal degradation or recycle them back to the membrane [88, 73].

In [172] it was reported that mono-ubiquitination (mono-Ub) of the EGF Receptor could only be observed at high EGF concentrations, raising the question whether mono-Ub might serve as a discriminative feature, which, when appended to the receptor, selectively targets the receptor to CIE [70, 2]. This, however, conflicts with reports on the involvement of the ubiquitin-binding adaptor proteins epsin and EPS15 during CDE [2, 88, 38].

To address this controversy, we built a mathematical model of the sorting process. Mathematical modeling has previously played a significant role in elucidating the mechanisms of EGF receptor signaling and endocytosis [180, 167, 110, 199, 100]. The question of how the distribution of activated

receptors into the different endocytosis routes is controlled, however, has not been treated mathematically thus far. Here, we demonstrate that a switch-like response of CIE may result simply from a saturation effect of the CDE pathway. The unexpected steepness of the response (indicated by high Hill-coefficients) as well as its robustness towards parameter variations suggest it as a plausible mechanism to generate ultrasensitivity in cellular signaling. Importantly, the mechanism imposes only weak assumptions on the underlying interaction structure and parameter values. We thus give evidence for the hypothesis that the main purpose of post-ligand binding modifications of the EGF receptor such as ubiquitination does not lie in the discrimination between alternative endocytosis pathways.

4.2 Ultrasensitivity in EGFR endocytosis

$d(\text{EGF})/dt = -k_f \cdot \text{EGF} \cdot R + k_r \cdot R \cdot \text{EGF}$	1
$d(R)/dt = -k_f \cdot \text{EGF} \cdot R + k_r \cdot R \cdot \text{EGF}$	2
$d(R \cdot \text{EGF})/dt = k_f \cdot \text{EGF} \cdot R - k_r \cdot R \cdot \text{EGF} - k_{cde} \cdot R \cdot \text{EGF} \cdot \text{CDE} - k_{cie} \cdot R \cdot \text{EGF} \cdot \text{CIE}$	3
$d(\text{CDE})/dt = -k_{cde} \cdot R \cdot \text{EGF} \cdot \text{CDE}$	4
$d(\text{CIE})/dt = -k_{cie} \cdot R \cdot \text{EGF} \cdot \text{CIE}$	5
$d(R_{i \cdot cde})/dt = k_{cde} \cdot R \cdot \text{EGF} \cdot \text{CDE}$	6
$d(R_{i \cdot cie})/dt = k_{cie} \cdot R \cdot \text{EGF} \cdot \text{CIE}$	7

Table 4.1: The system of ODEs constituting the model .

We built a system of ordinary differential equations (ODEs) that models the sorting of EGF receptor into the two pathways (Table 4.1). The model contains the binding reaction of EGF to receptor R, which leads to one form of activated receptor (R_EGF), capable of entering clathrin-dependent or -independent endocytosis.

In order to simulate the entry of ligand-bound receptor into an endocytosis pathway, we introduced variables CDE and CIE, representing adaptors for clathrin-dependent and -independent endocytosis which R_EGF can enter with rates k_{cde} and k_{cie} , respectively. The variables CDE and CIE represent the amount of the limiting factor in each pathway, which could be adaptor- or cage-proteins. In accordance with previous findings (e.g. [172]) we assume that the affinity of activated receptors R_EGF is significantly higher for the CDE-pathway ($k_{cde} \gg k_{cie}$). To quantify the fraction of receptor

going either pathway, we introduced variables $R_{i,cde}$ and $R_{i,cie}$. The steady-state values of these variables represent the amount of R_EGF internalized via CDE and CIE, respectively. The model equations were derived according to law of mass-actions (see, for example, [187]).

4.3 CIE-internalization depends on number of receptors and strength of EGF-stimulation

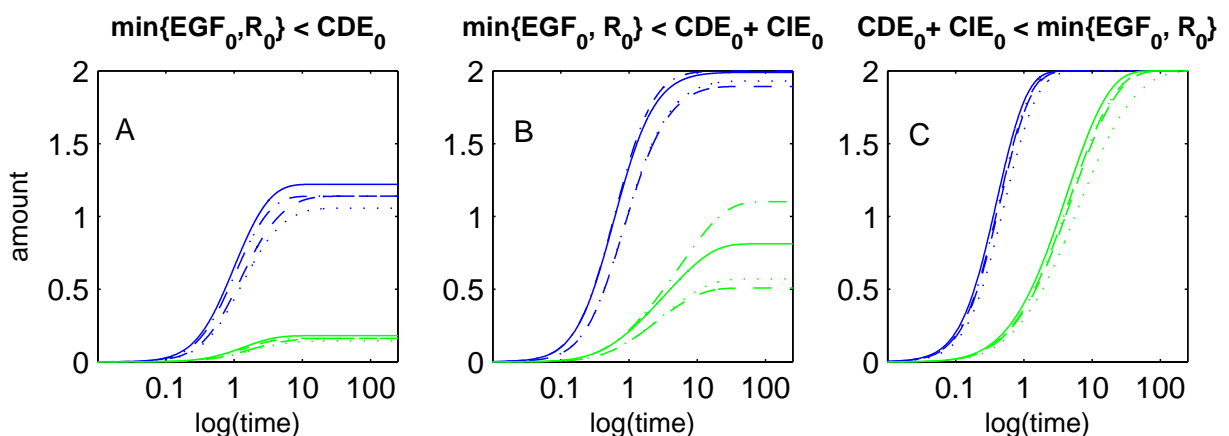


Figure 4.2: Time trajectories of $R_{i,cde}$ (blue) and $R_{i,cie}$ (green) for three different classes of initial conditions. In case A (B) at least one of EGF_0 or R_0 stays below CDE_0 ($CDE_0 + CIE_0$). In case C, both EGF_0 and R_0 exceed $CDE_0 + CIE_0$. Initial values were chosen arbitrarily such that these conditions are satisfied. In all three cases $CDE_0 = 2.0$, $CIE_0 = 2.0$ and (A) $(EGF_0, R_0) = (1.2, 1.5)$, $(1.6, 1.3)$, $(2.3, 1.3)$, $(1.4, 2.5)$; (B) $(2.5, 3.0)$, $(3.1, 2.4)$, $(3.1, 4.5)$, $(5.0, 2.8)$; (C) $(4.3, 4.7)$, $(5.0, 5.2)$, $(5.5, 5.0)$, $(5.3, 6.0)$.

We systematically scanned the space of initial values of the model in Table 4.1 to investigate the effect of EGF stimulation on receptor distribution into CDE or CIE (see Methods). Figure 4.2 shows the time trajectories of $R_{i,cde}$ and $R_{i,cie}$ for three different classes of initial conditions, each represented by four different sets of values (see Figure caption). The three classes of initial values have distinct effects on the internalization-behavior of R_EGF, the activated receptor. They represent assumptions on the relative quantities of EGF-molecules, unbound receptors and endocytosis adaptors.

The first class of initial values (Fig. 4.2A) represents the case that either the initial number of unbound receptors (R_0) or EGF-molecules (EGF_0) is lower than the capacity of the CDE-pathway

$(CDE_0)^1$. This corresponds to an experimental setting where cells are stimulated with low EGF-concentrations, i.e. $EGF_0 < CDE_0$. Initial values from the second class are such that either R_0 or EGF_0 are below the capacity of both internalization pathways ($CDE_0 + CIE_0$) (Fig. 4.2B), whereas the third class reflects the case that both R_0 and EGF_0 exceed the capacity of both internalization pathways (Fig. 4.2C).

It can be seen that in case A, $R_{i,cie}$ -production stays close to zero. In case B, internalization via CIE does occur, albeit to a lesser degree than CDE. For case C, receptors are equally partitioned between CDE and CIE.

4.4 Conditions on receptor number for switch-effect of CIE-internalization

The simulations shown in Fig. 4.2 suggest conditions on the receptor number under which an EGF-dependent switch of CIE-internalization will occur. If a cell possesses less receptors than CDE-adaptors, CIE-internalization will be low independent of EGF-stimulation (cf. Fig. 4.2A). If the cell exhibits more receptors than adaptors for CDE, but less than for both pathways, then, for EGF-stimulations exceeding CDE_0 , a moderate fraction of receptor will internalize via CIE (cf. Fig. 4.2B). Finally, if the amount of receptors is higher than the combined capacity of both pathways, CIE-internalization will be switched on equally strong as CDE-internalization for EGF-stimulations that are higher than this combined capacity (cf. Fig. 4.2C).

To test this hypothesis, we performed the following virtual experiment. We chose three sets of initial values for receptor R , CDE- and CIE-adaptors such that they fall within the three respective classes: $R_0 < CDE_0$, $R_0 < CDE_0 + CIE_0$ or $CDE_0 + CIE_0 < R_0$, and stimulated the system with increasing amounts of EGF. Fig. 4.3 shows the steady-state amounts of $R_{i,cde}$ (blue) and $R_{i,cie}$ (green) as a function of EGF_0 .

¹Generally, X_0 denotes the initial value of variable X .

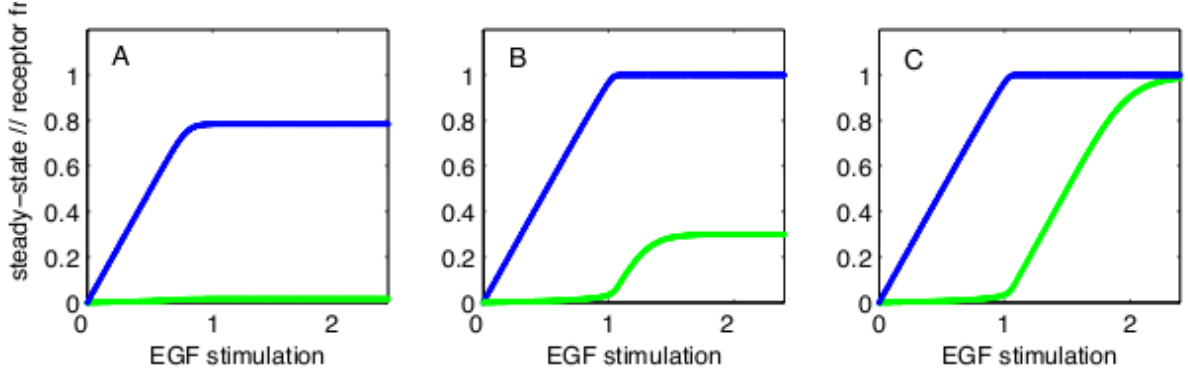


Figure 4.3: Plotted are steady-state values of R_{i_cde} (blue) and R_{i_cie} (green) as a function of EGF-stimulation (EGF_0). An ultrasensitive response of CIE-internalization with respect to EGF occurs if $R_0 > CDE_0$ (B) or $R_0 > CDE_0 + CIE_0$ (C), but not if $R_0 < CDE_0$ (A). In (B) and (C), when EGF_0 exceeds the amount of CDE_0 , CIE-internalization switches on abruptly, with a maximal response if $(CDE_0 + CIE_0) < \min\{EGF_0, R_0\}$ (C). In all three cases $CDE_0 = 1.0$, $CIE_0 = 1.0$ and (A) $R_0 = 0.8$, (B) $R_0 = 1.3$ and (C) $R_0 = 2.4$.

As predicted, for receptor levels lower than CDE_0 (4.3A), CIE-internalization stays close to zero, independently of EGF-stimulation. If the initial amount of receptors is greater than the capacity of CDE, CIE-internalization sets in abruptly, albeit to a moderate degree compared to CDE-internalization, for EGF-stimulations greater than CDE_0 (4.3B). Finally, if the initial number of receptors is greater than the capacity of both pathways, the CIE pathway switches on to an equal extent as CDE-internalization (4.3C).

We have thus derived an ultrasensitive response of CIE-internalization with respect to EGF-stimulation, without assuming any discriminative receptor modifications. Rather, it is necessary and sufficient that the initial amount of receptors is higher than the capacity of the CDE-pathway ($CDE_0 < R_0$, moderate switch) or both pathways ($CDE_0 + CIE_0 < R_0$, maximal switch).

4.5 Correspondence to distinct classes of steady-state

For dynamical systems with multiple steady-states, a certain steady-state will be reached depending on whether the system starts in the corresponding basin of attraction [46, 19]. Thus, a switch between steady-states occurs for different vectors of initial values, provided that the separatrix, i.e. the

hypersurface between neighboring basins of attraction, is crossed.

We investigated, whether the switch-effect of CIE-internalization corresponds to such a transition between distinct steady-states of the system. Analytically, one derives two classes of steady-states (see Methods for derivation of conditions):

$$(EGF^* = 0 \vee R^* = 0) \wedge R_EGF^* = 0, \quad (I)$$

$$CDE^* = 0 \wedge CIE^* = 0 \wedge R_EGF^* = \frac{k_f}{k_r} EGF^* * R^*, \quad (II)$$

where X^* denotes the steady-state concentration of the respective component.

Note that *classes* of steady-states are used since not all variables are assigned specific values. For example, in both cases $R_{i_cie}^*$ and $R_{i_cde}^*$ are not uniquely determined and depend on the corresponding initial values.

Steady-state class I reflects the case that either all available EGF ($EGF^* = 0$) or all free receptors R ($R^* = 0$) have been absorbed in the binding reaction and all activated receptors R_EGF have been internalized. In steady-state class II neither receptors nor ligand are limiting for the internalization process and have come to an equilibrium with R_EGF . Instead, the capacity of both internalization pathways has been depleted ($CIE^* = CDE^* = 0$).

The systematic scan of initial values and subsequent solving of the system until steady-state revealed initial conditions under which each steady-state class is reached. We found that if both EGF-stimulation and initial receptor level are higher than the capacity of both internalization pathways ($CDE_0 + CIE_0 < \min\{R_0, EGF_0\}$, initial value class C), the system tends towards steady-state class II. Otherwise, steady-state class I will be reached. In this case, if EGF-stimulation is below the amount of receptors, all EGF will be depleted in the binding reaction ($EGF^* = 0$), whereas if it is above, all receptors will be consumed ($R^* = 0$).

Note that for a given set of initial values the system exhibits exactly one steady-state. However, which one of the two analytically possible steady-state classes is reached depends on the relative

initial values	steady-state	CIE-internalization
$EGF_0 < CDE_0$	I	low
$CDE_0 + CIE_0 < EGF_0$	II	high

Table 4.2: Assuming that the initial number of receptors is higher than the combined capacity of both pathways ($R_0 > CDE_0 + CIE_0$), low and high EGF-stimulations lead to two different steady-states, respectively. In steady-state I, the receptor internalizes primarily via CDE, whereas in steady-state II it is equally partitioned between CDE and CIE.

initial values of the system as described (for details see protocol S1). In [172] it was reported that for high ligand concentrations, the activated receptor is equally partitioned between CDE and CIE. Assuming similar initial abundance levels of adaptors, our simulations show that this is the case for initial receptor levels higher than the sum of both initial adaptor values (Fig. 4.2C, Fig. 4.3C). We thus hypothesize that in cells, where the steady-state levels of internalized receptors via CIE and CDE are similar, the amount of receptors exceeds the capacity of both pathways. In this case, treatment of the cells with low vs high EGF-stimulations, corresponds to a transition of the system between steady-state classes I and II (see Table 4.2).

4.6 Conditions on initial values for steady-states

For a given set of initial values the system in Table 4.1 exhibits exactly one steady-state. However, which one of the two analytically possible steady-state classes is reached depends on the relative initial values of the system as described in the Results section. Briefly, if both EGF-stimulation and initial receptor level are higher than the capacity of both internalization pathways ($CDE_0 + CIE_0 < \min\{R_0, EGF_0\}$, initial value class C in Fig. 4.2 and Fig. 4.3), the system tends towards steady-state class II, i.e. $CDE^* = 0 \wedge CIE^* = 0 \wedge R_EGF^* = \frac{k_f}{k_r} EGF^* * R^*$. Otherwise, steady-state class I will be reached, with $(EGF^* = 0 \vee R^* = 0) \wedge R_EGF^* = 0$.

This is exemplified in Fig. 4.4, where the steady-state value of ligand-bound receptor (R_EGF^*) is plotted as a function of EGF-stimulation for different initial receptor levels R_0 . Here, $CIE_0 = CDE_0 = 1$. For $R_0 = 1.7$ (orange), i.e. $R_0 < CDE_0 + CIE_0$ (2), the system reaches steady-state class

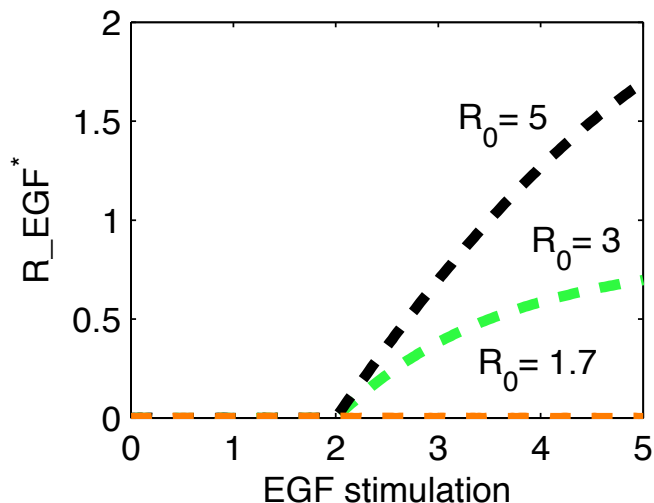


Figure 4.4: Plotted are steady-state values of ligand-bound receptor (R_{EGF^*}) as a function of EGF-stimulation for different initial receptor levels R_0 . If $R_0 < CDE_0 + CIE_0$ (orange curve), the system tends towards steady-state class I independently of the strength of EGF-stimulation (see text). Here, $CIE_0 = CDE_0 = 1$.

I independently of EGF-stimulation, as seen from $R_{EGF^*} = 0$. If $R_0 = 3$ (green) or $R_0 = 5$ (black), i.e. $CDE_0 + CIE_0 < R_0$, the steady-state value of R_{EGF} becomes positive for EGF-stimulations higher than 2 (steady-state class II).

4.7 New mechanism of ultrasensitivity - steepness of switch effect

An ultrasensitive response of a signaling system is characterized by a low, or damped response up to a certain threshold of stimulus, followed by an abrupt increase towards maximal response when this threshold is exceeded [46, 21, 187, 142]. Generally, a positive feedback or multisite-phosphorylation has been considered a prerequisite to achieve this kind of behaviour [90, 123, 8, 187, 139]. Ultrasensitivity has also been shown to arise in phosphorylation-dephosphorylation cycles if the enzymes operate near saturation [67], which makes the mechanism very sensitive to small parameter changes [21], or if the abundance levels of unphosphorylated substrate and kinase are sufficiently high (ultrasensitization,

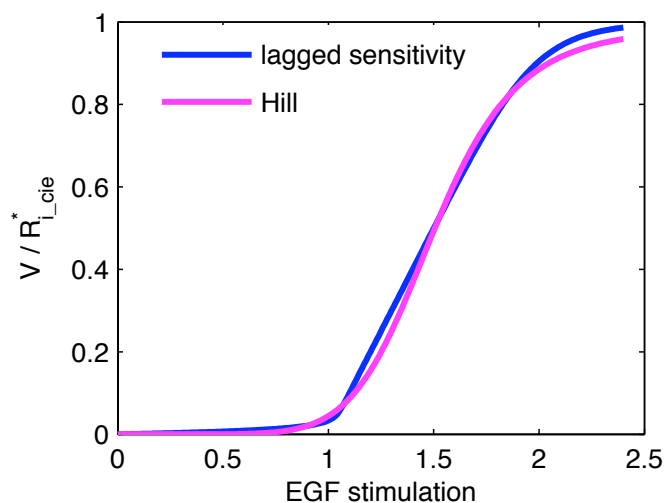


Figure 4.5: Comparison between Hill-type response and lagged sensitivity. Plotted are steady-state values of R_{i_cie} (lagged sensitivity) and reaction velocity V (Hill-kinetics). Parameter and initial values used were the same as for Fig. 4.3C. Hill-parameters extracted from the stimulus-response curve were: $h = 7.5$, $V_{max} = 1.0$, $K_m = 1.4$

[113]). Our model demonstrates that the even simpler module of a branching signaling molecule also results in ultrasensitivity.

To characterize the steepness of this 'lagged sensitivity module', we compared its response to a Hill-type reaction (see Methods).

Fig. 4.6 shows the reaction velocity V of the Hill-formula, compared to $R_{i_cie}^*$ -production of the lagged sensitivity module (stimulus-response curve) as a function of EGF-stimulation. To generate the stimulus-response curve, we chose the same parameter set as for Fig. 4.3C as a reference. From this curve we extracted the Hill-coefficient h , V_{max} and K_m to compute the corresponding Hill-curve, which will be used as a reference curve later on. Clearly, the lagged sensitivity module produces a comparably steep response as a Hill-reaction.

The Hill-kinetics given by equation (1) is merely a phenomenological model in that it includes no explication for the underlying mechanisms causing the ultrasensitivity. It primarily serves as a descriptive model that can be used to quantify the sigmoidality of a computed or measured response.

Contrary to that, biological interpretation substantiates the lagged sensitivity module. The ul-

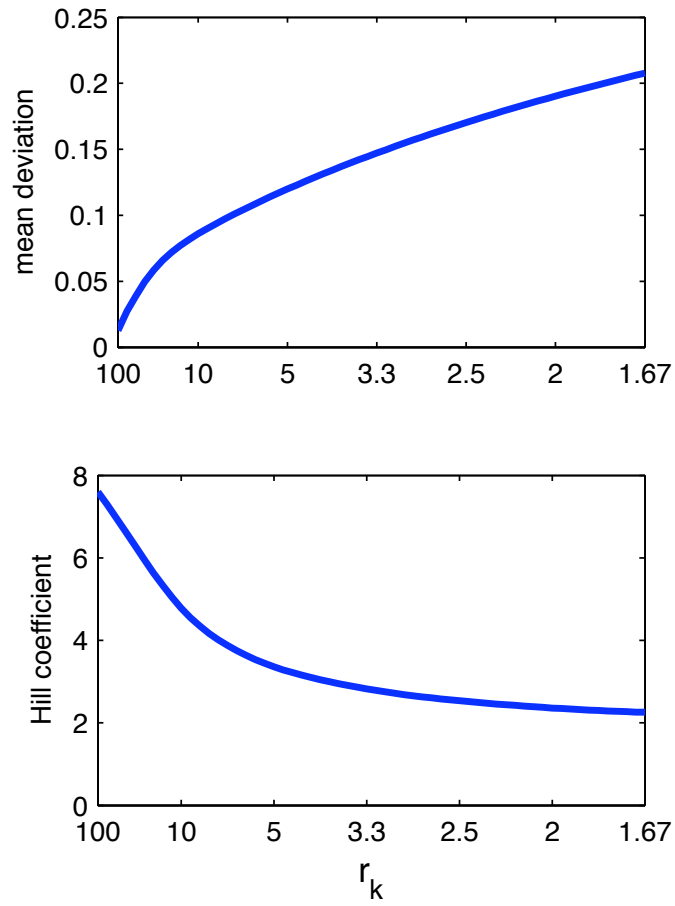


Figure 4.6: Comparison between Hill-type response and lagged sensitivity. Plotted are steady-state values of R_{i_cie} (lagged sensitivity) and reaction velocity V (Hill-kinetics). Parameter and initial values used were the same as for Fig. 4.3C. Hill-parameters extracted from the stimulus-response curve were: $h = 7.5$, $V_{max} = 1.0$, $K_m = 1.4$

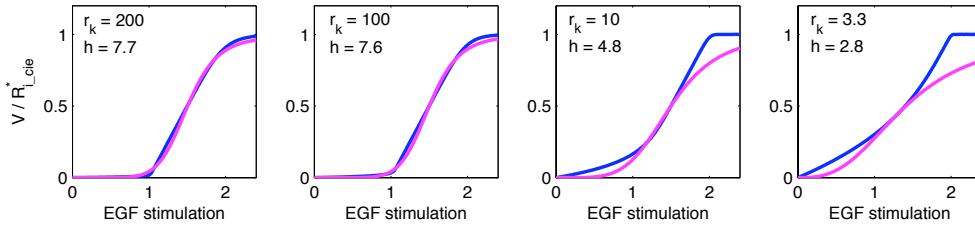


Figure 4.7: Comparison between stimulus-response curve (with Hill-coefficient h) and corresponding Hill-curve for selected r_k values. Here, $k_{cde} = 1.0$ and k_{cie} was varied. Plotted are steady-state values of $R_{i,cie}$ (lagged sensitivity, blue) or reaction velocity V (Hill-kinetics, magenta)

trasensitivity is caused by the higher binding kinetics with which the EGF receptor enters CDE. The threshold EGF concentration of CIE-internalization corresponds to the initial amount of CDE-adaptors. Finally, the model predicts that the initial number of free receptors must be higher than the capacity of CDE in order to observe CIE-internalization at high EGF-concentrations (Fig. 4.3).

4.8 Robustness of solution

It has been argued that biologically functional modules or pathways need to be robust against variations of reaction parameters and protein concentrations in order to ensure proper functioning [78]. The concept of robustness refers to the 'purpose' of a certain module or pathway: it is expected that intracellular network structures have undergone an evolution that guarantees their proper functioning independently of precise parameter values [78].

To transfer this concept to the question of receptor sorting into alternative pathways, we asked to what extent the functioning of the here described module depends on exact parameter or initial values. As $\hat{\text{functioning}}$ we defined the clear-cut sorting of the receptor into distinct routes, namely CDE at low, respectively CDE and CIE at high ligand concentrations.

The key parameter and initial concentrations that affect the strength of the switch effect are the initial concentrations of CDE- and CIE-adaptors as well as $r_k = \frac{k_{cde}}{k_{cie}}$. Obviously, the ultrasensitive response will be steeper the higher the difference in binding kinetics for the respective pathways is,

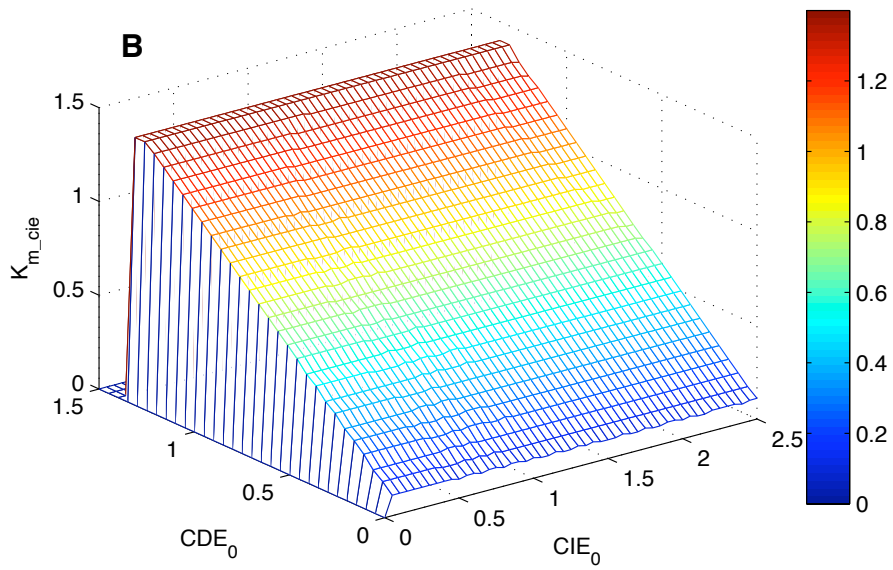
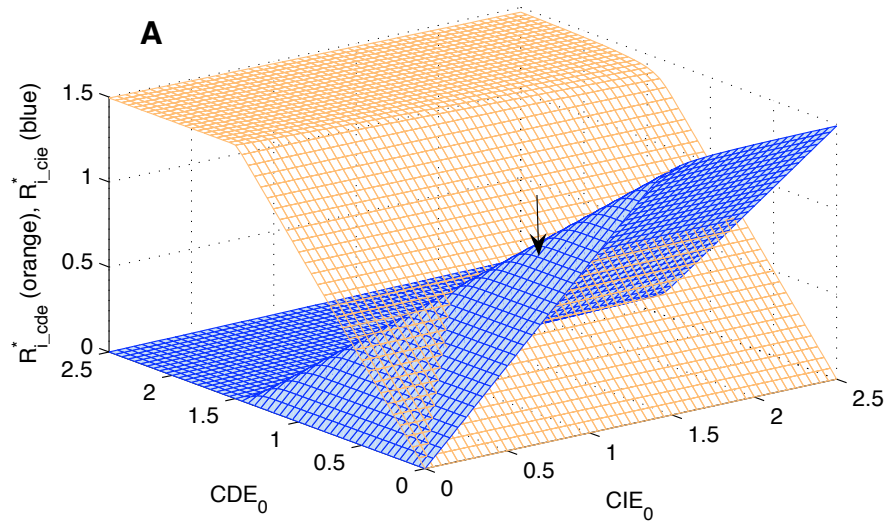


Figure 4.8: Plotted are $R_{l_{cie}}^*$ (blue) and $R_{l_{cde}}^*$ (orange) as a function of CDE_0 and CIE_0 . $EGF_0 = R_0 = 1.5$. See text for interpretation.

i.e. the greater r_k . We systematically varied r_k and from each thus obtained stimulus response curve of $R_{i_cie}^*$ -values extracted the Hill-coefficient h as a measure of steepness (see Methods). We also computed the mean deviation between the obtained stimulus response curves and the reference Hill-curve (Fig. 4.7), showing that for considerable variations of r_k the stimulus-response curve remains approximable by a Hill-curve.

In Fig 4.8A we plotted the steady-state values of R_{i_cde} and R_{i_cie} (V_{max} values of the stimulus-response curves) as a function of initial adaptor values CDE_0 and CIE_0 . Here, R_0 and EGF_0 were chosen 1.5. Consider the curve for $R_{i_cie}^*$ (blue). For initial adaptor values such that $CDE_0 + CIE_0 < R_0$, EGF_0 (see arrow), the curve is largely independent of CDE_0 and increases linearly as a function of CIE_0 up to the threshold of 1.5. The independence of CDE_0 reflects the fact that if neither receptors nor ligand are limiting for the internalization reaction (steady-state class II), the steady-state amount of receptor internalized via CIE is solely dependent on the initially available number of CIE-adaptors. Outside of this range, $R_{i_cie}^*$ decreases with increasing CDE_0 and becomes zero for $CDE_0 > 1.5$ (cf. Fig 4.3A). $R_{i_cde}^*$ (orange curve) is largely independent of CIE_0 and increases linearly with CDE_0 up to the threshold of 1.5 when ligand or receptor number become limiting.

The threshold of CIE-internalization (K_m of the stimulus-response curves) is independent of CIE_0 (for $CIE_0 > 0$) and is equal to CDE_0 as shown in Fig 4.8B.

4.9 Role of Receptor modifications

It is well-known that ligand-induced receptor modifications in the form of phosphorylation and/or ubiquitination play a functional role in signaling and contribute to the specificity of adaptor-binding. However, our analysis focused on the question, whether for a precise sorting of receptors into the two alternative endocytosis pathways discussed here a *discriminative* modification is necessary. In this light, R_EGF , which in our model indicates the activated receptor species capable of interacting with the endocytosis adaptors, could also represent an already modified form of the receptor. To illustrate this point, we extended the model as given in Table 4.1 to include the binding of the

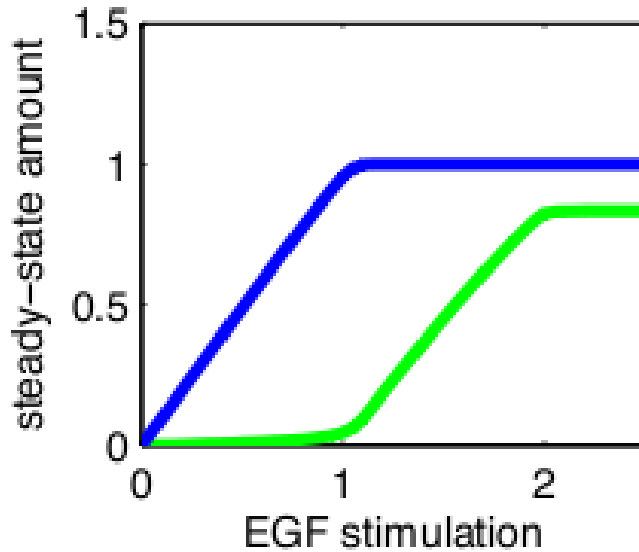


Figure 4.9: Plotted are steady-state values of $R_{i,cd\epsilon}$ (blue) and $R_{i,cie}$ (green) as a function of EGF-stimulation (EGF_0) for the extended model, including receptor ubiquitination. The switch effect is preserved under the assumption of receptor modifications.

ubiquitin-ligase Cbl followed by ubiquitination of the receptor (see protocol S2 for equations). Again, we tested whether the assumption that both pathways consume the thus modified, i.e. the same, form of receptor would comply with the observation of an ultrasensitive response of CIE-internalization to increasing EGF-stimulation (see Fig. S4.9). We found that the response of CIE is comparably steep as for the previous, simpler model (Fig. 4.3C), proving that the existence of receptor modifications prior to internalization does not affect our results.

4.10 Ultrasensitivity with inclusion of receptor modification

We extended the model in Table 4.1 for binding of the ubiquitin-ligase Cbl and subsequent ubiquitination as an example of ligand-induced receptor modification. For this, we assumed Ubiquitin (Ub) to be present in non-limiting amounts, so that the differential equations for the extended model read:

$$d(\text{EGF})/dt = -k_f * \text{EGF} * R + k_r * R_EGF \quad (4.10.1)$$

$$d(R)/dt = -k_f * \text{EGF} * R + k_r * R_EGF \quad (4.10.2)$$

$$\begin{aligned} d(R_EGF)/dt &= k_f * \text{EGF} * R - k_r * R_EGF \\ &\quad -k_{\text{onCbl}} * R_EGF * \text{Cbl} \\ &\quad +k_{\text{offCbl}} * R_EGF_Cbl \end{aligned} \quad (4.10.3)$$

$$\begin{aligned} d(\text{Cbl})/dt &= -k_{\text{onCbl}} * R_EGF * \text{Cbl} \\ &\quad +k_{\text{offCbl}} * R_EGF_Cbl \\ &\quad +k_{\text{catCbl}} * R_EGF_Cbl \end{aligned} \quad (4.10.4)$$

$$\begin{aligned} d(R_EGF_Cbl)/dt &= k_{\text{onCbl}} * R_EGF * \text{Cbl} \\ &\quad -k_{\text{offCbl}} * R_EGF_Cbl \\ &\quad -k_{\text{catCbl}} * R_EGF_Cbl \end{aligned} \quad (4.10.5)$$

$$\begin{aligned} d(R_EGF_Ub)/dt &= k_{\text{catCbl}} * R_EGF_Cbl \\ &\quad -k_{\text{cde}} * R_EGF_Ub * \text{CDE} \\ &\quad -k_{\text{cie}} * R_EGF_Ub * \text{CIE} \end{aligned} \quad (4.10.6)$$

$$d(\text{CDE})/dt = -k_{\text{cde}} * R_EGF_Ub * \text{CDE} \quad (4.10.7)$$

Here, k_{onCbl} and k_{offCbl} are the rate constants for the association and dissociation of Cbl to ligand-bound receptor R_EGF, and k_{catCbl} is the rate of the ubiquitination step. In Fig. 4.9 we plotted the steady-state values of receptor internalized via CDE ($R_{i,\text{cde}}$, blue) and CIE ($R_{i,\text{cie}}$, green), respectively. Clearly, the response is comparable to the results of the simpler model (Fig 4.3 C). The rate constants and initial values : $k_f = 1.0$, $k_r = 0.01$, $k_{\text{onCbl}} = 1.0$, $k_{\text{offCbl}} = 0.01$, $k_{\text{catCbl}} = 1.0$, $k_{\text{cde}} = 1.0$, $k_{\text{cie}} = 0.01$, $R_0 = 2.0$, $\text{Cbl}_0 = 2.0$, $\text{CDE}_0 = 1.0$, $\text{CIE}_0 = 1.6$. All other initial values are zero.

4.11 Discussion

Our analysis reveals that a simple activation reaction (ligand binding) with subsequent branching of the activated molecule (receptor) is capable of producing nontrivial dynamics such as ultrasensitivity.

Generally, a feedback-loop, multisite-modification or cooperative binding mechanisms are assumed to be a prerequisite for such a behaviour [139, 187, 8, 90, 123, 128]. In particular, for the EGF receptor, a cooperative binding effect of the ubiquitin-ligase Cbl during the ubiquitination reaction has been proposed to be necessary for the observed switch-effect of CIE internalization [70]. Our analysis reveals that imposing weaker assumptions on the internalization machinery, namely that the two pathways are entered with distinct affinities, is sufficient to explain the observed switch-effect.

The lack of knowledge about the true parameter/initial values was accounted for by systematic variations over broad numerical ranges. The robustness of the switch-effect to exact parameter values argues for the plausibility of the introduced mechanism.

Mathematical models addressing the problem of receptor sorting into alternative endocytosis pathways do not currently exist. Previously proposed hypotheses based on experimental data only have not been able to give a satisfying answer to this question [111, 88, 2, 172, 55, 73, 71]. Generally, the problem is considered at the 'single-molecule-level' : a single receptor is envisioned, which is thought to enter either the CDE- or the CIE-route (see Figure 4.1). This picture misleadingly implies the necessity of a discriminative receptor modification.

Instead of thinking in terms of individual entities, we propose to consider the dynamical properties

of a system of interacting molecule *populations*. Applying methods from the theory of dynamical systems, we were able to conceive that an increase in the ligand concentration above the capacity of the CDE-pathway qualitatively alters the system behaviour by enforcing an alternative steady-state (Fig. 4.3, Table 4.2). Our model states that an abrupt, switch-like start of CIE occurs if the extracellular EGF concentration exceeds the capacity of the CDE machinery. This proposes an interesting implication of the regulation of receptor sorting: the cell achieves the switch-effect 'for free' since no extra cost has to be invested into a discriminative receptor modification. It can be assumed that cells have evolved to optimize energy efficiency [39]. Utilizing the kind of dynamics introduced here, where just one form of receptor is consumed by both pathways, could thus constitute an evolutionary advantage.

A second major observation we draw from the model is that the lagged sensitivity mechanism provides a means for an individual cell to sense its surrounding medium: clathrin-independent endocytosis is switched on precisely when the extracellular ligand concentration exceeds the number of CDE-adaptors. One might interpret this mechanism as a protein module, i.e. a small interaction network acting as a computational element, whose purpose is to store and process information [22, 79, 19].

One might argue that the simplicity of the model impairs its ability to uncover unanticipated results. While an initiation of clathrin-independent endocytosis upon saturation of the clathrin pathway might have been proposed without mathematical modeling, the unexpected steepness of this switching-behaviour as well as its robustness could not have been revealed by intuition alone [2, 111, 55]. Furthermore, we showed that extending the model by allowing a modification of the receptor does not increase the steepness of the response. Thus, we conclude that a modification of receptor is not required to discriminate between the pathways. This does notably not exclude the possibility that a modification of the receptor might have been chosen by nature to ensure proper endocytic sorting.

Finally, we want to emphasize that the generality of our model makes it applicable to ultrasensitivity in signaling processes other than the here discussed problem of receptor sorting. In fact, an

ultrasensitive response will emerge from any cellular situation, in which a key branching molecule (e.g. activated receptor R.EGF) alternatively binds two types of molecules (e.g. CDE or CIE), one of them with a much greater affinity (e.g. $k_{cde} \gg k_{cie}$). The complex corresponding to the low affinity binding (e.g. $R_{i,cie}$) will only be produced significantly if the amount of the branching molecule exceeds the initial amount of the dominant binding partner (e.g. CDE_0).

In summary, we revealed the dynamical consequences of an interaction motif, whose molecular basis has already been well established experimentally. Our mathematical model not only reproduces well-known experimental findings. It rather describes the sorting of receptors into different endocytosis routes and provides a novel explanation for achieving an ultrasensitive response of CIE without assuming any receptor modification to discriminate between the pathways. Because of the weak assumptions underlying our model we conclude that the here described mechanism of lagged sensitivity might be a general motif of ultrasensitivity in cellular signaling in contexts other than EGF receptor endocytosis.

Chapter 5

Experimental investigation of EGF receptor sorting into clathrin- vs. caveolin-dependent endocytosis

In order to experimentally test the theoretical prediction derived in the previous chapter, we monitored EGF-induced EGFR endocytosis by confocal microscopy using Rhodamine-tagged EGF. We used an automated imaging approach to detect features of the internalized vesicles over time, such as size and intensity (sections 5.1 and 5.2). In order to describe endocytic trafficking we evaluated colocalization of Rhodamine-EGF with Clathrin or Caveolin at various stages along the endocytic route in HeLa cells stably expressing GFP-tagged versions of these proteins. We found that while Rhodamine-EGF strongly colocalizes with GFP-Clathrin at early time points of induction ($\leq 2\text{min}$), colocalization with GFP-Caveolin mainly occurs most pronouncedly at stages *after* the actual internalization step ($> 2\text{min}$) (section 5.2). To further elucidate the role of Clathrin or Caveolin during EGFR endocytosis we selectively inhibited the clathrin-mediated pathways by overexpression of a AP180 truncation (AP180-mut)[207, 59] or the caveolin-pathway by RNA interference against Caveolin-1. We found

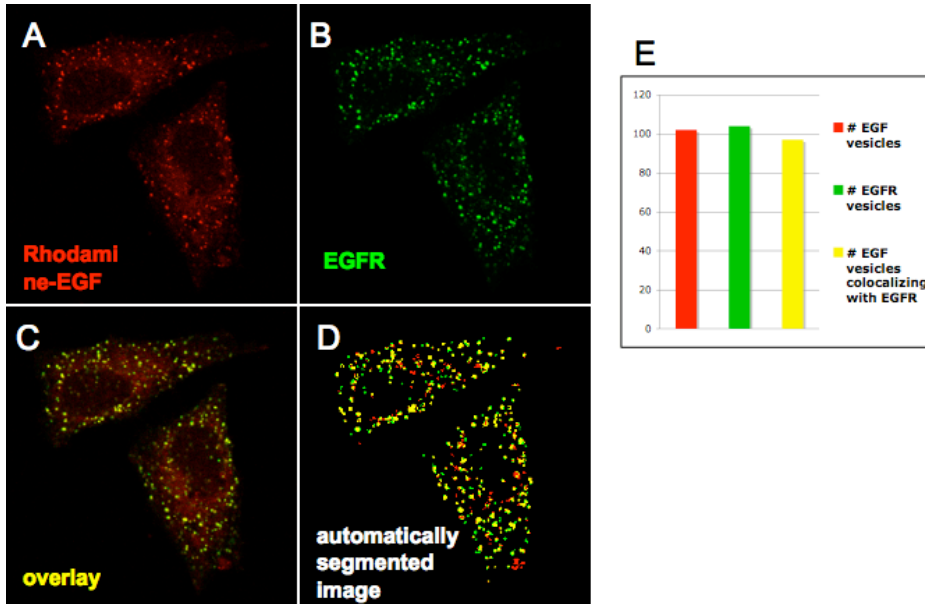


Figure 5.1: **Automated detection of vesicles and colocalization** HaCat cells were stimulated with 100 ng/ml Rhodamine-EGF (A) for 15 minutes and then stained for EGFR (B) by immunofluorescence. Colocalization is indicated in yellow in the overlay (C) as well as the segmented image (D) as produced by *ColocalizationFinder.java*. (E) shows detected number of EGF (red), EGFR (green) and EGF vesicles colocalizing with EGFR (yellow)

that while overexpression of AP180-mut effectively prevented EGF as well as Transferrin uptake, downregulation of caveolin-1 did not inhibit EGF internalization (section 5.3.1). This, together with the results of colocalization, suggests that caveolin participates in EGFR intracellular trafficking rather than internalization.

5.1 *ColocalizationFinder*: an ImageJ plugin for automated image analysis of vesicle features and colocalization

In order to be able to extract characteristics about endosomes, such as size and colocalization with endocytic markers, we developed a JAVA-based programme, *ColocalizationFinder.java*. The running program, full source code as well as a HTML-documentation can be found under <http://www.ibios.dkfz.de/schmidt-glenewinkel>.

In order to test (a) the ability of our image analysis tool to detect colocalization as well as (b) identify the timeline for which EGF remains associated with EGFR upon internalization, we stimulated cells with Rhodamine-EGF for various timepoints and used antibody staining against EGFR.

As a control to test the segmentation and colocalization results as produced by the software, we used cells stimulated with Rhodamine-EGF for 20 minutes and stained for EGFR by immunofluorescence (Figure 5.1). We expect to detect similar numbers of vesicles in each channel as well as close to 100% colocalization. As can be seen, the software faithfully detects vesicles numbers as well as colocalization events,

We conclude that our imaging tool is suited for automated detection of colocalization. Further, Rhodamine-EGF can be used as a marker for internalized EGFR until at least 20 minutes upon internalization.

5.2 EGF colocalizes with GFP-Clathrin at early and with GFP-Caveolin at later timepoints upon internalization

In HeLa cells, clathrin-dependent as well as clathrin-independent/caveolae endocytosis pathways have been described [172, 99].

Endocytosis consists of various steps, including translocation of ligand-bound receptors within the membrane prior to the actual internalization step, followed by intracellular trafficking to certain destinations [88, 43]. In order to elucidate at which steps of these processes clathrin or caveolin pathways play a role, we determined colocalization of EGF with clathrin or caveolin at various time points of stimulation. For this, we used HeLa cells stably expressing either GFP-Caveolin (GFP-Cav cells) or GFP-Clathrin Light Chain (CLC) (GFP-Clath cells) that were stimulated with Rhodamine-EGF and imaged by confocal microscopy to assess at which timepoints of after induction, the receptor was following which endocytosis pathway.

Figures 5.2 and 5.3 show microscopy results of GFP-Clath or GFP-Cav cells stimulated with

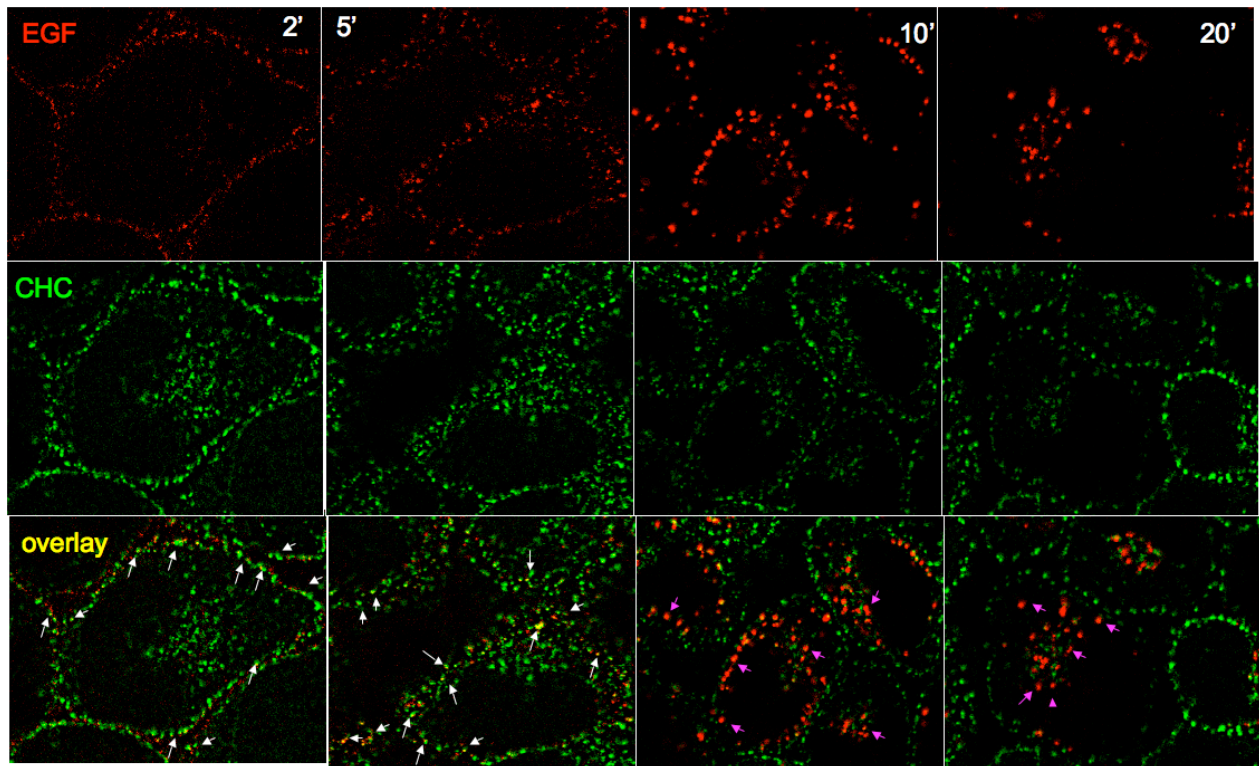


Figure 5.2: GFP-Clath HeLa cells were stimulated with 100 ng/ml Rhodamine-EGF for the indicated time points, fixed and imaged as described. Images were background subtracted (see section 5.1). Colocalization is indicated in yellow and marked with white arrows. Purple arrows indicate the loss of colocalization of EGF with clathrin in late endosomes (≥ 10 minutes)

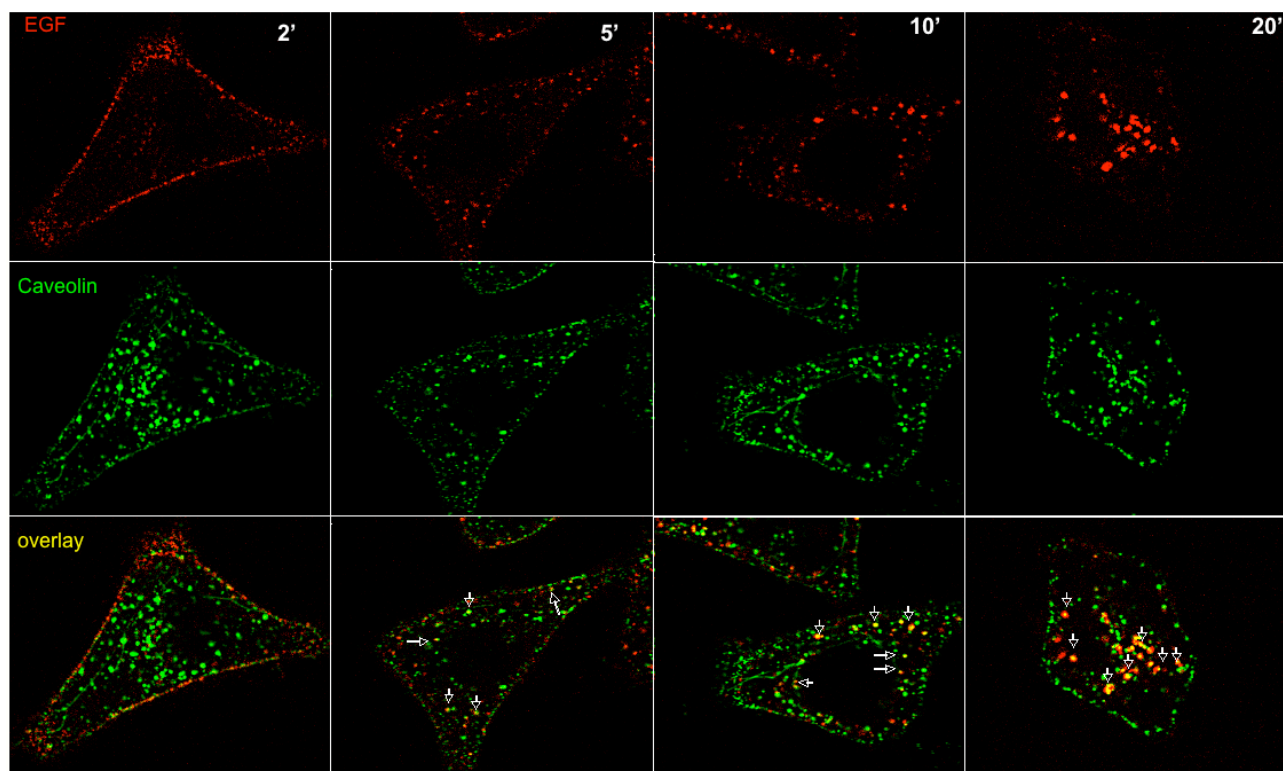


Figure 5.3: GFP-Cav HeLa cells were stimulated with 100 ng/ml Rhodamine-EGF for the indicated time points, fixed and imaged as described. Images were background subtracted (see section 5.1). Colocalization is indicated in yellow and marked with white arrows.

100 ng/ml Rhodamine-EGF for the indicated timepoints, respectively. Prior to imaging, cells were fixed. Shown are background subtracted images of the GFP and Rhodamine channels as well as the overlay. Colocalization is indicated in in yellow. White arrows mark EGF vesicles colocalizing with GFP-Caveolin (Figure 5.3) or GFP-Clathrin (5.2).

It can be seen that shortly after stimulation (< 2 minutes), EGF vesicles begin to form. At these early time points, these endomes are characterized by a small size and a close location to the plasma membrane. At longer time point of stimulation, the EGF vesicles increase in size, which is due to fusion processes [88, 129]. This maturation from early to late endosomes is accompanied by a translocation from the plasma membrane to the perinuclear region of the cell.

Figure 5.2 shows that colocalization of EGF and Clathrin occurs immediately upon internalization (2 min). These EGF vesicles which colocalize with Clathrin and form right after internalization, are typically small and are located close to the plasma membrane (Figure 5.2 (2') (colocalization is marked with white arrows) and Figure 5.4, upper row). As vesicles mature, the colocalization with clathrin is lost (Figure 5.2 (> 10 minutes), indicated by purple arrows.).

The opposite is observed when co-trafficking of EGF with GFP-Caveolin is monitored (Figure 5.3). After 2 minutes of stimulation, very little colocalization is observed (white arrows). At later timepoints of stimulation, however, the typical larger EGF vesicles frequently colocalize with Caveolin (purple arrows) in Figure 5.3.

Figure 5.4 illustrates this again. Shown are GFP-clath (upper row) or GFP-cav (lower row) cells that were stimulated with 100 ng/ml Rhodamine-EGF for 2 (left) or 20 (right) minutes. Colocalization is shown in yellow and marked with white arrows. It can be seen that while at 2 minutes strong colocalization is observed between clathrin and EGF, only little colocalization between EGF and caveolin occurs. At 20 minutes, this relationship is shifted and colocalization of EGF is strongest with caveolin.

These results suggest that whereas clathrin is mainly involved in the actual internalization step, caveolin might predominantly function in intracellular trafficking of EGF containing vesicles.

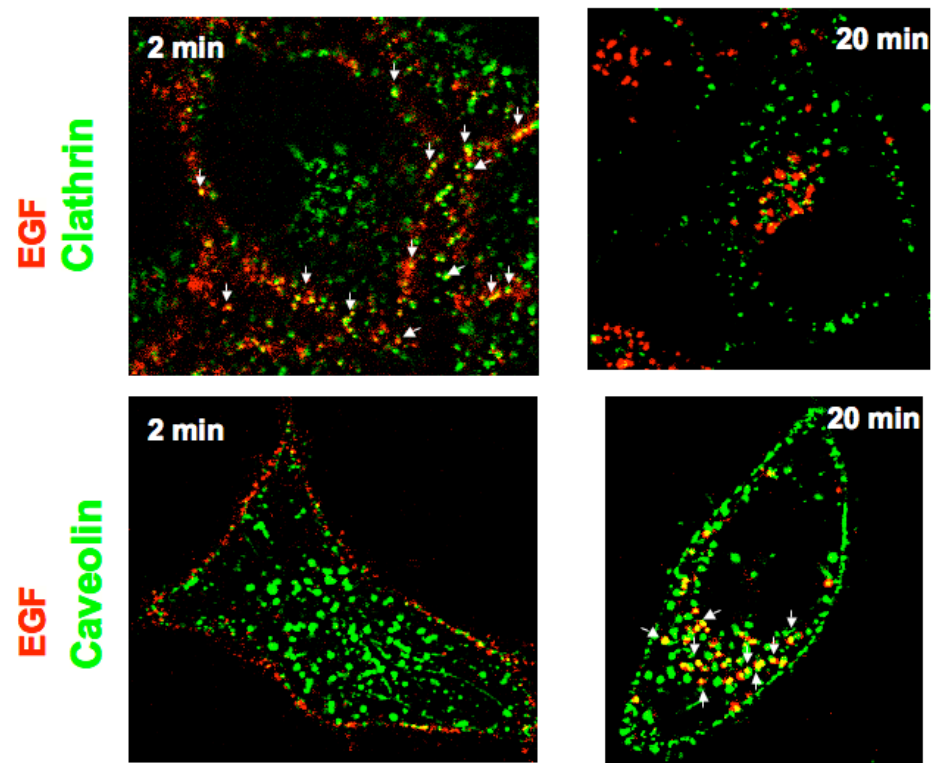


Figure 5.4: GFP-Clath (upper row) or GFP-Cav (lower row) HeLa cells were stimulated with 100 ng/ml Rhodamine-EGF for the 2 (left) or 20 minutes (right), fixed and imaged as described. Shown are the segmented images. Colocalization is shown in yellow and indicated by white arrows.

Cotrafficking of EGF- and Caveolin-vesicles

The maturation of internalized EGF vesicles from early to late endosomes is characterized by an increase in vesicle size due to fusion events. Since we observed that EGF vesicles colocalized with Caveolin along the endocytic route we asked whether the increase in size of EGF vesicles is also reflected in the population of caveolin vesicles which colocalized with EGF.

To determine this we stimulated GFP-Cav cells with Rhodamine-EGF for different time lengths, fixed and imaged the cells. Figure 5.5 shows original images (upper row) as well as segmented images (lower row). Shown are overlay images of DAPI (blue), Caveolin (green) and EGF (red), colocalization between EGF and Caveolin is indicated in yellow. The typical increase in size of EGF vesicles is accompanied by an increase of size of the colocalizing caveolin vesicles.

From the segmented images we extracted the sizes of EGF or caveolin vesicles. Figure 5.6A shows the average size of EGF (red) or Caveolin (green) vesicles at indicated time points of stimulation. Plotted are the mean values of ca 60 cells (see Material and Methods), errorbars denote standard deviation between three repetitions. It can be seen that while EGF vesicles increase in size over time, the size of the Caveolin vesicle population remains largely unaltered. Nevertheless, Figure 5.5B shows the same plot, separated into the Caveolin vesicles that do (Δ) or do not colocalize with an EGF vesicle (∇). We see that the EGF-colocalizing Caveolin vesicles mimic the behaviour of the EGF vesicles in that they increase in size over time.

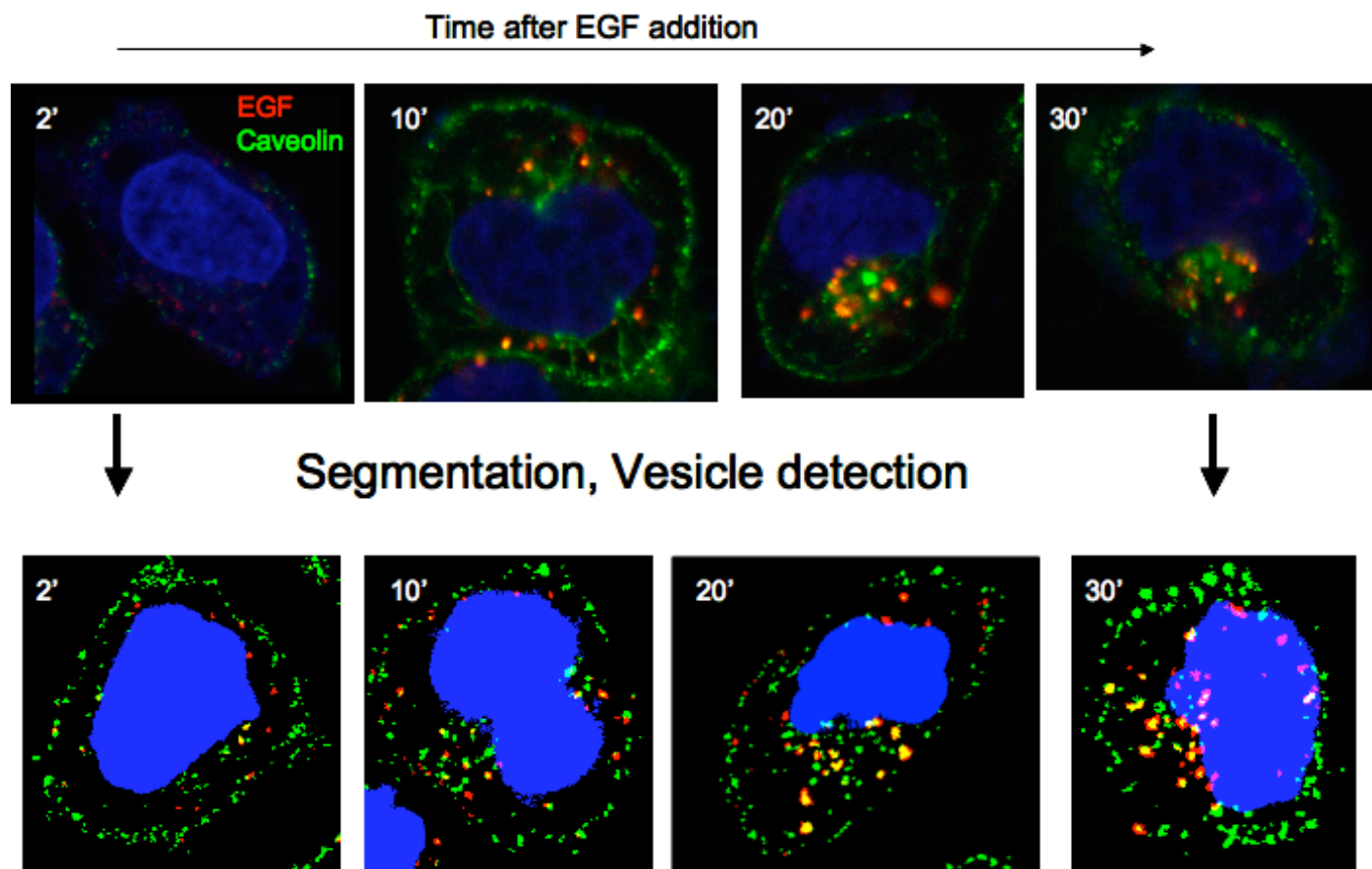


Figure 5.5:

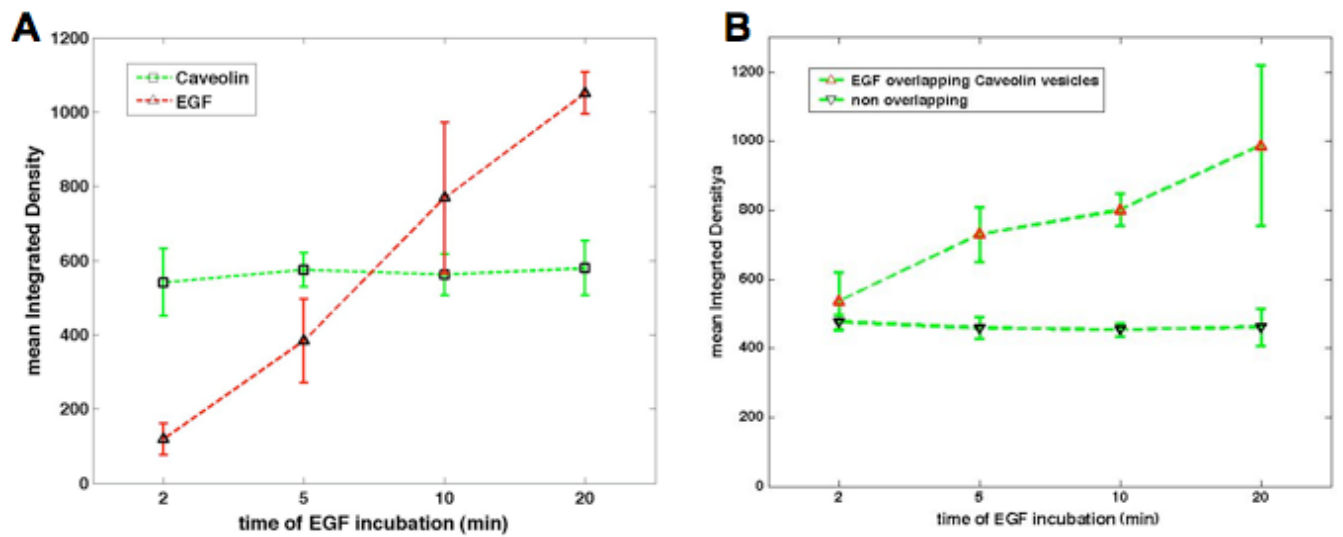


Figure 5.6: **Caveolin-1 vesicles colocalizing with Rhodamine-EGF increase in size over time** GFP-Cav HeLa cells were stimulated with 100ng/ml Rhodamine-EGF and fixed at the indicated timepoints. Intensities of Rhodamine-EGF or GFP-Caveolin vesicles were determined as described. (A) Intensities of EGF vesicles (red) or Caveolin vesicles (green) at indicated timepoints of EGF stimulation. (B) Intensities of Caveolin vesicles that do (Δ) or do not colocalize with an EGF vesicle (∇) at indicated timepoints of EGF stimulation. Plotted are the mean values of 60 cells, errorbar denote standard deviation.

5.3 Effect of inhibition of clathrin-mediated endocytosis or Caveolin-1 expression on EGF uptake and endocytic trafficking

5.3.1 RNAi-knockdown of Caveolin does not reduce EGF uptake but interferes with intracellular trafficking

While it seems clear that there are pathways that lead from the membrane to the cell interior which are clathrin-independent [149, 146, 159], the role of these pathways in EGFR endocytosis is controversial. Some groups report that caveolin participates in the internalization step of EGFR and in fact constitutes a pathway separable from clathrin-mediated endocytosis [172, 99, 149]. What speaks against this model are reports that upon disruption of Caveolin-mediated trafficking using a chemical inhibitor Nystatin, which depletes cholesterol from membrane and should thus disrupt lipid raft/caveolae regions, EGF uptake is unaltered [98]. Further, through inhibition of clathrin-mediated endocytosis by RNAi-mediated depletion of clathrin, EGF uptake is reduced efficiently, arguing against the existence of an alternative pathway [87, 92].

We used an RNAi approach against Caveolin to investigate whether it is directly participating in internalization of the receptor or whether its role is more in the intracellular trafficking of the internalized receptor-ligand complex.

We first tested the efficiency of the shRNA to inhibit Caveolin expression in GFP-Cav cells. Figure 5.7 shows GFP-Cav cells transfected with shRNAi against Caveolin (left) or control DNA (right). Cells from the same experiment were subjected to flow cytometry, see Figure 5.8. Figure 5.8 A (C) and B (D) show histograms and scatterplots of cells transfected with control (Caveolin) shRNA, respectively. E shows the quantification of GFP signal of gated cells.

GFP-Cav cells were estimated to express GFP-Caveolin at levels similar to the endogenous form [147]. The flow cytometry as well as microscopy measurements suggested that the RNAi-induced

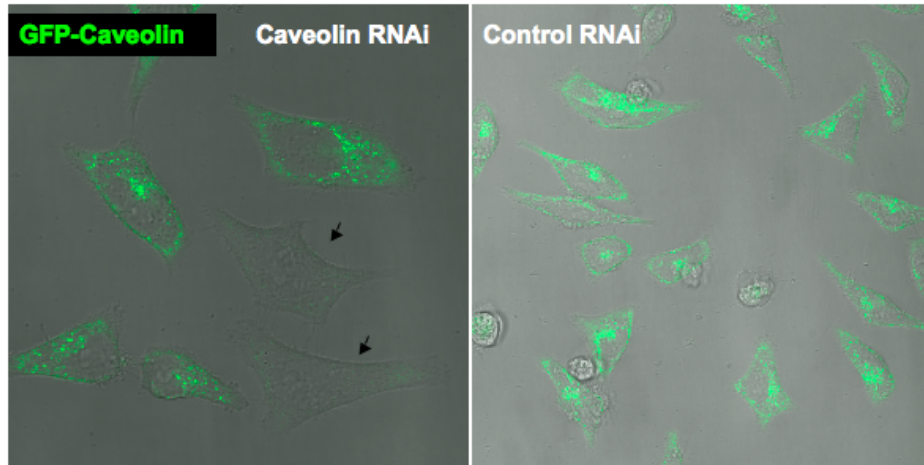


Figure 5.7: **Expression of RNAi inhibits GFP-Caveolin expression (microscopy)** Cells were treated as in Figure 5.8 and imaged by confocal microscopy. Transfected cells are marked by arrows.

downregulation of Caveolin is efficient in that transfected cells practically showed no GFP signal (cf. Figure 5.7 and Figure 5.8E). It is assumed that the RNAi targets the GFP- as well as the endogenous form in a non-discriminative manner and we thus expect that in RNAi-transfected cells overall Caveolin production is reduced efficiently.

We first evaluated the effect of Caveolin inhibition on intracellular trafficking of EGF. Figure 5.9 shows GFP-Cav cells that were transfected with control DNA (upper row) or shRNA against Caveolin-1 (lower row) and treated with 100 ng/ml Rhodamine-EGF for the indicated time points. Shown are segmented images. Control cells showed the typical trafficking behaviour: Vesicles colocalized with caveolin as they moved away from the plasma membrane, towards the perinuclear region of the cells (indicated by purple arrows). In Caveolin RNAi transfected cells (Figure 5.9, lower row) the morphology as well as localization of EGF vesicles began to differ from that in control cells starting at around 10-15 minutes of stimulation. At 5 minutes of stimulation EGF vesicles appeared normally: internalized vesicles formed and were localized in the cell periphery. However, at 15 minutes of EGF stimulation, EGF vesicles were still largely localized in the membrane near region (marked with white arrows). Further, after 30 minutes of stimulation, while in control cells EGF vesicles showed the typical appearance of late endosomes (increased size, localization to cell interior), vesicles in RNAi-positive

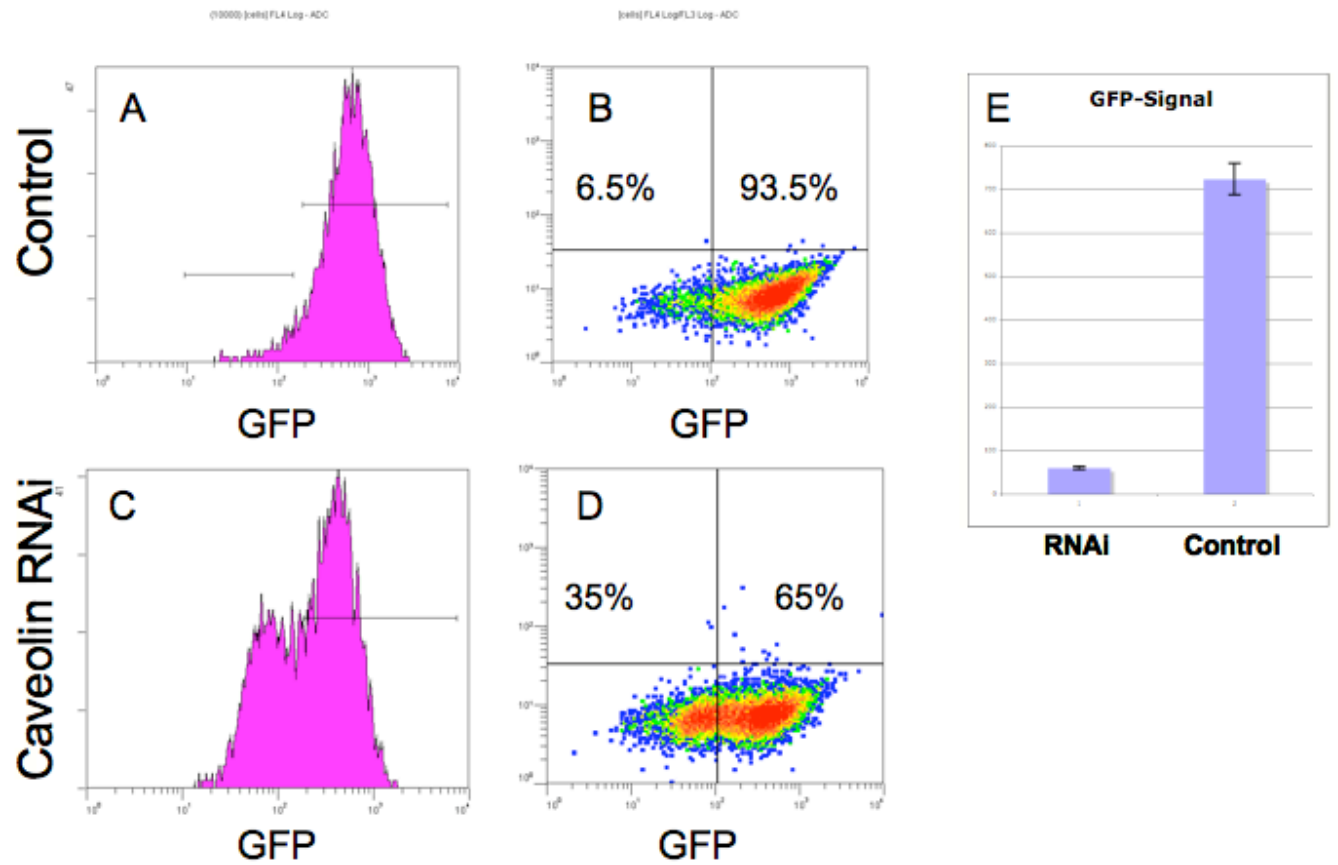


Figure 5.8: **Expression of RNAi inhibits GFP-Caveolin expression (FC)** GFP-Cav HeLa cells were transfected with control DNA (A, B) or shRNA against Caveolin (C, D). Shown are histograms (A, C) or scatterplots (B, D) of GFP signal.

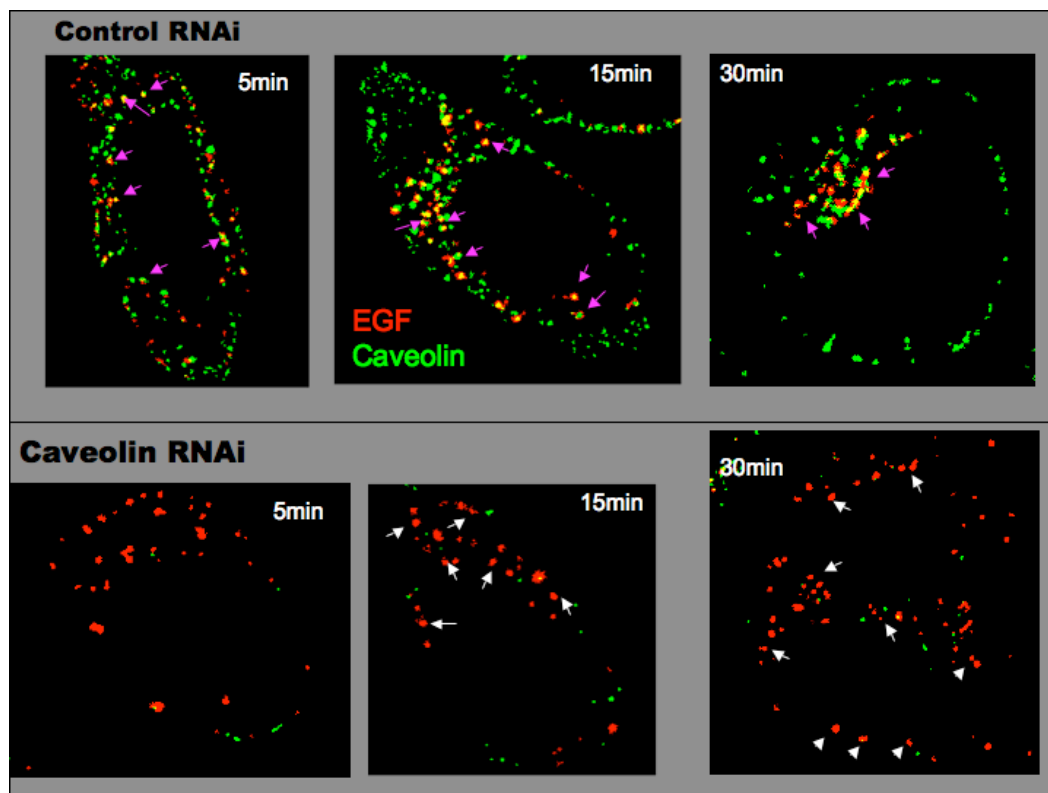


Figure 5.9: **Effect of Caveolin downregulation on EGF trafficking** GFP-Cav HeLa cells were transfected with control DNA (upper row) or shRNA against Caveolin-1 (lower row) and treated with 100 ng/ml Rhodamine-EGF for the indicated time points, fixed and imaged.

cells remained small in size and did not progress to the perinuclear region (purple arrows). These results suggest that presence of Caveolin is not necessary for internalization of EGF but is needed for proper trafficking along the endocytic route.

To further test the hypothesis that Caveolin is not needed for the actual internalization step of EGFR, we utilized (normal) HeLa cells transfected with the Caveolin shRNA. In order to be able to select those cells that were transfected by the DNA, we co-transfected the cells with BFP. The BFP signal can then be used in flow cytometry to select the cells that are transfected with the shRNA. First, we tested the cotransfection approach in GFP-Cav cell co-transfected with BFP and shRNA (Figure 5.10) GFP-Cav HeLa cells were co-transfected with BFP and shRNA against Caveolin-1 (upper row) or control DNA (lower row) in a ratio of 1:2. Shown are histograms of BFP (left) or GFP signal

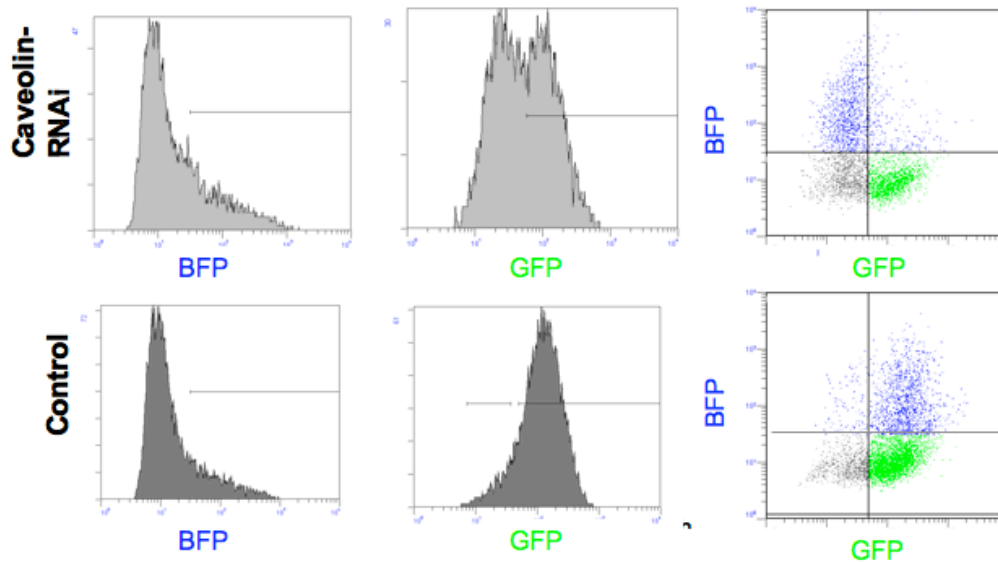


Figure 5.10: **Cotransfection with BFP can be used as marker for shRNA** GFP-Cav HeLa cells were co-transfected with BFP and shRNA against Caveolin-1 (upper row) or control DNA (lower row) in a ratio of 1:2. Shown are histograms of BFP (left) or GFP signal (middle), as well as scatterplots of the two (right panel, with GFP or BFP positive cells).

(middle), as well as scatterplots of the two (right pane, with GFP positive cells marked green and BFP positive cells marked in blue). It can be seen that presence of a BFP signal strongly correlates with reduction of GFP-Caveolin and we thus conclude that co-transfection can be used to conclude for the presence of shRNA in a given cell.

Figure 5.11 shows the results of flow cytometric detection of Rhodamine-EGF internalization in HeLa cells co-transfected with BFP and shRNA against Caveolin-1 (upper row) or control DNA (lower row) in a ratio of 1:2. Cells were stimulated with 100 ng/ml Rhodamine for 10 minutes. It can be seen that downregulation of Caveolin expression (as marked by presence of BFP signal) does not affect EGF internalization.

We conclude that Caveolin is not necessary for EGF internalization, but that it is involved in trafficking of the ligand-receptor complex post-internalization.

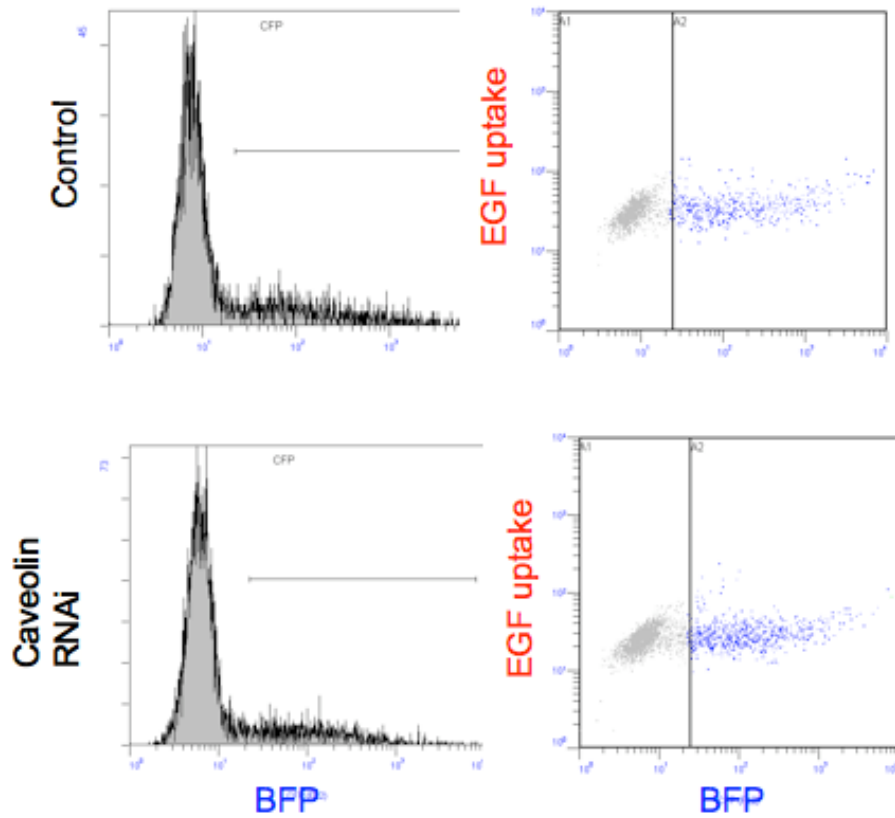


Figure 5.11: **Downregulation of Caveolin-1 expression does not reduce EGF uptake** HeLa cells were co-transfected with BFP and shRNA against Caveolin-1 (upper row) or control DNA (lower row) in a ratio of 1:2 and stimulated with 100 ng/ml Rhodamine-EGF for 10 minutes. Prior to measurement, cells were acid-stripped to remove surface bound EGF.

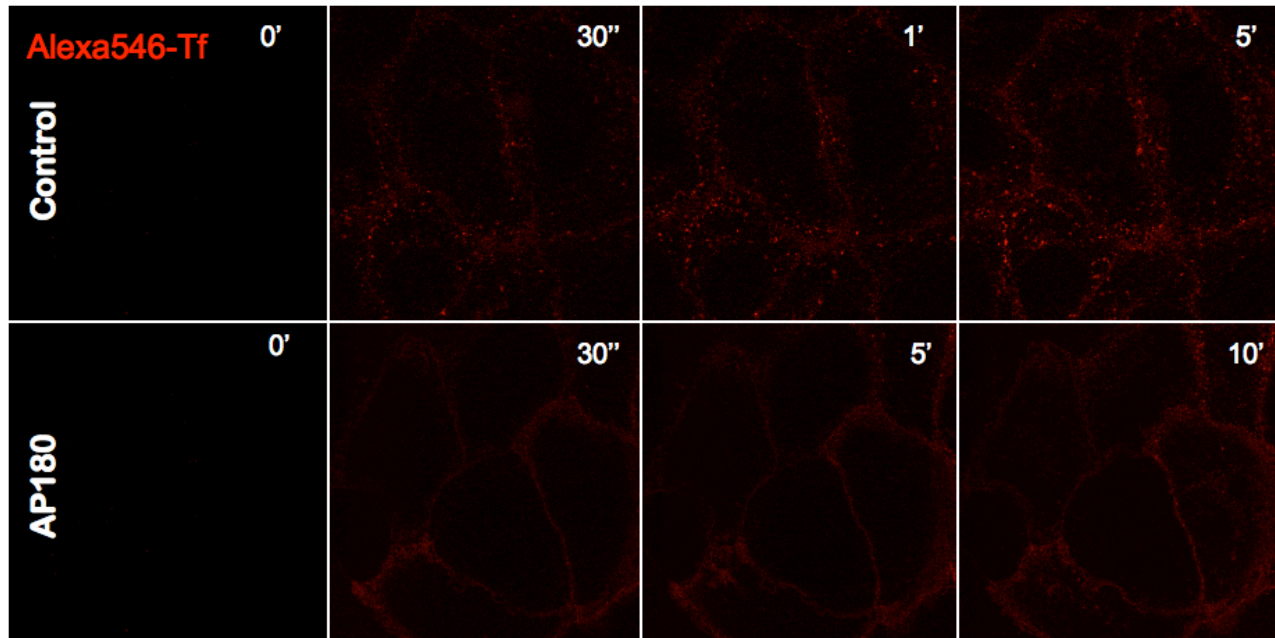


Figure 5.12:

5.3.2 Inhibition of Clathrin-mediated endocytosis reduces, but does not block EGF internalization

Clathrin-mediated endocytosis depends on the presence of a whole range of adaptor proteins which are necessary for the assembly of the clathrin-cage (AP-2, EPS15 [14, 162, 15]) or to recruit receptors to the forming pits (AP-2 [104, 31]) (see Introduction, page 29). Consequently, clathrin-mediated endocytosis can be inhibited by disrupting the function of these adaptor proteins.

Inhibition of Formation of functional clathrin-coated pits can also be achieved by overexpression of a truncated form of AP180 (AP180-mut), which functions during the recruitment of clathrin to the membrane as well as its polymerization into cage like structures [59].

When overexpressed in HeLa cells, we found that AP180-mut efficiently inhibited the internalization of Transferrin, a ligand that is known to be strictly dependent on clathrin-mediated endocytosis (Figure 5.12 [132, 87]). This result is consistent with previous studies on HeLa or Cos cells [207].

In order to learn about the relationship between clathrin- or caveolin-mediated endocytosis and

intracellular trafficking, we tested how disruption of the clathrin-pathway by overexpression of AP180-mut affects (a) EGF uptake and intracellular trafficking, as well as (b) colocalization with Caveolin and routing to perinuclear regions characteristic of late endosomes.

5.3.3 Overexpression of AP180-mut leads to accumulation of Caveolin in perinuclear region, suggesting a connection between the clathrin- and caveolae-pathways

We tested the effect of AP180-mut expression on EGF intracellular trafficking and colocalization with Caveolin. Figure 5.13 shows GFP-Cav cells co-transfected with BFP and AP180-mut in a ratio of 1:2, so that the presence of BFP can be used as a marker for the presence of AP180-mut (cf. Figure 5.10). The first effect we noted was that, in the absence of EGF stimulation, AP180-mut expressing cells (as indicated by BFP expression) showed a marked accumulation of Caveolin in the perinuclear region (Figure 5.13, purple arrows). This was unexpected, since, to our knowledge, a connection between the clathrin-pathway as defined by requirement of AP180 and the caveolin pathway has not been described.

The morphology and localization of these Caveolin-assemblies resemble lysosomal structures. When inhibiting the lysosome with bafilomycin, we found a marked increase of total cellular GFP-Caveolin levels, indicating that Caveolin gets constitutively degraded by the lysosome (not shown). Our results hint at the possibility that functional AP180 is necessary for the lysosomal degradation of Caveolin.

The AP180-mut expressing cells also showed markedly different EGF internalization behaviour: Up to 10 minutes after stimulation, hardly any EGF vesicles could be detected (Figure 5.13 white arrows).

Figure 5.14 shows a different field of view from the same experiment, with a higher resolution and enhanced image representation. Again, we see that the AP180 expressing cell shows accumulation of Caveolin. The internalization and trafficking of EGF is altered: Internalization itself does not seem to be inhibited completely as small vesicles very close to the membrane can still be seen. This would also

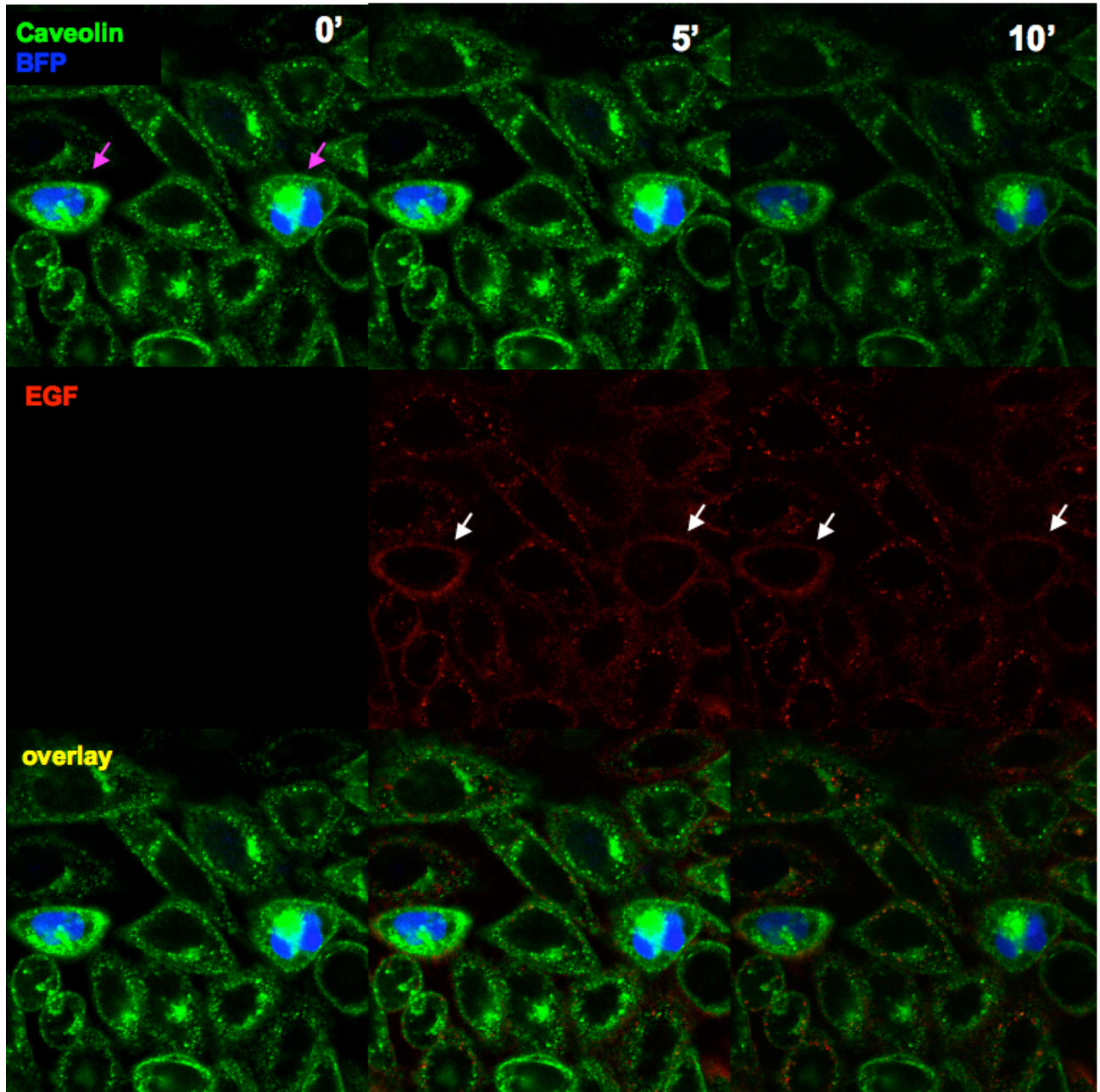


Figure 5.13: **Effect of AP180 overexpression on Caveolin distribution and EGF internalization** GFP-Cav cells were co-transfected with BFP and AP180 and stimulated with 100 ng/ml Rhodamine-EGF for the indicated time points. BFP positive cells show an accumulation of Caveolin in the perinuclear cell region in the absence of stimulation (purple arrows). Upon stimulation, AP180 expression cells show low or delayed EGF uptake (white arrows)

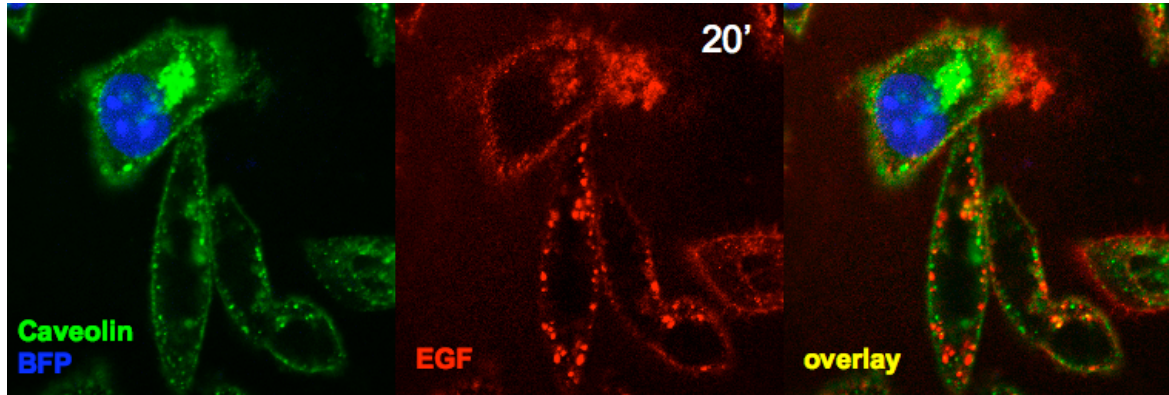


Figure 5.14: GFP-Cav cells were co-transfected with BFP and AP180. Cells were stimulated with 100ng/ml Rhodamine-EGF and imaged. For clarity, shown are images with enhanced image representation.

explain the results of the flow cytometry, according to which AP180 expressing cells still do internalize EGF. Nevertheless, as can be seen in the microscopy images, the subsequent intracellular routing of EGF vesicles is dramatically altered. Larger vesicles moving away from the membrane can not be observed at all.

5.4 Discussion

We have applied confocal microscopy and evaluated colocalization of Rhodamine-EGF with GFP-Clathrin or GFP-Caveolin in HeLa cells to investigate at which stages along the endocytic route the ligand-receptor complexes assemble with the different markers. We found that while EGF colocalizes with Clathrin during and immediately after internalization, colocalization with Caveolin was more sustained and most pronounced at later stages (5-20 minutes of stimulation, cf. Figures 5.2 and 5.3). This data suggested that Caveolin is not participating in the internalization step itself, which was further confirmed by RNAi-mediated downregulation of Caveolin and flow cytometric detection of the effect on EGF uptake (Figure 5.11). On the other hand, disruption of clathrin-dependent endocytosis by overexpression of AP180 inhibited EGF uptake efficiently (Figure 5.14), although it seemed that some internalization still took place, but only small vesicles close to the plasma membrane could

be observed (cf. Figure 5.14) This result is interesting as one study reported that RNAi-mediated downregulation of clathrin expression did not inhibit EGF uptake altogether but instead led to different vesicle morphology, in that only small vesicles could be observed [87]. One interpretation of this result could be that the clathrin-dependent internalization pathway which is specifically disrupted upon AP180 expression is normally responsible to the classical 'vesicle maturation' route from early to late endosomes, whereas an alternative internalization pathway still functioning upon AP180 expression leads to a different population of vesicles, possible recycling endosomes. In order to test in more detail whether EGF uptake still occurred in AP180 overexpressing cells, Flow Cytometry should be performed, since it is more sensitive than confocal microscopy. Further, the same experiment that was done in GFP-cav cells (Figure 5.14) should be done in GFP-clath cells.

As already mentioned in the introduction (section 1.2.2, page 29), the role of clathrin-independent (CIE)/caveolae-mediated internalization during EGFR endocytosis is discussed controversially. According to some reports, nystatin-treatment, which is thought to disrupt caveolae by cholesterol depletion, has failed to affect the rate of EGF uptake [98] in HeLa cells, which is challenged by other reports [172].

Our results suggest that Caveolin is not required for the internalization of the receptor but for proper intracellular routing, as in Caveolin-depleted cells vesicles seemed to be arrested in an earlier endosomal stage characterized by small size and proximity to the plasma membrane (Figure 5.9). It could thus be that Caveolin is required for routing the receptor to cellular compartments which are needed for signal attenuation, which would then agree with the previously described role of caveolin as a negative regulator of EGFR signaling [118]. A further sensible experiment would be to test for receptor degradation upon Caveolin-depletion.

Part IV

Material and Methods

Chapter 6

Experimental Procedures

6.1 Flow Cytometry

6.1.1 Laser and Filter

Samples were measured on a modified flow cytometer FC500 /MPL (Beckman Coulter). The standard argon-Ion laser (488nm /20 mW, Cyonics) was removed and a Sapphire 488 nm / 20 mW and a Compass 561 nm / 40 mW (Coherent) were installed on mounting platform (Figure ??) Additionally the standard Radius 635 laser was swapped with a Radius 405 nm / 25 mW (Coherent). All three lasers were aligned collinearly (Figure 6.2).

Spectra of the three fluorophores used in this study (BFP, GFP and Tetramethylrhodamine) as well as emission filter setup used are shown in Figure 6.3 A and B, respectively. Alexa 546 or Rhodamine-EGF labeled samples were analyzed with a 590/50 bandpass filter (indicated by red shading in Figure 6.3A). The same filters were used for DPSS 488-nm and 561-nm measurements. GFP or BFP labeled samples were analyzed with a 488/25 or a 450/50 bandpass filter, respectively (blue or green shading in Figure 6.3A).

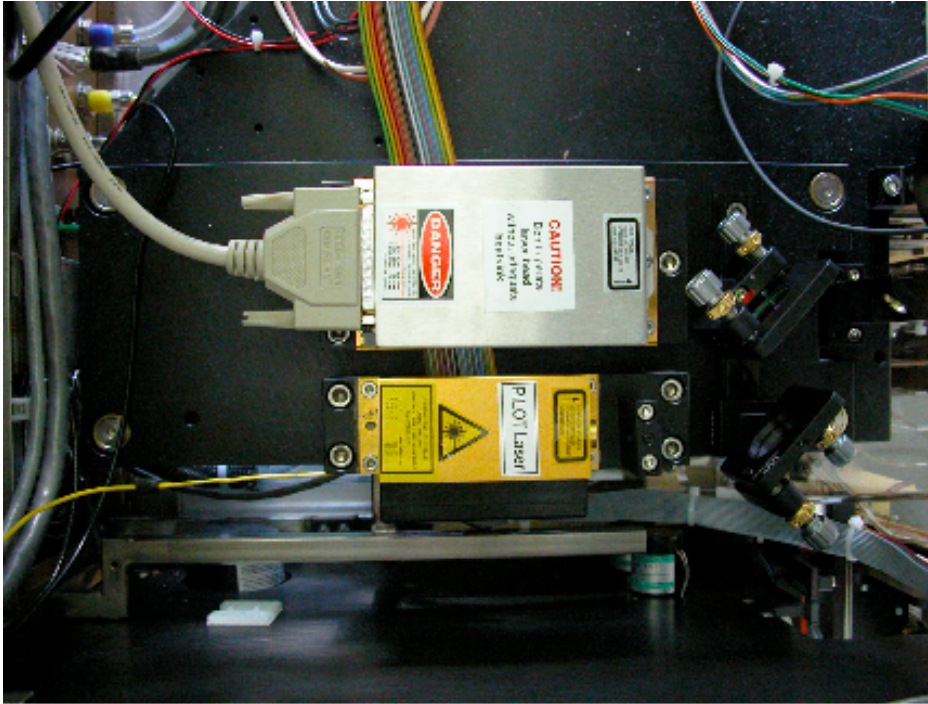


Figure 6.1: **Sapphire 488 nm / 20 mW and Compass 561 nm / 40 mW lasers** Top view on Lasers mounted on a subchassis with steering mirrors (mirror mounts by Newport, beam combiners by Chroma). The platform replaces the standard argon-ion laser.

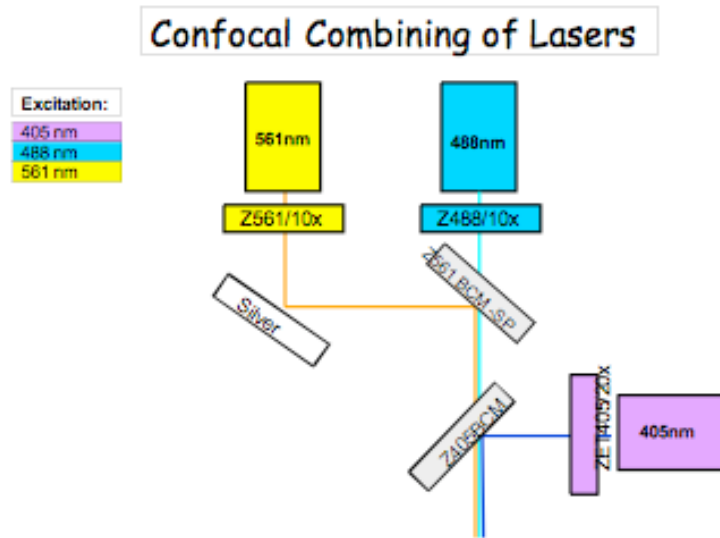


Figure 6.2: **Confocal Combination of Lasers** Three laser beams are combined collinearly using dichroic filters: Z561BCM-SP and Z405 BCM. Additional laser line filters were used to reduce background from laserdiode (bore glow).

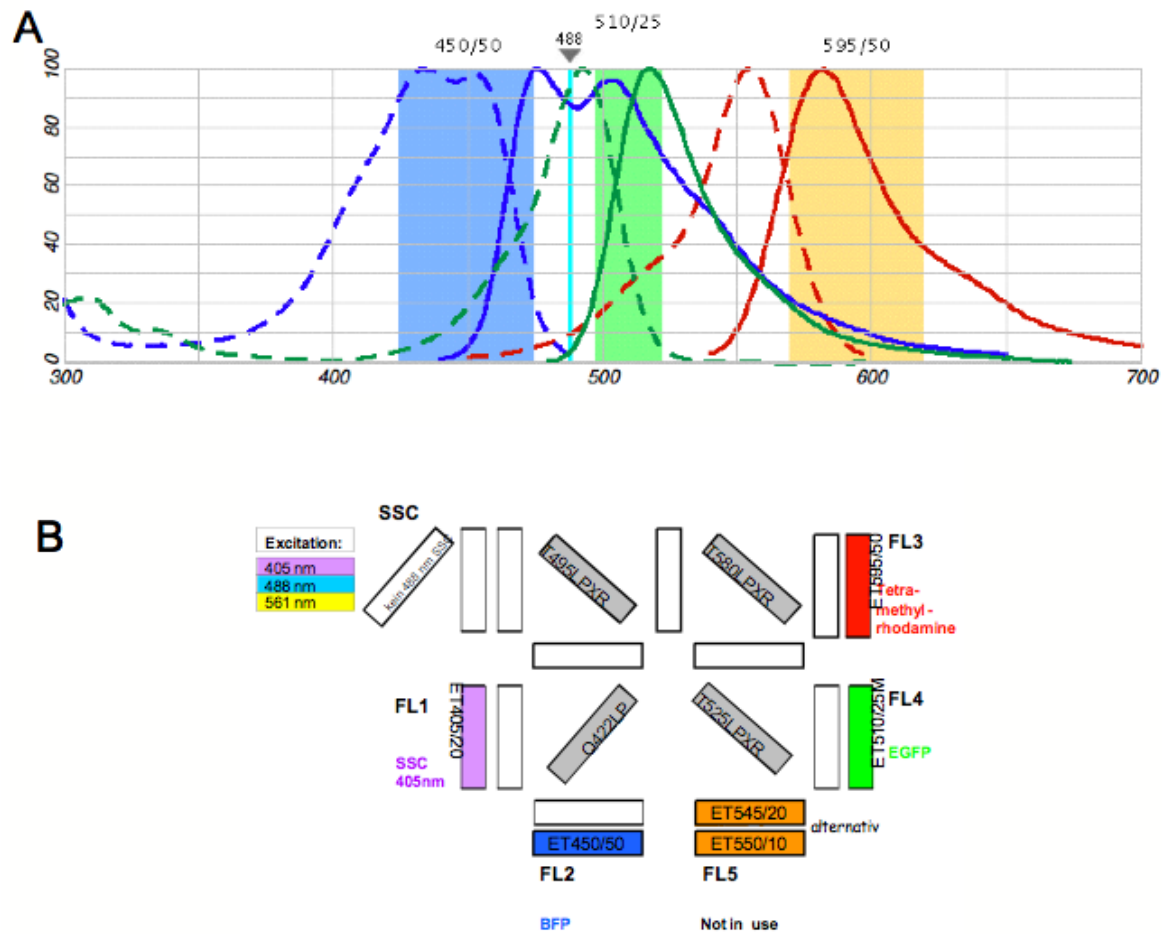


Figure 6.3: **Emmission filter setup** (A) Spectra of the fluorophores used in this study. Shown are the excitation (dashed) and emission (solid) spectra of BFP (blue), GFP (green) and tetramethylrhodamine (red). Indicated by shading in the corresponding color are the regions from which the used filters collected the light. (B) Transmission of the optical filters used

6.1.2 Sample preparation

Cells were kept in culture as described. Prior to flow cytometry measurements, cells were washed with PBS once and then kept in trypsin for 2 minutes. To break cell aggregates, samples were pipetted once or twice before returning them in full medium to inactivate the trypsin.

6.2 Cell Culture

HeLa cells were kept in DMEM supplemented with 10% FCS (full DMEM). Cells expressing GFP-Clathrin or GFP-Caveolin were kept in full DMEM plus 0.5 mg/ml G418.

6.2.1 EGF internalization studies

Before EGF stimulation experiments cells were starved overnight in DMEM without FCS for at least 12 hours. Cells were stimulated by adding EGF (or Rhodamine-EGF) directly into the starvation medium in the appropriate concentrations. To detect surface-bound as well as internalized ligand, cells were washed in PBS only. To remove surface bound ligand, cells were treated with a low pH acid buffer (50 mM glycine, 150mM NaCl, pH 3.0).

6.2.2 Transfection of cells, cell lines and plasmids

Transfection of HeLa cells with plasmid DNA was achieved using the Lipofectamine 2000 reagent. In co-transfection experiments using two plasmids, a ratio of 1:2 of the respective DNA was used.

HeLa cells stably expressing GFP-Caveolin (GFP-Cav cells) were a gift from Lucas Pelkmans [149]. HeLa cells stably expressing GFP-Clathrin (GFP-Clath cells) were obtained from Ernst Ungewickell [87].

The AP180 truncation mutant was obtained by Victor Laketa [59].

6.3 Confocal microscopy

Fixed or living cells were imaged on a confocal laser scanning microscope TCS SP5 (Leica Microsystems, Wetzlar, Germany) using a 63x oil immersion objective. A diode laser ($\lambda = 405\text{nm}$) was used for excitation of BFP. An argon ($\lambda = 488\text{nm}$) and a helium/neon ($\lambda = 543\text{nm}$) laser was used for excitation of GFP or Rhodamine/Alexa546, respectively.

6.3.1 Sample Preparation

Living cells were imaged in imaging medium (DMEM without phenylred). For fixation, cells were washed in PBS once, fixed in 4% PFA for 10 minutes on ice and then returned to PBS for imaging.

6.4 Image Processing

6.4.1 Image Background Reduction and Segmentation

The first step in vesicle detection and colocalization analysis is image segmentation. In general, segmentation of an image refers to the process of partitioning a digital image into distinct regions (objects) such that a binary image is created. The simplest method of creating a binary, segmented image is to set a threshold value for each pixel

For our purpose of detecting endosomal vesicles from confocal microscopy images I found the following method most suitable. In the first step, a background image is calculated from the original image by applying a mean filter: each pixel value in the original image is replaced with the mean ('average') value of its neighbors, including itself. This has the effect of eliminating pixel values which are unrepresentative of their surroundings. The process is exemplified in Figure 6.4. Figure 6.4A shows the original image, Figure 6.4B shows the result of the mean filter computation. In the second step this 'mean' image is subtracted from the original one in a pixel-by-pixel manner (Figure 6.4C), resulting in an image which is less blurred and contains less background noise. Simply applying a global gray value threshold on this background reduced image then yields a binary, segmented image (6.4D).

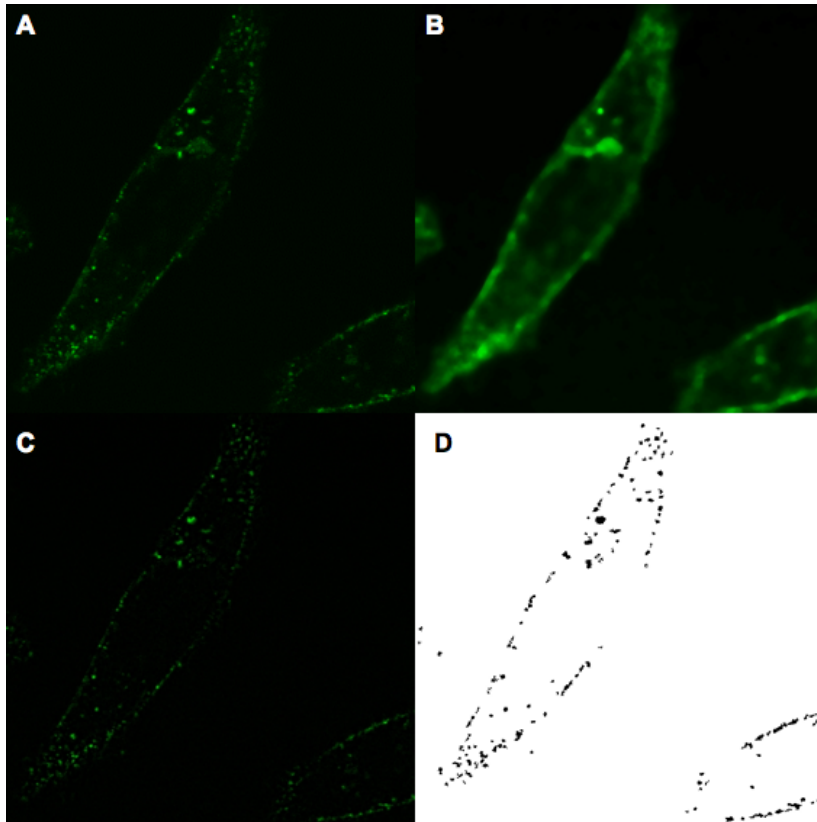


Figure 6.4: Creating a binary image by image segmentation

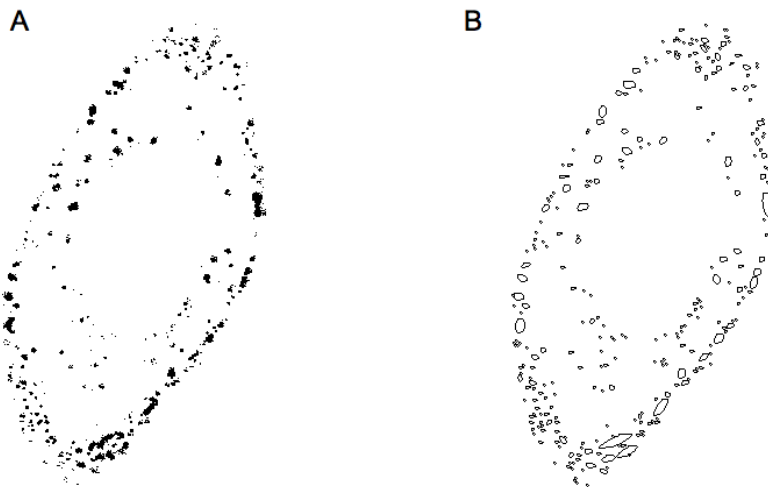


Figure 6.5: **Vesicle detection** From the binary image characteristics about each detected vesicles are obtained so that they become computer-recognized objects with certain characteristics such as position in the x/y-plane, size and intensity. (cf. Figure 6.6)

The image shows a screenshot of a software window titled "Results". The window contains a table with the following columns: Area, BX, BY, Width, Height, and IntDen. The table lists 28 rows of data, each representing a detected vesicle. The data is as follows:

	Area	BX	BY	Width	Height	IntDen
277	1	295	411	1	1	255
278	1	244	412	1	1	255
279	1	0	413	1	1	255
280	2	263	413	1	2	510
281	23	267	414	6	5	5865
282	7	3	415	5	3	1785
283	1	22	417	1	1	255
284	13	252	417	5	5	3315
285	8	259	418	5	3	2040
286	7	277	418	3	3	1785
287	48	280	418	13	8	12240
288	1	304	419	1	1	255
289	7	259	423	4	2	1785
290	11	0	424	5	4	2805
291	5	239	425	4	3	1275
292	33	267	425	9	7	8415
293	1	253	426	1	1	255
294	3	255	426	3	2	765
295	3	251	429	3	1	765
296	2	285	430	2	1	510
297	1	255	431	1	1	255
298	18	279	431	9	5	4590
299	2	264	432	2	2	510
300	1	2	436	1	1	255
301	2	258	439	2	2	510
302	1	257	441	1	1	255
303	1	259	443	1	1	255
304	2	268	445	2	1	510

Figure 6.6: **A list obtained with information about each detected vesicle** Through the vesicle recognition procedure information about each detected object is obtained, such as location, size and intensity

This binary image can then be used for the object recognition process (Figure 6.5), during which information about each detected vesicle is obtained (Figure 6.6).

Chapter 7

Differential equations

7.1 Modeling internalization with a single pathways (chapter 3, page 81)

7.1.1 Deriving $r(t)$ for non-constant $\hat{R}E_s$

From

$$\frac{d(\hat{R}E_s)}{dt} = -\hat{k}_i \cdot \hat{R}E_s$$

we obtain

$$\hat{R}E_s(t) = \hat{R}E_0 \cdot e^{-\hat{k}_i \cdot t}.$$

Further, we have

$$\hat{R}E_s + \hat{R}_i = \hat{R}E_{s0} + \hat{R}_{i0} = \hat{R}E_{s0}$$

due to conservation of mass and $\hat{R}_{i0} = 0$, so that

$$\hat{R}_i(t) = \hat{R}E_{s0} - \hat{R}E_s = \hat{R}E_{s0} - \hat{R}E_{s0} \cdot e^{-\hat{k}_i \cdot t}.$$

This leads to

$$r(t) = \frac{\hat{R}_i}{\hat{R}E_s} = \frac{\hat{R}E_{s0}(1 - e^{-k_1 t})}{\hat{R}E_{s0}e^{-\hat{k}t}} = e^{kt} - 1.$$

Deriving the second derivative of $r(t)$ with inclusion of $\hat{I}C$

The dynamics of reaction scheme (R1):



are given by a single equation:

$$d(\hat{R}E_s)/dt = d(\hat{I}C)/dt = -d(\hat{R}E_i)/dt = -k_2 \cdot \hat{R}E_s \cdot \hat{I}C$$

Again, due to mass conservation,

$$\hat{R}_i(t) = \hat{R}E_{s0} - \hat{R}E_s$$

as well as

$$\hat{I}C_i(t) = \hat{R}E_s - \hat{R}E_{s0} + \hat{I}C_{s0}.$$

Thus we have

$$\frac{d(\hat{R}E_s)}{dt} = -\hat{k}_i \cdot \hat{R}E_s (\hat{R}E_s - \hat{R}E_{s0} + \hat{I}C_{s0})$$

and

$$\hat{I}C(t) = \hat{R}E_{s0} - \hat{R}E_s$$

The first derivative of $r(t) = \frac{\hat{I}C}{\hat{R}E_s}$ is given by

$$\begin{aligned}
r(t)' &= \left(\frac{\hat{R}E_{s0} - \hat{R}E_s}{\hat{R}E_s} \right)' \\
&= \frac{-\hat{R}E_s' \cdot \hat{R}E_s - \hat{R}E_s' \cdot (\hat{R}E_{s0} - \hat{R}E_s)}{\hat{R}E_s^2} \\
&= -\hat{R}E_{s0} \frac{\hat{R}E_s'}{\hat{R}E_s^2} \\
&= -\hat{R}E_{s0} \frac{-k_2 \cdot \hat{R}E_s (\hat{R}E_s - \hat{R}E_{s0} + \hat{I}C_0)}{\hat{R}E_s^2} \\
&= \hat{R}E_{s0} \cdot k_2 \frac{\hat{R}E_s - \hat{R}E_{s0} + \hat{I}C_0}{\hat{R}E_s}
\end{aligned}$$

and

$$\begin{aligned}
r(t)'' &= \hat{R}E_{s0} \cdot k_2 \cdot \frac{\hat{R}E_s' \cdot \hat{R}E_s - \hat{R}E_s' (\hat{R}E_s - \hat{R}E_{s0} + \hat{I}C_0)}{\hat{R}E_s^2} \\
&= \hat{R}E_{s0} \cdot k_2 \cdot \frac{\hat{R}E_s'}{\hat{R}E_s^2} \cdot (\hat{R}E_{s0} - \hat{I}C_0)
\end{aligned}$$

7.2 Modeling of endocytic sorting into two pathways (section 4, page 97)

7.2.1 Numerical Simulations and Steady-State Analysis

To numerically solve the systems of equations (1.1 - 1.7) we used the MATLAB ODE15s function.

The existence of distinct classes of steady-states was derived as follows: The system of ODEs

exhibits four independent equations, namely equations (1.1), (1.3), (1.4) and (1.5). To obtain the values of the variables that represent a steady-state, we simultaneously set these equations equal to zero and solved for the variables.

Setting equations (1.4) and (1.5) equal to zero yields

$$-k_{cde} * R_EGF * CDE = 0 \quad (1.4')$$

$$-k_{cie} * R_EGF * CIE = 0 \quad (1.5')$$

Since all kinetic constants are assumed to be positive, one derives that either R_EGF^* or both CDE^* and CIE^* have to be zero. Consider the case that $R_EGF^* = 0$. Then, from setting equations (1.1) and (1.3) equal to zero, i.e.

$$k_f * EGF * R - k_r * R_EGF = 0 \quad (1.1')$$

$$k_f * EGF * R - k_r * R_EGF - k_{cde} * R_EGF * CDE \quad (1.3')$$

$$-k_{cie} * R_EGF * CIE = 0$$

it follows that either R^* or EGF^* have to be zero. We have thus derived steady-state class I (see Results). Consider now the second case derived from equations (1.4') and (1.5'), namely that $CDE^* = 0$ and $CIE^* = 0$. Substituting these values into equation (1.3), one obtains

$$R \cdot EGF^* = \frac{k_f}{k_r} EGF^* \cdot R^*, \quad (1.3')$$

which also leaves equation (1.1) equal to zero. This second set of values represents steady-state class II (see Results).

7.2.2 Approximability by Hill-curve

In order to assess the steepness of the derived switch-effect, we compared the obtained stimulus-response curve to the switch-effect described by the Hill-formula. This formula was originally introduced as a phenomenological model to describe the binding of oxygen to hemoglobin [86] and later often used to for cooperative enzyme reactions :

$$V = \frac{V_{\max} \cdot x^h}{K_m^h + x^h}. \quad (3.1)$$

Here, V denotes reaction velocity, V_{\max} the maximal velocity, x the substrate concentration, K_m the substrate concentration where half-maximal velocity is reached and h , the Hill-coefficient, represents the steepness of the response.

In order to investigate the sensitivity of the switch-effect of CIE-internalization on specific parameter values, we adapted a procedure applied in [21]. We systematically varied reaction parameters and initial values of the model (equations 1.1 - 1.7) using equidistant sampling points. For each thus obtained set we computed the stimulus-response curve and extracted the Hill-coefficient as

$h = \frac{\log 81}{\log(x_{0.9})\log(x_{0.1})}$ [90]. Here, $x_{0.1}$ and $x_{0.9}$ are the EGF-concentrations where 10% or 90% of the maximal response is reached, respectively.

To evaluate the approximability of the stimulus-response curve by the Hill-equation, we computed the mean deviation between the obtained stimulus-response curves and a reference Hill-curve. In this way we formally determined a broad range of parameter values for which an ultrasensitive response of CIE-internalization occurs (Fig. 5 and Fig. 6).

Bibliography

- [1] <http://mathworld.wolfram.com/>.
- [2] Rubén Claudio Aguilar and Beverly Wendland. Endocytosis of membrane receptors: two pathways are better than one. *Proc Natl Acad Sci USA*, 102(8):2679–80, Feb 2005.
- [3] U Alon, M G Surette, N Barkai, and S Leibler. Robustness in bacterial chemotaxis. *Nature*, 397:168–171, 1999.
- [4] Uri Alon. *An Introduction to Systems Biology*. Chapman & Hall, 2006.
- [5] Ido Amit, Ami Citri, Tal Shay, Yiling Lu, Menachem Katz, Fan Zhang, Gabi Tarcic, Doris Siwak, John Lahad, Jasmine Jacob-Hirsch, Ninette Amariglio, Nora Vaisman, Eran Segal, Gideon Rechavi, Uri Alon, Gordon B Mills, Eytan Domany, and Yosef Yarden. A module of negative feedback regulators defines growth factor signaling. *Nat Genet*, 39(4):503–12, Mar 2007.
- [6] Ido Amit, Ron Wides, and Yosef Yarden. Evolvable signaling networks of receptor tyrosine kinases: relevance of robustness to malignancy and to cancer therapy. *Mol Syst Biol*, 3:151, Jan 2007.
- [7] H A Anderson, Y Chen, and L C Norkin. Bound simian virus 40 translocates to caveolin-enriched membrane domains, and its entry is inhibited by drugs that selectively disrupt caveolae. *Mol Biol Cell*, 7(11):1825–34, Oct 1996.

- [8] David Angeli, Jr. Ferrell, James E., and Eduardo D. Sontag. Detection of multistability, bifurcations, and hysteresis in a large class of biological positive-feedback systems. *PNAS*, 101:1822–1827, 2004.
- [9] B. Antonsson, F. Conti, A. Ciavatta, S. Montessuit, S. Lewis, I. Martinou, L. Bernasconi, A. Bernard, J. J. Mermod, G. Mazzei, K. Maundrell, F. Gambale, R. Sadoul, and J. C. Martinou. Inhibition of bax channel-forming activity by bcl-2. *Science*, 277(5324):370–372, Jul 1997.
- [10] E. Z. Bagci, Y. Vodovotz, T. R. Billiar, G. B. Ermentrout, and I. Bahar. Bistability in apoptosis: roles of bax, bcl-2, and mitochondrial permeability transition pores. *Biophys J*, 90(5):1546–59, Mar 2006.
- [11] Lee Bardwell, Xiufen Zou, Qing Nie, and Natalia L Komarova. Mathematical models of specificity in cell signaling. *Biophys J*, Feb 2007.
- [12] Naama Barkai and Stanislas Leibler. Robustness in simple biochemical networks. *Nature*, 387:913–917, 1997.
- [13] A. Becskei, B. Séraphin, and L. Serrano. Positive feedback in eukaryotic gene networks: cell differentiation by graded to binary response conversion. *EMBO J*, 20(10):2528–35, May 2001.
- [14] A Benmerah, M Bayrou, N Cerf-Bensussan, and A Dautry-Varsat. Inhibition of clathrin-coated pit assembly by an eps15 mutant. *J Cell Sci*, 112 (Pt 9):1303–11, Apr 1999.
- [15] A Benmerah, C Lamaze, B Bègue, S L Schmid, A Dautry-Varsat, and N Cerf-Bensussan. Ap-2/eps15 interaction is required for receptor-mediated endocytosis. *J Cell Biol*, 140(5):1055–62, Mar 1998.
- [16] E M Bennett, S X Lin, M C Towler, F R Maxfield, and F M Brodsky. Clathrin hub expression affects early endosome distribution with minimal impact on receptor sorting and recycling. *Mol Biol Cell*, 12(9):2790–9, Aug 2001.

- [17] M. Bentele, I. Lavrik, M. Ulrich, S. Stosser, D.W. Heermann, H. Kalthoff, P.H. Kramer, and R. Eils. Mathematical modeling reveals threshold mechanism in cd95-induced apoptosis. *J Cell Biol*, 166:839–851, 2004.
- [18] O. G. Berg, J. Paulsson, and M. Ehrenberg. Fluctuations and quality of control in biological cells: zero-order ultrasensitivity reinvestigated. *Biophys J*, 79(3):1228–1236, Sep 2000.
- [19] U. S. Bhalla and R. Iyengar. Emergent properties of networks of biological signaling pathways. *Science*, 283:381–7, 1999.
- [20] Upinder S Bhalla, Prahlad T Ram, and Ravi Iyengar. Map kinase phosphatase as a locus of flexibility in a mitogen-activated protein kinase signaling network. *Science*, 297(5583):1018–23, Aug 2002.
- [21] Nils Bluthgen and Hanspeter Herzl. How robust are switches in intracellular signaling cascades? *J Theor Biol*, 225(3):293–300, December 2003.
- [22] D. Bray. Protein molecules as computational elements in living cells. *Nature*, 376:307–12, 1995.
- [23] A. Breitkreutz and M. Tyers. Mapk signaling specificity: It takes two to tango. *Trends Cell Biol*, 12:254–257, 2002.
- [24] G Brockhoff, E Endl, W Minuth, F Hofstädter, and R Knüchel. Options of flow cytometric three-colour dna measurements to quantitate egfr in subpopulations of human bladder cancer. *Analytical cellular pathology : the journal of the European Society for Analytical Cellular Pathology*, 11(1):55–70, May 1996.
- [25] G Brockhoff, W Wieland, G Woelfl, F Hofstaedter, and R Knuechel. Evaluation of flow-cytometric three-parameter analysis for egfr quantification and dna assessment in human bladder carcinomas. *Virchows Arch*, 432(1):77–84, Jan 1998.
- [26] F M Brodsky, C Y Chen, C Knuehl, M C Towler, and D E Wakeham. Biological basket weaving: formation and function of clathrin-coated vesicles. *Annu Rev Cell Dev Biol*, 17:517–68, Jan 2001.

- [27] B P Ceresa and S L Schmid. Regulation of signal transduction by endocytosis. *Curr Opin Cell Biol*, 12(2):204–10, Apr 2000.
- [28] Joshua L. Cherry and Frederick R. Adler. How to make a biological switch. *J Theor Biol*, 203:117–133, 2000.
- [29] Ami Citri and Yosef Yarden. Egf-erbB signalling: towards the systems level. *Nat Rev Mol Cell Biol*, 7(7):505–16, Jun 2006.
- [30] S?bastien Clodong, Ulf D?hring, Luiza Kronk, Annegret Wilde, Ilka Axmann, Hanspeter Herzel, and Markus Kollmann. Functioning and robustness of a bacterial circadian clock. *Mol Syst Biol*, 3:90, 2007.
- [31] Brett M Collins, Airlie J McCoy, Helen M Kent, Philip R Evans, and David J Owen. Molecular architecture and functional model of the endocytic ap2 complex. *Cell*, 109(4):523–35, May 2002.
- [32] Sean D Conner and Sandra L Schmid. Regulated portals of entry into the cell. *Nature*, 422(6927):37–44, Mar 2003. hgdjhasg.
- [33] J Couet, M Sargiacomo, and M P Lisanti. Interaction of a receptor tyrosine kinase, egf-r, with caveolins. caveolin binding negatively regulates tyrosine and serine/threonine kinase activities. *J Biol Chem*, 272(48):30429–38, Nov 1997.
- [34] H Damke, D D Binns, H Ueda, S L Schmid, and T Baba. Dynamin gtpase domain mutants block endocytic vesicle formation at morphologically distinct stages. *Mol Biol Cell*, 12(9):2578–89, Aug 2001.
- [35] S. R. Datta, A. Brunet, and M. E. Greenberg. Cellular survival: a play in three akts. *Genes Dev*, 13(22):2905–2927, Nov 1999.
- [36] C G Davis, J L Goldstein, T C Südhof, R G Anderson, D W Russell, and M S Brown. Acid-dependent ligand dissociation and recycling of ldl receptor mediated by growth factor homology region. *Nature*, 326(6115):760–5, Jan 1987.

- [37] Karla de Bruin, Nadia Ruthardt, Katharina von Gersdorff, Ralf Bausinger, Ernst Wagner, Manfred Ogris, and Christoph Bräuchle. Cellular dynamics of egf receptor-targeted synthetic viruses. *Mol Ther*, 15(7):1297–305, Jun 2007.
- [38] Annemieke A de Melker, Gerda van der Horst, and Jannie Borst. c-cbl directs egf receptors into an endocytic pathway that involves the ubiquitin-interacting motif of eps15. *J Cell Sci*, 117(Pt 21):5001–12, Sep 2004.
- [39] Erez Dekel and Uri Alon. Optimality and evolutionary tuning of the expression level of a protein. *Nature*, 436:588–92, 2005.
- [40] J. Demongeot, M. Kaufman, and R. Thomas. Positive feedback circuits and memory. *C R Acad Sci III*, 323(1):69–79, Jan 2000.
- [41] Q. L. Deveraux, N. Roy, H. R. Stennicke, T. Van Arsdale, Q. Zhou, S. M. Srinivasula, E. S. Alnemri, G. S. Salvesen, and J. C. Reed. Iaps block apoptotic events induced by caspase-8 and cytochrome c by direct inhibition of distinct caspases. *EMBO J*, 17(8):2215–2223, Apr 1998.
- [42] Q. L. Deveraux, R. Takahashi, G. S. Salvesen, and J. C. Reed. X-linked iap is a direct inhibitor of cell-death proteases. *Nature*, 388(6639):300–304, Jul 1997.
- [43] Ivan Dikic and Silvia Giordano. Negative receptor signalling. *Curr Opin Cell Biol*, 15(2):128–35, Apr 2003.
- [44] W. Driever and C. Nüsslein-Volhard. The bicoid protein is a positive regulator of hunchback transcription in the early drosophila embryo. *Nature*, 337(6203):138–143, Jan 1989.
- [45] Lei Duan, Yuko Miura, Manjari Dimri, Biswanath Majumder, Ingrid L Dodge, Alagarsamy L Reddi, Amiya Ghosh, Norvin Fernandes, Pengcheng Zhou, Karen Mullane-Robinson, Navin Rao, Stephen Donoghue, Rick A Rogers, David Bowtell, Mayumi Naramura, Hua Gu, Vimla Band, and Hamid Band. Cbl-mediated ubiquitinylation is required for lysosomal sorting of epidermal

- growth factor receptor but is dispensable for endocytosis. *J Biol Chem*, 278(31):28950–60, Jul 2003.
- [46] Leah Edelstein-Keshet. *Mathematical Models in Biology*. SIAM, Philadelphia, USA, 2005.
- [47] Thomas Eissing, Steffen Waldherr, Frank Allgöwer, Peter Scheurich, and Eric Bullinger. Steady state and (bi-) stability evaluation of simple protease signalling networks. *Biosystems*, Jan 2007.
- [48] Thomas Eissing, Holger Conzelmann, Ernst D Gilles, Frank Allgöwer, Eric Bullinger, and Peter Scheurich. Bistability analyses of a caspase activation model for receptor-induced apoptosis. *J Biol Chem*, 279(35):36892–36897, Aug 2004.
- [49] Avigdor Eldar, Ruslan Dorfman, Daniel Weiss, Hilary Ashe, Ben-Zion Shilo, and Naama Barkai. Robustness of the BMP morphogen gradient in Drosophila embryonic patterning. *Nature*, 419:304–8, 2002.
- [50] Avigdor Eldar, Dalia Rosin, Ben-Zion Shilo, and Naama Barkai. Self-enhanced ligand degradation underlies robustness of morphogen gradients. *Dev Cell*, 5:635–46, 2003.
- [51] Avigdor Eldar, Ben-Zion Shilo, and Naama Barkai. Elucidating mechanisms underlying robustness of morphogen gradients. *Curr Opin Genet Dev*, 14:435–9, 2004.
- [52] M. Enari, H. Sakahira, H. Yokoyama, K. Okawa, A. Iwamatsu, and S. Nagata. A caspase-activated dnase that degrades dna during apoptosis, and its inhibitor icad. *Nature*, 391(6662):43–50, Jan 1998.
- [53] J A Engelman, X L Zhang, B Razani, R G Pestell, and M P Lisanti. p42/44 map kinase-dependent and -independent signaling pathways regulate caveolin-1 gene expression. activation of ras-map kinase and protein kinase a signaling cascades transcriptionally down-regulates caveolin-1 promoter activity. *J Biol Chem*, 274(45):32333–41, Nov 1999.
- [54] B W Ennis, M E Lippman, and R B Dickson. The egf receptor system as a target for antitumor therapy. *Cancer Invest*, 9(5):553–62, Jan 1991.

- [55] Michela Felberbaum-Corti, Françoise Gisou Van Der Goot, and Jean Gruenberg. Sliding doors: clathrin-coated pits or caveolae? *Nat Cell Biol*, 5(5):382–4, Apr 2003.
- [56] J. E. Ferrell. Tripping the switch fantastic: how a protein kinase cascade can convert graded inputs into switch-like outputs. *Trends Biochem Sci*, 21(12):460–466, Dec 1996.
- [57] J. E. Ferrell. How responses get more switch-like as you move down a protein kinase cascade. *Trends Biochem Sci*, 22(8):288–289, Aug 1997.
- [58] J. E. Ferrell and E. M. Machleder. The biochemical basis of an all-or-none cell fate switch in *Xenopus* oocytes. *Science*, 280:895–8, 1998.
- [59] M G Ford, B M Pearse, M K Higgins, Y Vallis, D J Owen, A Gibson, C R Hopkins, P R Evans, and H T McMahon. Simultaneous binding of ptdins(4,5)p2 and clathrin by ap180 in the nucleation of clathrin lattices on membranes. *Science*, 291(5506):1051–5, Feb 2001.
- [60] Mark R Frey, Rebecca S Dize, Karen L Edelblum, and D Brent Polk. p38 kinase regulates epidermal growth factor receptor downregulation and cellular migration. *EMBO J*, 25(24):5683–92, Dec 2006.
- [61] L M Fujimoto, R Roth, J E Heuser, and S L Schmid. Actin assembly plays a variable, but not obligatory role in receptor-mediated endocytosis in mammalian cells. *Traffic*, 1(2):161–71, Jan 2000.
- [62] F Galbiati, D Volonte, J A Engelman, G Watanabe, R Burk, R G Pestell, and M P Lisanti. Targeted downregulation of caveolin-1 is sufficient to drive cell transformation and hyperactivate the p42/44 map kinase cascade. *EMBO J*, 17(22):6633–48, Nov 1998.
- [63] T. S. Gardner, C. R. Cantor, and J. J. Collins. Construction of a genetic toggle switch in *Escherichia coli*. *Nature*, 403(6767):339–42, Jan 2000.
- [64] Thomas P J Garrett, Neil M McKern, Meizhen Lou, Thomas C Elleman, Timothy E Adams, George O Lovrecz, Hong-Jian Zhu, Francesca Walker, Morry J Frenkel, Peter A Hoyne, Robert N

- Jorissen, Edouard C Nice, Antony W Burgess, and Colin W Ward. Crystal structure of a truncated epidermal growth factor receptor extracellular domain bound to transforming growth factor alpha. *Cell*, 110(6):763–73, Sep 2002.
- [65] A. Goldbeter and D. E. Koshland. An amplified sensitivity arising from covalent modification in biological systems. *Proc Natl Acad Sci U S A*, 78(11):6840–6844, Nov 1981.
- [66] A. Goldbeter and D. E. Koshland. Ultrasensitivity in biochemical systems controlled by covalent modification. interplay between zero-order and multistep effects. *J Biol Chem*, 259(23):14441–14447, Dec 1984.
- [67] A Goldbeter and Jr Koshland, D E. An amplified sensitivity arising from covalent modification in biological systems. *PNAS*, 78:6840–6844, 1981.
- [68] Albert Goldbeter. Zero-order switches and developmental thresholds. *Mol Syst Biol*, 1:msb4100042–E1–msb4100042–E2, 2005.
- [69] Y. Gotoh, N. Masuyama, K. Dell, K. Shirakabe, and E. Nishida. Initiation of xenopus oocyte maturation by activation of the mitogen-activated protein kinase cascade. *J Biol Chem*, 270(43):25898–25904, Oct 1995.
- [70] Barth D Grant and Anjon Audhya. The ins and outs of endocytic transport. *Nat Cell Biol*, 7(12):1151–4, Nov 2005.
- [71] Lene Melsaether Grovdal, Espen Stang, Alexander Sorkin, and Inger Helene Madshus. Direct interaction of cbl with ptyr 1045 of the egf receptor (egfr) is required to sort the egfr to lysosomes for degradation. *Exp Cell Res*, 300(2):388–395, November 2004.
- [72] Jean Gruenberg and Harald Stenmark. The biogenesis of multivesicular endosomes. *Nat Rev Mol Cell Biol*, 5(4):317–23, Apr 2004.

- [73] Gianni M Di Guglielmo, Christine Le Roy, Anne F Goodfellow, and Jeffrey L Wrana. Distinct endocytic pathways regulate tgf-beta receptor signalling and turnover. *Nat Cell Biol*, 5(5):410–21, Apr 2003.
- [74] K. Z. Guyton, Y. Liu, M. Gorospe, Q. Xu, and N. J. Holbrook. Activation of mitogen-activated protein kinase by h2o2. role in cell survival following oxidant injury. *J Biol Chem*, 271(8):4138–4142, Feb 1996.
- [75] Kaisa Haglund, Sara Sigismund, Simona Polo, Iwona Szymkiewicz, Pier Paolo Di Fiore, and Ivan Dikic. Multiple monoubiquitination of rtk is sufficient for their endocytosis and degradation. *Nat Cell Biol*, 5(5):461–6, Apr 2003.
- [76] Jack Hale and Huseyin Kocak. *Dynamics and Bifurcations*. Springer-Verlag New York, 1991.
- [77] P M Harari. Epidermal growth factor receptor inhibition strategies in oncology. *Endocr Relat Cancer*, 11(4):689–708, Nov 2004.
- [78] Leland H. Hartwell. Theoretical biology: A robust view of biochemical pathways. *Nature*, 387:855, 1997.
- [79] Leland H Hartwell, John J Hopfield, Stanislas Leibler, and Andrew W Murray. From molecular to modular cell biology. *Nature*, 402:C47–C52, 1999.
- [80] Bart S Hendriks, Lee K Opresko, H Steven Wiley, and Douglas Lauffenburger. Coregulation of epidermal growth factor receptor/human epidermal growth factor receptor 2 (her2) levels and locations: quantitative analysis of her2 overexpression effects. *Cancer Res*, 63(5):1130–7, Feb 2003.
- [81] Bart S Hendriks, Lee K Opresko, H Steven Wiley, and Douglas Lauffenburger. Quantitative analysis of her2-mediated effects on her2 and epidermal growth factor receptor endocytosis: distribution of homo- and heterodimers depends on relative her2 levels. *J Biol Chem*, 278(26):23343–51, Jun 2003.

- [82] Bart S Hendriks, H Steven Wiley, and Douglas Lauffenburger. Her2-mediated effects on egfr endosomal sorting: analysis of biophysical mechanisms. *Biophys J*, 85(4):2732–45, Sep 2003.
- [83] Roy S Herbst. Review of epidermal growth factor receptor biology. *Int J Radiat Oncol Biol Phys*, 59(2 Suppl):21–6, Jan 2004.
- [84] L Hicke. Protein regulation by monoubiquitin. *Nat Rev Mol Cell Biol*, 2(3):195–201, Mar 2001.
- [85] Linda Hicke, Heidi L Schubert, and Christopher P Hill. Ubiquitin-binding domains. *Nat Rev Mol Cell Biol*, 6(8):610–21, Aug 2005.
- [86] A. Hill. The possible effects of the aggregation of the molecules of haemoglobin on its dissociation curves. *J Physiol*, 40:iv–vii, 1910.
- [87] Lars Hinrichsen, Jens Harborth, Lars Andrees, Klaus Weber, and Ernst J Ungewickell. Effect of clathrin heavy chain- and alpha-adaptin-specific small inhibitory rnas on endocytic accessory proteins and receptor trafficking in hela cells. *J Biol Chem*, 278(46):45160–70, Nov 2003.
- [88] Daniela Hoeller, Sinisa Volarevic, and Ivan Dikic. Compartmentalization of growth factor receptor signalling. *Curr Opin Cell Biol*, 17(2):107–11, Mar 2005.
- [89] Fran?ois Houle, Simon Rousseau, Nick Morrice, Mario Luc, S?bastien Mongrain, Christopher E Turner, Sakae Tanaka, Pierre Moreau, and Jacques Huot. Extracellular signal-regulated kinase mediates phosphorylation of tropomyosin-1 to promote cytoskeleton remodeling in response to oxidative stress: impact on membrane blebbing. *Mol Biol Cell*, 14(4):1418–1432, Apr 2003.
- [90] Chi-Ying F. Huang and Jr. Ferrell, James E. Ultrasensitivity in the mitogen-activated protein kinase cascade. *PNAS*, 93:10078–10083, 1996.
- [91] Fangtian Huang, Lai Kuan Goh, and Alexander Sorkin. Egf receptor ubiquitination is not necessary for its internalization. *Proc Natl Acad Sci USA*, 104(43):16904–9, Oct 2007.

- [92] Fangtian Huang, Anastasia Khvorova, William Marshall, and Alexander Sorkin. Analysis of clathrin-mediated endocytosis of epidermal growth factor receptor by rna interference. *J Biol Chem*, 279(16):16657–61, Apr 2004.
- [93] Haiming Huang, Lei Li, Chenggang Wu, David Schibli, Karen Colwill, Sukan Ma, Chengjun Li, Protiva Roy, Krystina Ho, Zhou Songyang, Tony Pawson, Youhe Gao, and Shawn S-C Li. Defining the specificity space of the human src homology 2 domain. *Mol Cell Proteomics*, 7(4):768–84, Apr 2008.
- [94] D. St Johnston and C. Nüsslein-Volhard. The origin of pattern and polarity in the drosophila embryo. *Cell*, 68(2):201–219, Jan 1992.
- [95] Arvi Jers, Viljar Jaks, Johanna Kase, and Toivo Maimets. p53-dependent transcription can exhibit both on/off and graded response after genotoxic stress. *Oncogene*, 23(37):6175–85, Aug 2004.
- [96] Veena Kapoor, Fedor V Subach, Vladimir G Kozlov, Anatoly Grudinin, Vladislav V Verkhusha, and William G Telford. New lasers for flow cytometry: filling the gaps. *Nat Methods*, 4(9):678–9, Aug 2007.
- [97] David J Katzmann, Greg Odorizzi, and Scott D Emr. Receptor downregulation and multivesicular-body sorting. *Nat Rev Mol Cell Biol*, 3(12):893–905, Dec 2002.
- [98] Maja Kazazic, Kirstine Roepstorff, Lene E Johannessen, Nina M Pedersen, Bo van Deurs, Espen Stang, and Inger H Madshus. Egf-induced activation of the egf receptor does not trigger mobilization of caveolae. *Traffic*, 7(11):1518–27, Oct 2006.
- [99] Elaine M Khan, Jill M Heidinger, Michal Levy, Michael P Lisanti, Tommer Ravid, and Tzipora Goldkorn. Epidermal growth factor receptor exposed to oxidative stress undergoes src- and caveolin-1-dependent perinuclear trafficking. *J Biol Chem*, 281(20):14486–93, May 2006.

- [100] B N Kholodenko, O V Demin, G Moehren, and J B Hoek. Quantification of short term signaling by the epidermal growth factor receptor. *J Biol Chem*, 274(42):30169–81, Oct 1999.
- [101] Boris N Kholodenko. Untangling the signalling wires. *Nat Cell Biol*, 9(3):247–9, Mar 2007.
- [102] Boris N Kholodenko, Anatoly Kiyatkin, Frank J Bruggeman, Eduardo Sontag, Hans V Westerhoff, and Jan B Hoek. Untangling the wires: a strategy to trace functional interactions in signaling and gene networks. *Proc Natl Acad Sci U S A*, 99(20):12841–12846, Oct 2002.
- [103] Y. M. Kim, T. H. Kim, D. W. Seol, R. V. Talanian, and T. R. Billiar. Nitric oxide suppression of apoptosis occurs in association with an inhibition of bcl-2 cleavage and cytochrome c release. *J Biol Chem*, 273(47):31437–31441, Nov 1998.
- [104] Tom Kirchhausen. Clathrin adaptors really adapt. *Cell*, 109(4):413–6, May 2002.
- [105] A J Koleske, D Baltimore, and M P Lisanti. Reduction of caveolin and caveolae in oncogenically transformed cells. *Proc Natl Acad Sci USA*, 92(5):1381–5, Feb 1995.
- [106] Markus Kollmann, Linda Lovdok, Kilian Bartholome, Jens Timmer, and Victor Sourjik. Design principles of a bacterial signalling network. *Nature*, 438:504–507, 2005.
- [107] Natalia L Komarova, Xiufen Zou, Qing Nie, and Lee Bardwell. A theoretical framework for specificity in cell signaling. *Mol Syst Biol*, 1:2005.0023, 2005.
- [108] D. E. Koshland, A. Goldbeter, and J. B. Stock. Amplification and adaptation in regulatory and sensory systems. *Science*, 217(4556):220–225, Jul 1982.
- [109] Galit Lahav, Nitzan Rosenfeld, Alex Sigal, Naama Geva-Zatorsky, Arnold J Levine, Michael B Elowitz, and Uri Alon. Dynamics of the p53-Mdm2 feedback loop in individual cells. *Nat Genet*, 36(2):147–50, Feb 2004.
- [110] Douglas Lauffenburger and Jennifer Linderman. *Receptors. Models for Binding, Trafficking and Signaling*. Douglas Lauffenburger, 1993.

- [111] C. Le Roy and J. Wrana. Clathrin- and non-clathrin mediated endocytic regulation of cell signalling. *Nat Rev Mol Cell Biol*, 6:112 – 126, 2005.
- [112] Stefan Legewie, Nils Blüthgen, and Hanspeter Herzel. Mathematical modeling identifies inhibitors of apoptosis as mediators of positive feedback and bistability. *PLoS Comput Biol*, 2(9):e120, Sep 2006.
- [113] Stefan Legewie, Nils Blüthgen, Reinhold Schäfer, and Hanspeter Herzel. Ultrasensitization: switch-like regulation of cellular signaling by transcriptional induction. *PLoS Comput Biol*, 1(5):e54, Oct 2005.
- [114] A E Lenferink, R Pinkas-Kramarski, M L van de Poll, M J van Vugt, L N Klapper, E Tzahar, H Waterman, M Sela, E J van Zoelen, and Y Yarden. Differential endocytic routing of homo- and hetero-dimeric erbB tyrosine kinases confers signaling superiority to receptor heterodimers. *EMBO J*, 17(12):3385–97, Jun 1998.
- [115] J. Lewis, J. M. Slack, and L. Wolpert. Thresholds in development. *J Theor Biol*, 65(3):579–90, Apr 1977.
- [116] P. Li, D. Nijhawan, I. Budihardjo, S. M. Srinivasula, M. Ahmad, E. S. Alnemri, and X. Wang. Cytochrome c and datp-dependent formation of apaf-1/caspase-9 complex initiates an apoptotic protease cascade. *Cell*, 91(4):479–489, Nov 1997.
- [117] Diane S Lidke, Peter Nagy, Rainer Heintzmann, Donna J Arndt-Jovin, Janine N Post, Hernan E Grecco, Elizabeth A Jares-Erijman, and Thomas M Jovin. Quantum dot ligands provide new insights into erbB/her receptor-mediated signal transduction. *Nat Biotechnol*, 22(2):198–203, Jan 2004.
- [118] M P Lisanti, P E Scherer, Z Tang, and M Sargiacomo. Caveolae, caveolin and caveolin-rich membrane domains: a signalling hypothesis. *Trends Cell Biol*, 4(7):231–5, Jul 1994.

- [119] E Livneh, M Benveniste, R Prywes, S Felder, Z Kam, and J Schlessinger. Large deletions in the cytoplasmic kinase domain of the epidermal growth factor receptor do not affect its lateral mobility. *J Cell Biol*, 103(2):327–31, Aug 1986.
- [120] K A Lund, L K Opresko, C Starbuck, B J Walsh, and H S Wiley. Quantitative analysis of the endocytic system involved in hormone-induced receptor internalization. *J Biol Chem*, 265(26):15713–23, Sep 1990.
- [121] X. Luo, I. Budihardjo, H. Zou, C. Slaughter, and X. Wang. Bid, a bcl2 interacting protein, mediates cytochrome c release from mitochondria in response to activation of cell surface death receptors. *Cell*, 94(4):481–490, Aug 1998.
- [122] Nick I Markevich, Jan B Hoek, and Boris N Kholodenko. Signaling switches and bistability arising from multisite phosphorylation in protein kinase cascades. *J Cell Biol*, 164(3):353–359, Feb 2004.
- [123] Nick I. Markevich, Jan B. Hoek, and Boris N. Kholodenko. Signaling switches and bistability arising from multisite phosphorylation in protein kinase cascades. *J Cell Biol*, 164:353–359, 2004.
- [124] Mina D Marmor, Kochupurakkal Bose Skaria, and Yosef Yarden. Signal transduction and oncogenesis by erbB/her receptors. *Int J Radiat Oncol Biol Phys*, 58(3):903–13, Mar 2004.
- [125] Satyajit Mayor and Richard E Pagano. Pathways of clathrin-independent endocytosis. *Nat Rev Mol Cell Biol*, 8(8):603–12, Jul 2007.
- [126] Megan N McClean, Areez Mody, James R Broach, and Sharad Ramanathan. Cross-talk and decision making in map kinase pathways. *Nat Genet*, 39(3):409–414, Mar 2007.
- [127] Gustavo J Melen, Sagi Levy, Naama Barkai, and Ben-Zion Shilo. Threshold responses to morphogen gradients by zero-order ultrasensitivity. *Mol Syst Biol*, 1:msb4100036–E1–msb4100036–E11, 2005.

- [128] Gustavo J Melen, Sagi Levy, Naama Barkai, and Ben-Zion Shilo. Threshold responses to morphogen gradients by zero-order ultrasensitivity. *Mol Syst Biol*, 1:2005.0028, Dec 2005.
- [129] Marta Miaczynska, Savvas Christoforidis, Angelika Giner, Anna Shevchenko, Sandrine Uttenweiler-Joseph, Bianca Habermann, Matthias Wilm, Robert G Parton, and Marino Zerial. Appl proteins link rab5 to nuclear signal transduction via an endosomal compartment. *Cell*, 116(3):445–56, Feb 2004.
- [130] Marta Miaczynska, Lucas Pelkmans, and Marino Zerial. Not just a sink: endosomes in control of signal transduction. *Curr Opin Cell Biol*, 16(4):400–6, Jul 2004.
- [131] C Mineo, G L James, E J Smart, and R G Anderson. Localization of epidermal growth factor-stimulated ras/raf-1 interaction to caveolae membrane. *J Biol Chem*, 271(20):11930–5, May 1996.
- [132] Alison Motley, Nicholas A Bright, Matthew N J Seaman, and Margaret S Robinson. Clathrin-mediated endocytosis in ap-2-depleted cells. *J Cell Biol*, 162(5):909–18, Aug 2003.
- [133] S. Nagata. Apoptosis by death factor. *Cell*, 88(3):355–65, Feb 1997.
- [134] Venugopalan D Nair, Tony Yuen, C. Warren Olanow, and Stuart C Sealfon. Early single cell bifurcation of pro- and antiapoptotic states during oxidative stress. *J Biol Chem*, 279(26):27494–501, Jun 2004.
- [135] A Nesterov, R E Carter, T Sorkina, G N Gill, and A Sorokin. Inhibition of the receptor-binding function of clathrin adaptor protein ap-2 by dominant-negative mutant mu2 subunit and its effects on endocytosis. *EMBO J*, 18(9):2489–99, May 1999.
- [136] Karleen M Nicholson and Neil G Anderson. The protein kinase b/akt signalling pathway in human malignancy. *Cell Signal*, 14(5):381–395, May 2002.

- [137] H Ohno, J Stewart, M C Fournier, H Bosshart, I Rhee, S Miyatake, T Saito, A Gallusser, T Kirchhausen, and J S Bonifacino. Interaction of tyrosine-based sorting signals with clathrin-associated proteins. *Science*, 269(5232):1872–5, Sep 1995.
- [138] E. M. O’Neill, I. Rebay, R. Tjian, and G. M. Rubin. The activities of two ets-related transcription factors required for drosophila eye development are modulated by the ras/mapk pathway. *Cell*, 78(1):137–147, Jul 1994.
- [139] Rong Li Onn Brandman, James E. Ferrell Jr and Tobias Meyer. Interlinked fast and slow positive feedback loops drive reliable cell decisions. *Science*, 310:496–498, 2005.
- [140] L K Opresko and H S Wiley. Receptor-mediated endocytosis in xenopus oocytes. i. characterization of the vitellogenin receptor system. *J Biol Chem*, 262(9):4109–15, Mar 1987.
- [141] L K Opresko and H S Wiley. Receptor-mediated endocytosis in xenopus oocytes. ii. evidence for two novel mechanisms of hormonal regulation. *J Biol Chem*, 262(9):4116–23, Mar 1987.
- [142] Fernando Ortega, Luis Acerenza, Hans V. Westerhoff, Francesc Mas, and Marta Cascante. Product dependence and bifunctionality compromise the ultrasensitivity of signal transduction cascades. *PNAS*, 99:1170–1175, 2002.
- [143] T Pawson, G D Gish, and P Nash. Sh2 domains, interaction modules and cellular wiring. *Trends Cell Biol*, 11(12):504–11, Dec 2001.
- [144] B M Pearse. Clathrin: a unique protein associated with intracellular transfer of membrane by coated vesicles. *Proc Natl Acad Sci USA*, 73(4):1255–9, Apr 1976.
- [145] L Pelkmans, J Kartenbeck, and A Helenius. Caveolar endocytosis of simian virus 40 reveals a new two-step vesicular-transport pathway to the er. *Nat Cell Biol*, 3(5):473–83, Apr 2001.
- [146] Lucas Pelkmans, Thomas Bürli, Marino Zerial, and Ari Helenius. Caveolin-stabilized membrane domains as multifunctional transport and sorting devices in endocytic membrane traffic. *Cell*, 118(6):767–80, Sep 2004.

- [147] Lucas Pelkmans, Eugenio Fava, Hannes Grabner, Michael Hannus, Bianca Habermann, Eberhard Krausz, and Marino Zerial. Genome-wide analysis of human kinases in clathrin- and caveolae/raft-mediated endocytosis. *Nature*, 436(7047):78–86, Jul 2005.
- [148] Lucas Pelkmans and Ari Helenius. Endocytosis via caveolae. *Traffic*, 3(5):311–20, Apr 2002.
- [149] Lucas Pelkmans and Marino Zerial. Kinase-regulated quantal assemblies and kiss-and-run recycling of caveolae. *Nature*, 436(7047):128–33, Jul 2005.
- [150] B. Pettmann and C. E. Henderson. Neuronal cell death. *Neuron*, 20(4):633–647, Apr 1998.
- [151] N. Plesnila, S. Zinkel, D. A. Le, S. Amin-Hanjani, Y. Wu, J. Qiu, A. Chiarugi, S. S. Thomas, D. S. Kohane, S. J. Korsmeyer, and M. A. Moskowitz. Bid mediates neuronal cell death after oxygen/glucose deprivation and focal cerebral ischemia. *Proc Natl Acad Sci U S A*, 98(26):15318–15323, Dec 2001.
- [152] Simona Polo, Sara Sigismund, Mario Faretta, Monica Guidi, Maria Rosaria Capua, Giovanna Bossi, Hong Chen, Pietro De Camilli, and Pier Paolo Di Fiore. A single motif responsible for ubiquitin recognition and monoubiquitination in endocytic proteins. *Nature*, 416(6879):451–5, Mar 2002.
- [153] Babak Razani, Scott E Woodman, and Michael P Lisanti. Caveolae: from cell biology to animal physiology. *Pharmacol Rev*, 54(3):431–67, Sep 2002.
- [154] Babak Razani, Scott E. Woodman, and Michael P. Lisanti. Caveolae: From Cell Biology to Animal Physiology. *Pharmacol Rev*, 54(3):431–467, 2002.
- [155] J. C. Reed. Dysregulation of apoptosis in cancer. *J Clin Oncol*, 17(9):2941–53, Sep 1999.
- [156] Markus Rehm, Heiko Dussmann, Reiner U Janicke, Jeremy M Tavaré, Donat Kogel, and Jochen H M Prehn. Single-cell fluorescence resonance energy transfer analysis demonstrates that caspase activation during apoptosis is a rapid process. Role of caspase-3. *J Biol Chem*, 277(27):24506–14, Jul 2002.

- [157] Jochen Rink, Eric Ghigo, Yannis Kalaidzidis, and Marino Zerial. Rab conversion as a mechanism of progression from early to late endosomes. *Cell*, 122(5):735–49, Sep 2005.
- [158] K G Rothberg, J E Heuser, W C Donzell, Y S Ying, J R Glenney, and R G Anderson. Caveolin, a protein component of caveolae membrane coats. *Cell*, 68(4):673–82, Feb 1992.
- [159] Christine Le Roy and Jeffrey L Wrana. Clathrin- and non-clathrin-mediated endocytic regulation of cell signalling. *Nat Rev Mol Cell Biol*, 6(2):112–26, Jan 2005.
- [160] L. M. Roy, O. Haccard, T. Izumi, B. G. Lattes, A. L. Lewellyn, and J. L. Maller. Mos proto-oncogene function during oocyte maturation in xenopus. *Oncogene*, 12(10):2203–2211, May 1996.
- [161] Y Sako, S Minoghchi, and T Yanagida. Single-molecule imaging of egfr signalling on the surface of living cells. *Nat Cell Biol*, 2(3):168–72, Mar 2000.
- [162] A E Salcini, H Chen, G Iannolo, P De Camilli, and P P Di Fiore. Epidermal growth factor pathway substrate 15, eps15. *Int J Biochem Cell Biol*, 31(8):805–9, Jul 1999.
- [163] Silvia D M Santos, Peter J Verveer, and Philippe I H Bastiaens. Growth factor-induced mapk network topology shapes erk response determining pc-12 cell fate. *Nat Cell Biol*, 9(3):324–30, Mar 2007.
- [164] Silvia D M Santos, Peter J Verveer, and Philippe I H Bastiaens. Growth factor-induced mapk network topology shapes erk response determining pc-12 cell fate. *Nat Cell Biol*, 9(3):324–330, Mar 2007.
- [165] M Sargiacomo, P E Scherer, Z Tang, E Kübler, K S Song, M C Sanders, and M P Lisanti. Oligomeric structure of caveolin: implications for caveolae membrane organization. *Proc Natl Acad Sci USA*, 92(20):9407–11, Sep 1995.
- [166] H Schmidt-Glenewinkel, I Vacheva, D Hoeller, I Dikic, and R Eils. An ultrasensitive sorting mechanism for egf receptor endocytosis. *BMC systems biology*, 2(1):32, Apr 2008.

- [167] Birgit Schoeberl, Claudia Eichler-Jonsson, Ernst Dieter Gilles, and Gertraud Müller. Computational modeling of the dynamics of the map kinase cascade activated by surface and internalized egf receptors. *Nat Biotechnol*, 20(4):370–5, Apr 2002.
- [168] Waltraud X Schulze, Lei Deng, and Matthias Mann. Phosphotyrosine interactome of the erbb-receptor kinase family. *Mol Syst Biol*, 1:2005.0008, Jan 2005.
- [169] Monica A Schwartz and Hiten D Madhani. Principles of map kinase signaling specificity in *saccharomyces cerevisiae*. *Annu Rev Genet*, 38:725–748, 2004.
- [170] M. Serrano and M. A. Blasco. Putting the stress on senescence. *Curr Opin Cell Biol*, 13(6):748–753, Dec 2001.
- [171] Nathan C Shaner, Robert E Campbell, Paul A Steinbach, Ben N G Giepmans, Amy E Palmer, and Roger Y Tsien. Improved monomeric red, orange and yellow fluorescent proteins derived from *discosoma* sp. red fluorescent protein. *Nat Biotechnol*, 22(12):1567–72, Dec 2004.
- [172] Sara Sigismund, Tanja Woelk, Claudia Puri, Elena Maspero, Carlo Tacchetti, Pietro Transidico, Pier Paolo Di Fiore, and Simona Polo. Clathrin-independent endocytosis of ubiquitinated cargos. *Proc Natl Acad Sci USA*, 102(8):2760–5, Feb 2005.
- [173] Kai Simons and Derek Toomre. Lipid rafts and signal transduction. *Nat Rev Mol Cell Biol*, 1:31–39, 2000.
- [174] D J Slamon, G M Clark, S G Wong, W J Levin, A Ullrich, and W L McGuire. Human breast cancer: correlation of relapse and survival with amplification of the her-2/neu oncogene. *Science*, 235(4785):177–82, Jan 1987.
- [175] E. A. Slee, S. A. Keogh, and S. J. Martin. Cleavage of bid during cytotoxic drug and uv radiation-induced apoptosis occurs downstream of the point of bcl-2 action and is catalysed by caspase-3: a potential feedback loop for amplification of apoptosis-associated mitochondrial cytochrome c release. *Cell Death Differ*, 7(6):556–565, Jun 2000.

- [176] Alexander Sorkin. Cargo recognition during clathrin-mediated endocytosis: a team effort. *Curr Opin Cell Biol*, 16(4):392–9, Aug 2004.
- [177] Philippe Soubeyran, Katarzyna Kowanetz, Iwona Szymkiewicz, Wallace Y Langdon, and Ivan Dikic. Cbl-cin85-endophilin complex mediates ligand-induced downregulation of egf receptors. *Nature*, 416(6877):183–7, Mar 2002.
- [178] S. M. Srinivasula, M. Ahmad, T. Fernandes-Alnemri, and E. S. Alnemri. Autoactivation of procaspase-9 by apaf-1-mediated oligomerization. *Mol Cell*, 1(7):949–957, Jun 1998.
- [179] E Stang, J Kartenbeck, and R G Parton. Major histocompatibility complex class i molecules mediate association of sv40 with caveolae. *Mol Biol Cell*, 8(1):47–57, Dec 1997.
- [180] C Starbuck and D A Lauffenburger. Mathematical model for the effects of epidermal growth factor receptor trafficking dynamics on fibroblast proliferation responses. *Biotechnol Prog*, 8(2):132–43, Jan 1992.
- [181] S W Straight, B Herman, and D J McCance. The e5 oncoprotein of human papillomavirus type 16 inhibits the acidification of endosomes in human keratinocytes. *J Virol*, 69(5):3185–92, Apr 1995.
- [182] S W Straight, P M Hinkle, R J Jewers, and D J McCance. The e5 oncoprotein of human papillomavirus type 16 transforms fibroblasts and effects the downregulation of the epidermal growth factor receptor in keratinocytes. *J Virol*, 67(8):4521–32, Jul 1993.
- [183] William Telford, Matilde Murga, Teresa Hawley, Robert Hawley, Beverly Packard, Akira Komoriya, Fred Haas, and Charles Hubert. Dpss yellow-green 561-nm lasers for improved fluorescence detection by flow cytometry. *Cytometry A*, 68(1):36–44, Oct 2005.
- [184] Yuji Teramura, Junya Ichinose, Hiroaki Takagi, Kenji Nishida, Toshio Yanagida, and Yasushi Sako. Single-molecule analysis of epidermal growth factor binding on the surface of living cells. *EMBO J*, 25(18):4215–22, Sep 2006.

- [185] Peter Thomsen, Kirstine Roepstorff, Martin Stahlhut, and Bo van Deurs. Caveolae are highly immobile plasma membrane microdomains, which are not involved in constitutive endocytic trafficking. *Mol Biol Cell*, 13(1):238–50, Dec 2002.
- [186] John J Tyson, Katherine C Chen, and Bela Novak. Sniffers, buzzers, toggles and blinkers: dynamics of regulatory and signaling pathways in the cell. *Curr Opin Cell Biol*, 15(2):221–231, Apr 2003.
- [187] John J Tyson, Katherine C Chen, and Bela Novak. Sniffers, buzzers, toggles and blinkers: dynamics of regulatory and signaling pathways in the cell. *Curr Opin Cell Biol*, 15:221–231, 2003.
- [188] A V Vieira, C Lamaze, and S L Schmid. Control of egf receptor signaling by clathrin-mediated endocytosis. *Science*, 274(5295):2086–9, Dec 1996.
- [189] Qian Wang, Greg Villeneuve, and Zhixiang Wang. Control of epidermal growth factor receptor endocytosis by receptor dimerization, rather than receptor kinase activation. *EMBO Rep*, 6(10):942–8, Sep 2005.
- [190] R A Warren, F A Green, and C A Enns. Saturation of the endocytic pathway for the transferrin receptor does not affect the endocytosis of the epidermal growth factor receptor. *J Biol Chem*, 272(4):2116–21, Jan 1997.
- [191] H Waterman, I Sabanai, B Geiger, and Y Yarden. Alternative intracellular routing of erbB receptors may determine signaling potency. *J Biol Chem*, 273(22):13819–27, May 1998.
- [192] H Waterman and Y Yarden. Molecular mechanisms underlying endocytosis and sorting of erbB receptor tyrosine kinases. *FEBS Lett*, 490(3):142–52, Feb 2001. this paper is awesome p1 - yarden is my hero.

- [193] Hadassa Waterman, Menachem Katz, Chanan Rubin, Keren Shtiegman, Sara Lavi, Ari Elson, Thomas Jovin, and Yosef Yarden. A mutant egf-receptor defective in ubiquitylation and endocytosis unveils a role for grb2 in negative signaling. *EMBO J*, 21(3):303–13, Jan 2002.
- [194] Keng Boon Wee and Baltazar D Aguda. Akt versus p53 in a network of oncogenes and tumor suppressor genes regulating cell survival and death. *Biophys J*, 91(3):857–65, Aug 2006.
- [195] A Wells, J B Welsh, C S Lazar, H S Wiley, G N Gill, and M G Rosenfeld. Ligand-induced transformation by a noninternalizing epidermal growth factor receptor. *Science*, 247(4945):962–4, Feb 1990.
- [196] A Wilde, E C Beattie, L Lem, D A Riethof, S H Liu, W C Mobley, P Soriano, and F M Brodsky. Egf receptor signaling stimulates src kinase phosphorylation of clathrin, influencing clathrin redistribution and egf uptake. *Cell*, 96(5):677–87, Mar 1999.
- [197] H S Wiley. Anomalous binding of epidermal growth factor to a431 cells is due to the effect of high receptor densities and a saturable endocytic system. *J Cell Biol*, 107(2):801–10, Jul 1988.
- [198] H S Wiley and D D Cunningham. The endocytotic rate constant. a cellular parameter for quantitating receptor-mediated endocytosis. *J Biol Chem*, 257(8):4222–9, Apr 1982.
- [199] H. S. Wiley and D. D. Cunningham. The endocytotic rate constant. a cellular parameter for quantitating receptor-mediated endocytosis. *J Biol Chem*, 257(8):4222–4229, Apr 1982.
- [200] H Steven Wiley. Trafficking of the erbb receptors and its influence on signaling. *Exp Cell Res*, 284(1):78–88, Mar 2003.
- [201] R Worthyake, L K Opreko, and H S Wiley. Erbb-2 amplification inhibits down-regulation and induces constitutive activation of both erbb-2 and epidermal growth factor receptors. *J Biol Chem*, 274(13):8865–74, Mar 1999.
- [202] Wen Xiong and James E Ferrell. A positive-feedback-based bistable 'memory module' that governs a cell fate decision. *Nature*, 426:460–5, 2003.

- [203] Yosef Yarden and Ben-Zion Shilo. Snapshot: Egfr signaling pathway. *Cell*, 131(5):1018, Nov 2007.
- [204] N. Yew, M. L. Mellini, and G. F. Vande Woude. Meiotic initiation by the mos protein in xenopus. *Nature*, 355(6361):649–652, Feb 1992.
- [205] X. M. Yin, K. Wang, A. Gross, Y. Zhao, S. Zinkel, B. Klocke, K. A. Roth, and S. J. Korsmeyer. Bid-deficient mice are resistant to fas-induced hepatocellular apoptosis. *Nature*, 400(6747):886–891, Aug 1999.
- [206] W Zhang, B Razani, Y Altschuler, B Bouzahzah, K E Mostov, R G Pestell, and M P Lisanti. Caveolin-1 inhibits epidermal growth factor-stimulated lamellipod extension and cell migration in metastatic mammary adenocarcinoma cells (mtln3). transformation suppressor effects of adenovirus-mediated gene delivery of caveolin-1. *J Biol Chem*, 275(27):20717–25, Jul 2000.
- [207] X Zhao, T Greener, H Al-Hasani, S W Cushman, E Eisenberg, and L E Greene. Expression of auxilin or ap180 inhibits endocytosis by mislocalizing clathrin: evidence for formation of nascent pits containing ap1 or ap2 but not clathrin. *J Cell Sci*, 114(Pt 2):353–65, Jan 2001.
- [208] Hua Zou, Ruomei Yang, Junshan Hao, Jean Wang, Chaohong Sun, Stephen W Fesik, Joe C Wu, Kevin J Tomaselli, and Robert C Armstrong. Regulation of the apaf-1/caspase-9 apoptosome by caspase-3 and xiap. *J Biol Chem*, 278(10):8091–8098, Mar 2003.
- [209] Yaara Zwang and Yosef Yarden. p38 map kinase mediates stress-induced internalization of egfr: implications for cancer chemotherapy. *EMBO J*, 25(18):4195–206, Sep 2006.